Rôles respectifs des isoformes de ferrédoxine-NADP-oxydoréductase dans la cyanobactérie Synechocystis sp. PCC 6803

Anja Korn

Faculté des sciences d'Orsay

UNIVERSITÉ PARIS-SUD 11

Numéro d'ordre 9782

Respective roles of the ferredoxin:NADP-oxidoreductase isoforms in the cyanobacterium *Synechocystis* sp. PCC 6803

Anja Korn

Service de Bioénergétique, Biologie Structurale et Mécanismes (SB2SM)
Institut de Biologie et de Technologies de Saclay (IBITEC-S)
CNRS-CEA Saclay

JURY

Soutenue le 19 février 2010 devant le jury composé de :

Présidente du jury	Chantal Astier
Rapporteurs	Caroline Bowsher
	Giovanni Finazzi
Examinateurs	Ghada Ajlani
	Laurent Cournac
Directeur de thèse	Pierre Sétif

cea

cnrs
dépasser les frontières

Contents

List of Figures

List of Tables

Résumé

Ce travail de thèse concerne la photosynthèse oxygénique, le processus utilisé par les cyanobactéries, les algues et les plantes pour convertir la lumière solaire en énergie chimique et stocker cette énergie. Lors des étapes initiales dépendant de la lumière, ce processus rejette de l'oxygène et forme de l'ATP et du NADPH, qui sont produits lors d'un flux linéaire d'électrons. Ces deux molécules énergétiques sont utilisées pour réduire le CO_2 et l'assimiler sous forme de sucres. Des modes alternatifs de transfert d'électrons, cyclique et pseudo-cyclique, conduisent seulement à la formation d'ATP. Deux flux d'électrons cycliques majeurs ont été proposés: un flux qui dépend de la ferrédoxine et un flux qui dépend du NADPH. Le premier et le deuxième flux sont respectivement les flux cycliques majeurs dans les plantes et les cyanobactéries. D'une part, le transfert cyclique implique chez les cyanobactéries le recyclage des excès de NADPH vers le pool des plastoquinones (PQ) dans la membrane thylakoïdale. D'autre part, le transfert pseudo-cyclique implique chez les cyanobactéries la formation de NADPH, dont les électrons ne sont pas recyclés vers le pool de PQ mais "perdus" pour réduire l'oxygène en eau.

Dans les membranes photosynthétiques des cyanobactéries et également à un degré moindre des chloroplastes se déroulent des transferts d'électrons respiratoires, producteurs d'ATP à partir du NAD(P)H lui-même issu de la dégradation des sucres. La cyanobactérie étudiée ici - *Synechocystis* sp. PCC6803 (*Synechocystis*) - est un organisme non seulement photoautotrophe mais aussi hétérotrophe facultatif.

Le phycobilisome (PBS) est le complexe majeur collecteur de lumière chez les cyanobactéries. Il transfert l'énergie capturée essentiellement vers le photosystème (PS) II. De plus, il constitue jusqu'à 30% des protéines dans la cyanobactérie et peut être dégradé en conditions de carence en nutriments. Le PS I (PSI) est responsable de la formation photosynthétique de NADPH, les électrons étant transportés des accepteurs du PSI vers la ferrédoxine (Fd) et finalement vers le $NADP^+$ *via* la ferrédoxine:NADP oxydoréductase (FNR).

Chez les plantes, différentes isoformes de Fd et de FNR sont présentes dans différents tissus et codées par différents gènes. Ainsi dans les chloroplastes de feuilles, des Fds réduisent la FNR photosynthétique pour former le NADPH. Par contre, dans les plastes des racines, la FNR

hétérotrophe réduit une autre Fd en oxydant le NADPH et la Fd ainsi réduite est impliquée entre autres dans l'assimilation de l'azote. Chez *Synechocystis*, la Fd codée par le gène *fed1* est indispensable en conditions de croissance photoautotrophe aussi bien qu'hétérotrophe cependant que trois autres gènes codant des Fd photosynthétiques sont faiblement exprimés. Le produit du gène *fed1* est donc probablement impliqué dans la réduction du $NADP^+$ et l'oxydation du NADPH.

A partir d'un seul gène, deux isoformes de FNR de taille différente ont été trouvées chez *Synechocystis*. Grâce à un domaine de type linker, la plus grande, FNR_L, est liée au PBS, contrairement à la plus petite, FNR_S, qui est dépourvue de ce domaine. Ces observations posent deux questions qui ont motivé ce travail de thèse: quelle est la fonction de l'attachement de FNR_L au PBS et quelles sont les rôles respectifs des deux isoformes de FNR? Des mutants exprimant uniquement une des isoformes ont été récemment obtenus. De l'étude de la croissance des mutants en différentes conditions a été formulée l'hypothèse de ce travail que FNR_L est impliquée dans la réduction du $NADP^+$ (transfert d'électrons linéaire) et FNR_S dans l'oxydation du NADPH (transfert d'électrons respiratoire/cyclique).

Ce travail de thèse a fait l'objet de deux approches différentes. D'une part, les activités catalytiques des deux isoformes ont été étudiées *in vitro*. D'autre part, les mutants de FNR ont été comparés au type sauvage (WT) dans différentes études *in vivo*.

FNR_L étant toujours liée au PBS *in vivo* et étant protéolysée lorsqu'elle n'est pas liée, nous avons choisi de purifier un sous-complexe du PBS comprenant FNR_L et un hexamère de phycocyanine (PC) du PBS. Ce complexe, appelé FNR_L-PC, est stable tout en présentant des propriétés d'absorption compatibles avec des études de spectroscopie d'absorption. FNR_L-PC a été purifié à partir d'une souche mutée de *Synechocystis* possédant d'une part un seul hexamère de PC par bâtonnet (au lieu de trois) et d'autre part une étiquette histidine insérée dans le domaine charnière de la FNR_L (situé entre le domaine linker et les domaines catalytiques). Puisqu'une à deux FNR_L sont attachées par PBS aussi bien dans le mutant que dans le WT, nous avons multiplié par trois le rapport FNR_L/PC dans le matériel de départ. De plus, la présence de l'étiquette histidine a facilité la purification du complexe par l'utilisation d'une étape de chromatographie d'affinité au nickel, les impuretés restantes étant ensuite éliminées par filtration sur tamis moléculaire.

Grâce à cette approche, nous avons atteint notre premier objectif qui était de purifier FNR_L-PC à l'homogénéité et d'augmenter son rendement de purification. Le complexe FNR_L-PC contient FNR_L, un hexamère de PC et un linker bâtonnet-coeur appelé L_{RC}, pour une masse moléculaire d'environ 330 kDa. Il possède un groupe prosthétique FAD par FNR_L et est stable à 4°C, ce qui confirme que la liaison à l'hexamère de PC protège FNR_L de la protéolyse. Nous avons également initié des études de reconstitution du PBS et de FNR_L, ce qui permet d'envisager la production de grandes quantités de complexe en vue d'une analyse structurale.

Nous avons ensuite effectué une étude enzymologique détaillée des activités $NADP^+$-réductase et NADPH-oxydase de FNR_L-PC que nous avons comparées à celles de FNR_S. Nous avons caractérisé l'activité d'oxydation du NADPH par des tests classiques d'enzymologie et commencé l'étude de l'inhibition par le produit de la réaction. L'activité $NADP^+$-réductase a été mesurée par spectroscopie d'absorption différentielle résolue en temps en présence de PSI.

Bien que dans l'ensemble assez proches, les mesures d'activité présentent quelques différences majeures entre FNR_L-PC et FNR_S. La différence la plus importante concerne l'affinité réduite de la Fd oxydée (Fd_{ox}) pour FNR_L-PC *vs.* FNR_S lors de l'oxydation du NADPH. L'effet observé peut s'expliquer par l'encombrement stérique de l'hexamère de PC dans le complexe FNR_L-PC. Comme il est généralement admis que la dissociation de Fd_{ox} est cinétiquement limitante lors de la réduction du $NADP^+$, cet effet pourrait favoriser la réduction du $NADP^+$ par le complexe. Ceci est en accord avec les caractéristiques de croissance des mutants de FNR, le mutant exprimant uniquement FNR_L poussant mieux en photoautotrophie (réduction du $NADP^+$). Cet effet d'encombrement s'est aussi manifesté pour les cinétiques de réduction de la FNR par Fd_{red}.

L'augmentation d'affinité pour le NADPH de FNR_L-PC *vs.* FNR_S a été également observée. Cette augmentation pourrait ne pas avoir d'effet négatif sur l'oxydation *in vivo* du NADPH par FNR_S, car l'induction de FNR_S chez le WT en conditions de stress ou d'hétérotrophie est corrélée à une augmentation, au moins transitoire, de la concentration de NADPH. Une meilleure affinité pour le substrat $NADP^+$/NADPH pourrait par contre renforcer la réduction du $NADP^+$ par FNR_L-PC. Nous avons de plus mis en évidence que dans les conditions de force ionique élevée que nous utilisons pour garder intact FNR_L-PC, la première réduction de la FNR par Fd_{red} est limitante pour la réduction du $NADP^+$, ce qui n'est pas le cas à faible force ionique.

Les différences que nous avons observées sont en désaccord avec les différences observées chez les isoformes de FNR de plantes (feuilles *vs.* racines). Les isoformes de *Synechocystis* correspondent peut-être mieux aux différentes isoformes trouvées dans les feuilles d'un même organisme. D'autres facteurs que les propriétés catalytiques, tels que la disponibilité des substrats (Fd_{ox}/Fd_{red} et $NADP^+$/NADPH) et la localisation de la FNR, sont probablement essentiels pour expliquer les rôles physiologiques respectifs des deux isoformes de la FNR de *Synechocystis*. Ainsi FNR_L est liée au PBS tandis que FNR_S est soit soluble, soit liée à la membrane, soit liée à des complexes membranaires (cytochrome b_6f, NADPH déshydrogénase NDH-1).

C'est pourquoi nous avons commencé des études *in vivo* sur le WT ainsi que sur des mutants appelés MI6 et FS1 qui expriment une seule isoforme, respectivement FNR_L et FNR_S. Nous avons effectué trois types de mesure. D'abord nous avons caractérisé l'état rédox du pool de NADP par la mesure du rapport $NADP^+$/NADPH. Ensuite nous avons mesuré la réduction transitoire du pool des PQ de la membrane, à l'obscurité juste après une période d'éclairement, par des mesures de fluorescence chlorophyllienne. Enfin nous avons identifié le(s) mode(s) prédominant(s) de

transfert d'électrons (linéaire *vs.* respiratoire/cyclique) par les cinétiques de photooxydation du donneur primaire P700 du PSI lors d'une excitation sélective du PSI. L'interprétation de ces dernières données requiert l'utilisation d'inhibiteurs qui bloquent sélectivement les transferts d'électrons du PSII (DCMU) ou du cytochrome b_6f (DBMIB) ou qui inhibent les réactions de recombinaison du PSI (méthyl viologène).

Les trois souches (WT, MI6 et FS1) ont d'abord été étudiées en conditions de croissance photoautotrophes en présence d'un excès de CO_2/HCO_3^-, conditions dans lesquelles seule FNR_L est exprimée dans le WT. Nous avons déterminé que le pool de NADP est plus oxydé dans FS1 que dans le WT et MI6, ce qui suggère que FNR_S est soit peu apte à réduire le $NADP^+$, soit recycle efficacement les électrons du NADPH vers le pool de PQ. Les mesures de réduction transitoire du pool de PQ à l'obscurité sont en plein accord avec la deuxième possibilité, avec un signal de réduction plus élevé pour FS1 que pour WT/MI6. Les cinétiques de photooxydation du P700 sont également cohérentes avec les mesures précédentes: la photooxydation est rapide chez WT/MI6 et beaucoup plus lente chez FS1. Ces résultats s'expliquent par un transfert d'électrons linéaire (et peut-être pseudo-cyclique) dominant chez WT/MI6 et un transfert d'électrons respiratoire/cyclique beaucoup plus efficace chez FS1.

Nous avons ensuite répété les mesures de photooxydation du P700 sur les trois souches cultivées à faible CO_2 (CO_2 atmosphérique, pas de bicarbonate) car ces conditions sont connues pour induire le transfert d'électrons cyclique/respiratoire. MI6 et FS1 montrent pas ou peu de différences phénotypiques avec les observations précédentes tandis que le comportement du WT se rapproche de celui du FS1: le P700 est beaucoup plus lentement photooxydé. Nous proposons que cela est dû à l'accumulation de FNR_S qui se produit généralement chez le WT en situation de stress (manque d'azote, excès de lumière). La mesure de MI6 (comportement identique à fort ou faible CO_2) renforce cette interprétation car ce mutant est incapable d'exprimer FNR_S. L'accumulation de FNR_S dans le WT favorise ainsi un transfert d'électrons respiratoire/cyclique, en accord avec l'idée que ces modes de transfert d'électrons sont induits à faible CO_2, lorsque le cycle de Calvin est ralenti.

L'implication de FNR_L dans le transfert d'électron linéaire/pseudo-cyclique et de FNR_S dans le transfert d'électron respiratoire/cyclique est donc confirmée par nos études *in vivo*. Pour remplir son rôle, FNR_S pourrait se lier à d'autres complexes membranaires comme le cytochrome b_6f ou les complexes NDH-1. Nous favorisons la dernière hypothèse car le mode dominant de transfert cyclique ainsi que la respiration chez les cyanobactéries implique les complexes NDH-1 et qu'un des complexes NDH-1 est fortement induit à faible CO_2.

Les résultats *in vitro* ainsi que les mesures de l'état rédox du pool de NADP sont décrits dans un article publié en 2009 dans "The Journal of Biological Chemistry" joint à la fin du manuscrit.

Ce travail ouvre de nombreuses perspectives pour des études *in vitro* et *in vivo*. Les études

d'inhibition de l'oxydation du NADPH par le produit de la réaction ($NADP^+$) permettront de comparer les affinités relatives de FNR_S pour le $NADP^+$ et le NADPH. La production massive d'une FNR_L contenant une étiquette histidine favorisera l'obtention par reconstitution de grandes quantités de complexes FNR_L-PC pour des études structurales ou spectroscopiques. Les études *in vivo* suivantes doivent être entreprises pour préciser le rôle de FNR_S et ses partenaires dans la réduction du pool de PQ chez les cyanobactéries hétérotrophes facultatives: accumulation de FNR_S dans le WT à faible CO_2, étude de l'état rédox du pool de PQ à l'obscurité et de sa réduction transitoire à fort et faible CO_2, mesures en temps réel du NADPH par fluorescence. L'étude transcriptomique des mutants de FNR permettra d'identifier les régulations induites par l'accumulation d'une seule isoforme. Une étude génétique est en cours afin d'étudier le rôle de la région 5' non-codante de l'ARN messager du gène *petH* dans l'accumulation de FNR_S.

Abbreviations

A_0^-	Chlorophyll of PSI, reduced in the primary electron transfer
AL	Actinic light
AP	Allophycocyanin PB subunit of an phycobiliprotein, PB indicates the protein
ATP	Adenosine 5′-triphosphate
α^{PC} and β^{PC}	Subunits of phycocyanin
b_6f	Cytochrome b_6f complex
chl	Chlorophyll
CP43	Core antenna complex with apparent mass of 43 kDa
CP47	Core antenna complex with apparent mass of 47 kDa
Cys	Cysteine
cyt *c*	Cytochrome *c*
Da	Dalton
DBMIB	2,5-Dibromo-3-methyl-6-isopropylbenzoquinone
DCMU	3-(3′,4′-Dichlorophenyl)-1,1-dimethylurea
DCPIP	2,6-Dichlorophenolindophenol
EDTA	Ethylene diaminetetraacetic acid
E_m	Midpoint redox potential
ET	Electron transfer
(F_A,F_B)	(4Fe-4S) Clusters, the terminal acceptors of PSI
Fd	Ferredoxin
(4Fe-4S) and (2Fe-2S)	Iron sulfur clusters
FNR	Ferredoxin-NADP(H)-oxidoreductase
FNR_L	Large *Synechocystis* FNR isoform, *Synechocystis* indicates the cyanobacterium
FNR_S	Small *Synechocystis* FNR isoform, *Synechocystis* indicates the cyanobacterium
FNR_{sq}	Singly reduced FNR/semiquinone form
FR	Far red
GDH	Glucose dehydrogenase
HC	high CO_2

IMAC	Immobilized metal affinity chromatography
LC	low CO_2
L_C	Core-linker polypeptide
L_{CM}	Core-membrane-linker polypeptide
L_{RC}	Rod-core-linker polypeptide
L_R (L_R^M)	Rod-linker polypeptide, M indicates its molecular mass
MES	2-Morpholinoethanesulfonic acid
MV	Methylviologen
$NADP^+$ (NADPH)	Nicotinamide adenine dinucleotide phosphate (reduced form)
NDH	NADPH dehydrogenase
OD	Optical density
P680	Primary electron donor of photosystem II
P700	Primary electron donor of photosystem I
PAM	Pulse amplitude modulation
PBP	Phycobiliprotein
PBS	Phycobilisome
Pc	Plastocyanin
PC	Phycocyanin, an $\alpha\beta$ protomer
PCB	Phycocyanobilin
PCC	Pasteur Culture Collection
PCR	Polymerase chain reaction
pdb	protein data bank
PQ	Plastoquinone
ps	picosecond, 1 ps=10^{-12} s
PSI	Photosystem I
PSII	Photosystem II
Q_A	Primary electron acceptor quinone of photosystem II
Q_B	Secondary electron acceptor quinone of photosystem II
SDS	Sodium dodecyl sulphate
SDS-PAGE	Polyacrylamide gel electrophoresis in the presence of SDS
Synechocystis	*Synechocystis* sp. PCC6803
TCA	Trichloroacetic acid
Tricine	N-[2-Hydroxy-1,1-bis(hydroxymethyl)ethyl]glycine
Tris	Tris hydroxymethyl methylamine
UV-Vis	Ultraviolet-visible
Y_Z	Tyrosine residue of photosystem II
WT	Wild type

Acknowledgments

First of all, I thank my Supervisor Pierre Sétif from the Laboratoire de Photocatalyse et Biohydrogène (LPB) for accepting me as a PhD students and guiding me through the three and half years. I thank Bernard Lagoutte and Véronique Mary from the LPB for providing various purified enzymes for activity tests and for help in biochemical techniques.

I am grateful to a second lab I collaborated strongly with, the Laboratoire de Bioénergétique Membranaire et Stress (LBMS) and especially to Ghada Ajlani. I thank Amin Nasser and Andrew Gall from the LBMS for fruitful collaborations and Bill Rutherford and Bruno Robert for funding.

I am grateful to all the members of the jury and especially to the two reviewers Caroline Bowsher and Giovanni Finazzi for judging my manuscript. Thanks to Chantal Astier for presiding the jury and to Laurent Cournac for helpful suggestions.

Jean-Claude Thomas, Cindy Bordot and Bettina Ughy are acknowledged for initiating the work on the two FNR isoforms. Francis Haraux is acknowledged for discussions and Alain Boussac for the gift of *T. elongatus* soluble extracts. Diana Kirilovsky and Anja Liszkay are acknowledged for help during *in vivo* studies. I thank the topic of my thesis for teaching me diverse techniques and challenging me during the time of my PhD.

I thank the people that supported me, mostly from the building 532 in CEA Saclay, especially Klaus Brettel, Tiona Andrianaivomananjaona, Katya Sybirna, Sameh Herga, Eiri Heyno, Adrienne Gomez de Gracia, Naoko Ishida-Blanc, Thanh-Lan Lai, Clémence Boulay, Thiagu Virutachalam, Adjélé Wilson, Sandrine Cot, Arezki Sedoud, Alain Rambourg and Christian Chauvin and many others. Last but not least, I am grateful to my family, friends and my boyfriend Rami Ajaj for support.

Chapter 1

Introduction

The field of photosynthesis research is very broad and comprises research at various levels - from eco-systems to isolated proteins [Messinger et al., 2009]. We will introduce in the following sections photosynthesis and bioenergetics and present various pathways of electron transfer. The antenna complexes and the photosystem I acceptor side are described in detail.

1.1 Photosynthesis and bioenergetics

Photosynthesis is the process that transforms light energy into electrochemical energy following the basic stoichiometry shown in Reaction 1.1.1 [Kiang et al., 2007]:

$$CO_2 + 2H_2A + h\nu \xrightarrow[\text{pigments}]{} (CH_2O) + H_2O + 2A \tag{1.1.1}$$

When H_2A is H_2O, this reaction is called oxygen-evolving photosynthesis. This reaction is divided in the photochemical reactions (formerly known as light reactions) and a series of enzymatic reactions involved in the Calvin-Benson-Bassham cycle (Calvin cycle) for CO_2 assimilation (formerly known as dark reactions) [Dubbs and Tabita, 2004]. The different stages of energy storage will be detailed later. In the following, we will describe the photosynthetic organisms.

Autotrophs derive all their cellular carbon from CO_2, whereas heterotrophs derive cellular carbon from organic carbon compounds [Blankenship, 2002]. In this way, heterotrophs depend on autotrophs to provide them with the organic carbon compounds. A further distinction can be made concerning the energy source. Phototrophs derive their energy from sunlight, whereas chemotrophs derive energy from different chemical compounds. Organisms that derive their

energy from the sunlight and derive all their cellular carbon from CO_2 are called photoautotrophs. Most of the photosynthetic organisms grow photoautotrophically. Species capable of performing photosynthesis are among prokaryotes and eukaryotes.

Five distinct major groups of prokaryotes are found that are capable of photosynthesis. Four of them are anoxygenic. H_2A does not correspond to water in this case. Thus, oxygen is not produced as a byproduct. The anoxygenic phototrophic bacteria include purple bacteria, green sulfur bacteria, green nonsulfur bacteria and heliobacteria. The only oxygen-evolving group of bacteria are called cyanobacteria (formerly known as blue-green algae).

Eukaryotic photosynthetic organisms such as plants and algae contain a subcellular organelle (plastid) called chloroplast. Chloroplasts originated by endosymbiosis from cyanobacteria. Initially a cyanobacterial-like cell was a symbiont with a protoeukaryotic cell and became a semi-autonomous part of the host cell. This explains the similar mechanism of photosynthesis of cyanobacteria compared to that of photosynthetic eukaryotes.

In the chloroplast as well as in cyanobacteria an extensive internal membrane system called the thylakoid contains chlorophyll and the electron transport chain that carries out initial light energy capture and storage.

1.1.1 Linear electron transfer and membrane complexes

In oxygenic photosynthetic organisms, the major mode of electron transfer (ET) is the linear ET (noncyclic). It involves water oxidation to molecular oxygen and the reduction of $NADP^+$ into NADPH. This is achieved by two sequential photoreactions involving two photosystems (Figure 1.1). We will further introduce the four integral membrane protein complexes involved in photosynthetic electron transfer and ATP build-up that are photosystem II (PSII), cytochrome b_6f (cyt b_6f), photosystem I (PSI) and ATP-synthase (ATPase).

PSI and PSII contain numerous pigments that harvest light and funnel the excitation to the primary electron donors, which can reduce an electron acceptor and accept electrons from specific electron donors. The cyt b_6f complex mediates electron transport between PSII and PSI and converts redox energy into a high-energy intermediate (protonmotive force; pmf) for ATP formation. The reaction catalyzed by PSII is shown in Equation 1.1.2:

$$2H_2O + 2PQ + 4H^+_{stroma} \longrightarrow O_2 + 2PQH_2 + 4H^+_{lumen} \tag{1.1.2}$$

The reaction involves the reduction of plastoquinone (PQ) into plastoquinol (PQH_2) and the oxidation of water into molecular oxygen. The PSII reaction center is composed of two similar

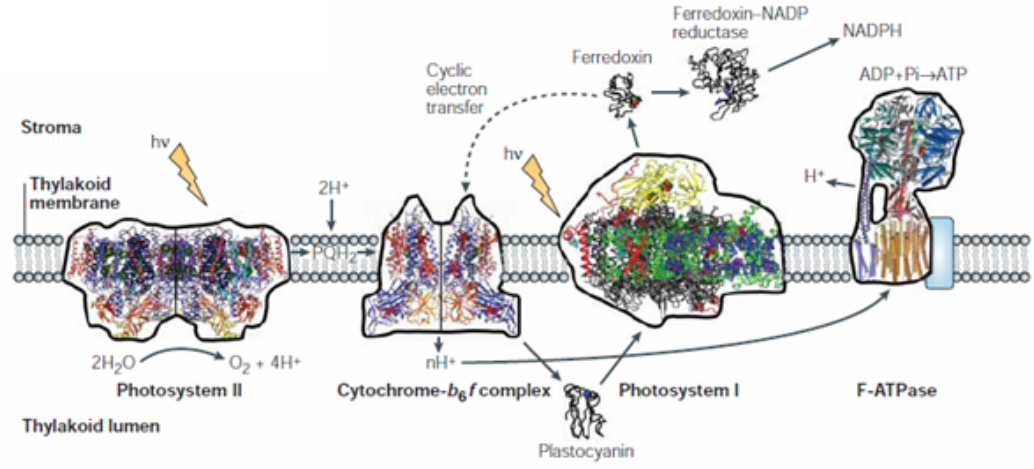

Figure 1.1 The structures of the four large membrane-protein complexes in thylakoid membranes that drive oxygenic photosynthesis taken from [Nelson and Ben-Shem, 2004].

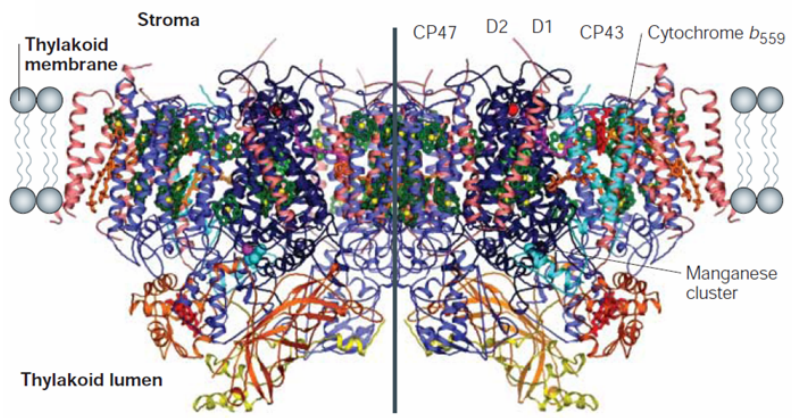

Figure 1.2 The structure of photosystem II from the cyanobacterium *Thermosynechococcus elongatus* [Ferreira et al., 2004].

proteins (D1 and D2). These proteins coordinate both the manganese cluster of PSII and all of the electron-transfer components involved in the main pathway of charge separation and stabilization (Figure 1.2). Following photoexcitation, a charge separation involving $P680^+$ and a reduced pheophytin occurs rapidly. To avoid recombination of the charges, a series of fast secondary electron transfer reactions is carried out. The main electron carriers in PSII include a bound PQ, Q_A, and a dissociable PQ, Q_B, after the pheophytin (Figure 1.3). The oxygen-evolving complex (OEC) *via* Tyr_Z reduces the $P680^+$ back to P680 and accumulates in this way the oxidizing equivalents necessary to oxidize water. The reduced Q_B then transfers electrons to the cyt b_6f. The widely used inhibitor 3-(3',4'-dichlorophenyl)-1,1-dimethylurea (DCMU) displaces Q_B from its PSII binding site.

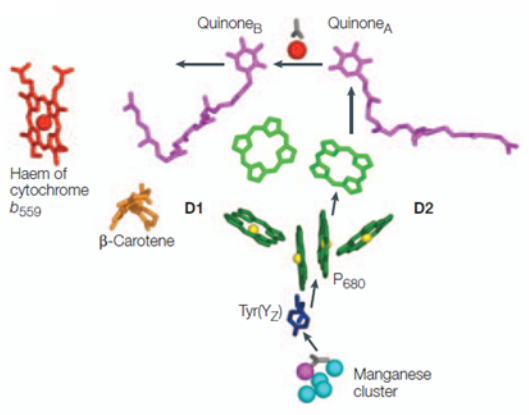

Figure 1.3 The cofactors of photosystem II published in [Ferreira et al., 2004].

The cyt b_6f complex (Figure 1.4a) is also called "plastoquinol-plastocyanin oxidoreductase". The complex operates following the "Q-cycle" [Mitchell, 1976, Trumpower, 1990] and is similar in structure and function to the cytochrome bc_1 complex from the respiratory ET chain. It exhibits two PQ binding sites, the Q_o site close to haem b_L binds quinol (lumenal side) and the Q_i site close to haem b_H binds quinone (stromal side). The PQH_2 looses a first electron, which is transferred to the Rieske iron-sulfur protein, the cyt f and finally to plastocyanin. The second electron from PQH_2 is transferred *via* two cyt b to the Q_i site where another PQ is reduced (Figure 1.4b). The quinone analogue 2,5-dibromo-3-methyl-6-isopropylbenzoquinone (DBMIB) acts as an inhibitor of cyt b_6f as it is thought to bind at the Q_o site. The presence of a further haem group that is covalently bound to cytochrome b_6 is puzzling [Kurisu et al., 2003, Stroebel et al., 2003]. Overall, two protons will be translocated across the thylakoid membrane for one electron that is passed to PSI *via* plastocyanin.

Plastocyanin (Pc), a single copper containing protein, transfers its electron to PSI (Figure 1.5a). Controlled by the Cu availability in the growth media, cytochrome c_6 can replace Pc in its function in many algae and cyanobacteria. The bulk of the reaction center of PSI is built of two,

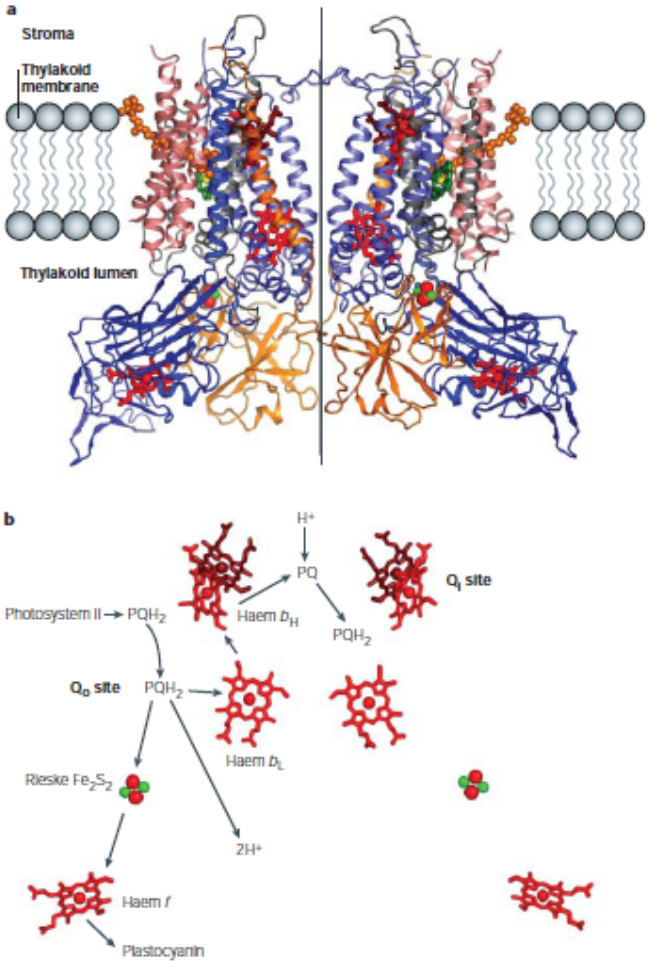

Figure 1.4 The structure of cytochrome-b_6f complex (a) and its cofactors (b) from the alga *Chlamydomonas reinhardtii* [Stroebel et al., 2003].

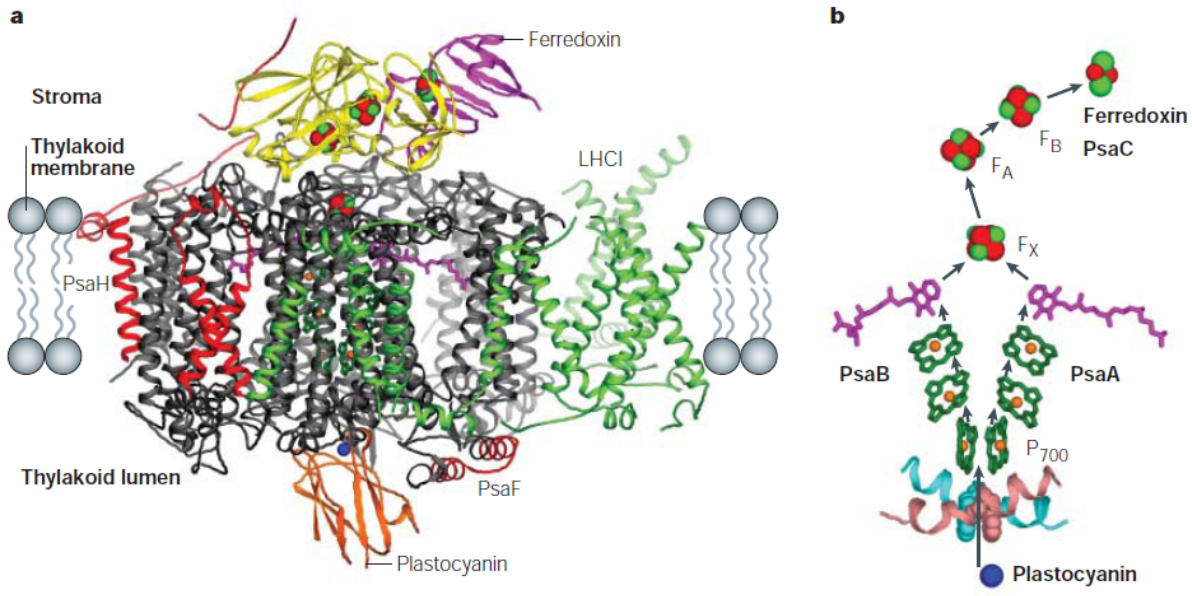

Figure 1.5 The model of a super-complex containing photosystem I, plastocyanin and ferredoxin (a) and their cofactors (b) from a higher plant (*Pisum sativum* var. *alaska*) [Ben-Shem et al., 2003].

homologous, large subunits (PsaA and PsaB) that harbor most of the PSI pigments and all of the cofactors up to F_X. Photoexcitation gives rapidly (ps time range) $P700^+$ and A_1^-. An electron from Pc (or cyt c_6) regenerates the special pair P700. The electron on the phylloquinone A_1 is passed through the F_X and F_A/F_B iron sulfur centers (Figure 1.5b). The electrons at the acceptor side of PSI are transferred to the soluble ferredoxin (Fd) and finally lead to $NADP^+$ reduction. This reaction is catalyzed by the enzyme ferredoxin-$NADP^+$ oxidoreductase (FNR) which is the subject of this thesis and will be described in section 1.3.3. N,N-dimethyl-4,4'-bipyridinium dichloride (methylviologen; MV) is an efficient electron acceptor, from (F_A,F_B) and Fd. Reduced MV reacts very rapidly with O_2 (contrary to (F_A,F_B) and Fd which react much more slowly).

A total of six protons are translocated, for 2 PSII charge separations and cyt b_6f ET, to the lumen that lead to an electrochemical-potential gradient (proton motive force; pmf) across the thylakoid membrane. The pmf will be used in the fourth complex, the ATPase, in order to synthesize ATP. During this process, protons flow from the lumen to the stroma through the integral membrane part of the ATPase CF_0 and ATP is generated at the level of the soluble part CF_1 (Figure 1.6).

Most of the details shown so far concern the photosynthetic electron transfer in higher plants and algae [Nelson and Ben-Shem, 2004]. All the complexes cited above are identical in cyanobacteria. Photosynthetic and respiratory electron transfers are carried out in the same compartment in cyanobacteria. This phenomenon is also present in chloroplasts and is called chlororespiration [Bennoun, 1982, Rumeau et al., 2007].

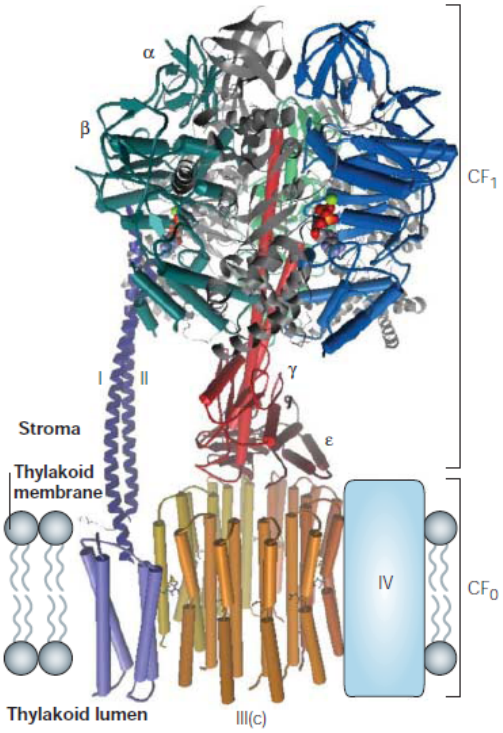

Figure 1.6 A composite model for the structure of the chloroplast F-ATPase. This model was created by W. Frasch using available structural data for mitochondrial F-ATPase subcomplexes [Abrahams et al., 1994, Stock et al., 1999, Gibbons et al., 2000].

1.1.2 Respiration

Both photosynthesis and respiration use membrane protein complexes located in the thylakoid membrane (Figure 1.7). Several components such as PQ, the cyt b_6f complex and soluble electron transporters are common to both bioenergetic processes.

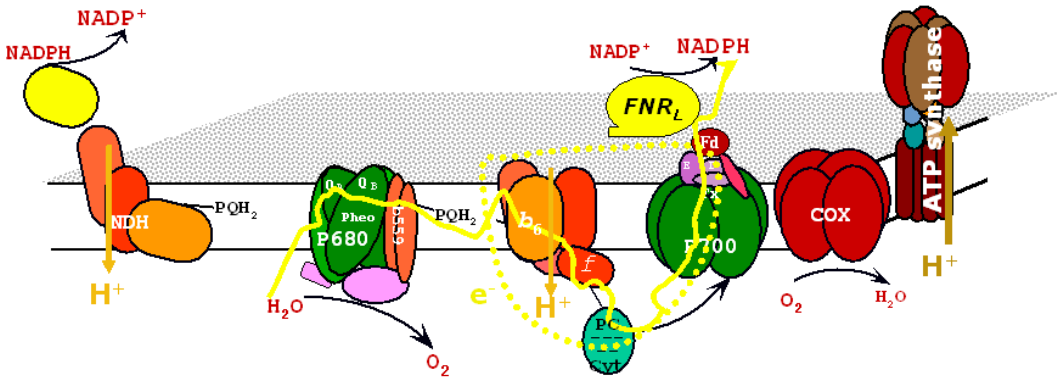

Figure 1.7 Scheme of the thylakoid membrane. The different electron translocating complexes are shown. Respiratory complexes involve the COX: cytochrome oxidase complex, NDH: NAD(P)H dehydrogenase (NDH-1) complex.

Succinate dehydrogenase (SDH) is the only enzyme of the tricarboxylic acid pathway which is found attached to the membrane. This complex functions in the respiratory ET as complex II. Evidence was found for the implication of SDH in the PQ pool reduction in *Synechocystis* [Cooley et al., 2000].

In the thylakoids of both cyanobacteria and plastids, distinct NAD(P)H dehydrogenases are found that oxidize NAD(P)H (NDH-1) and are equivalent to complex I involved in respiration. In cyanobacteria, the NDH-1 is extensively studied and is involved in a variety of functions like respiration, cyclic electron flow (introduced later) around PSI and CO_2 uptake [Battchikova and Aro, 2007].

In addition to that, three respiratory terminal oxidases (RTOs, complex IV) exist in *Synechocystis*: cytochrome c oxidase (CCox), quinol oxidase (Cyd), and alternative RTO (ARTO) [Pils and Schmetterer, 2001, Hart et al., 2005]. ET through the respiratory complexes lead to a proton gradient, hence to ATP formation, at the expense of reductants (NADPH and succinate).

1.1.3 Alternative electron sinks and cyclic electron transfer

Light-induced linear electron transfer between the two photosystems generate ATP and reducing equivalents in the form of NADPH. ATP and NADPH are used in a variety of metabolic processes. Under photoautotrophic growth conditions, CO_2 assimilation in the Calvin cycle constitutes the major electron sink for NADPH. However, stress conditions may lead to electron redirection

toward alternative electron sinks. Alternative electron sinks involve essentially the Mehler-reaction, cyclic electron transfer or respiration.

A substantial part of electrons can be transferred from PSI to molecular oxygen, which results in photoreduction of O_2 *via* superoxide anion to H_2O_2 in chloroplasts, *i.e.* the Mehler-reaction [Mehler, 1951, Asada, 1999]. The produced reactive oxygen species (ROS) are quickly detoxified by the combined action of superoxide dismutase and peroxidases. Thereby, the photoreduction of O_2 acts as an electron sink (pseudocyclic ET) under certain conditions, where up to 30% of the electrons from the light reactions can be directed to oxygen [Hackenberg et al., 2009]. For *Synechocystis* sp. PCC6803 (*Synechocystis*), it was shown that O_2 is reduced directly to water in one reaction mediated by A-type flavoproteins [Helman et al., 2003]. The genome of *Synechocystis* encodes four putative A-type flavoproteins, but only two of them, Flv1 and Flv3, are apparently involved in light-dependent O_2 reduction activity [Helman et al., 2003]. Recently, a role in the photoprotection of PSII has been shown for the two other *Synechocystis* flavoproteins, Flv2 and Flv4 [Zhang et al., 2009]. For pseudocyclic ET, which involves the Mehler-reaction or photorespiration, redox poising was proposed as a plausible function [Allen, 2003].

Under CO_2-limiting conditions, the Calvin cycle activity is strongly reduced and photorespiration, a Rubisco oxygenase reaction, increases. The so-called photorespiratory 2PG-metabolism helps to avoid depletion of Calvin-cycle intermediates. Due to the efficient inorganic carbon concentrating mechanism [Badger et al., 2006], it was assumed that cyanobacteria do not possess a photorespiratory 2PG-metabolism. In contrast to this earlier view, it was recently demonstrated that an active photorespiratory 2PG-metabolism involving three different pathways exists in *Synechocystis* [Eisenhut et al., 2008]. The complete loss of all three pathways leads to a high-CO_2-requiring-phenotype and highlights the essential function of photorespiratory 2PG-metabolism for cyanobacteria despite the carbon concentrating mechanism [Eisenhut et al., 2008]. The contribution of the Mehler-reaction may be controlled by inorganic carbon [Badger et al., 2000]. Transcription of one of the A-type flavoproteins, Flv3, essential for photoreduction of O_2 in cyanobacteria, is increased under high-light and low-CO_2 conditions [Eisenhut et al., 2007]. This may indicate an increase in pseudocyclic ET under low CO_2.

We will focus in the following especially on cyclic electron flow. This is an alternative electron flow that generates exclusively a proton gradient to build up ATP without accumulation of NADPH. It is assumed to involve PSI and the cyt b_6f (Figure 1.8). In addition to that, several partners are proposed to catalyze donation of electrons from the acceptor side of PSI (Fd, FNR, NADPH) back into the PQ pool.

The assimilation of CO_2 in the Calvin cycle requires ATP and NADPH in a 3:2 ratio [Allen, 2002]. The number of protons that are translocated through the membrane per ATP is function-specific [Stock et al., 1999, Seelert et al., 2000]. On one side, it was recently calculated in spinach

chloroplasts that the 3:2 ratio cannot be completely satisfied by linear electron transfer [Seelert et al., 2000]. On the other side, a new reconstitution method and a chemiosmotic model system were described to determine the H^+/ATP ratio of the ATP synthase from spinach chloroplasts and resulted in a value of exactly 3 ATP /2 NADPH [Turina et al., 2003]. Thus, the importance of cyclic electron transfer to participate in building up an additional proton gradient without accumulating NADPH is still not shown under non-stressed photoautotrophic growth. We should however keep in mind that NADPH and ATP are both used for a variety of metabolic processes (*e.g.* nitrogen, carbon and sulfur assimilation, transport).

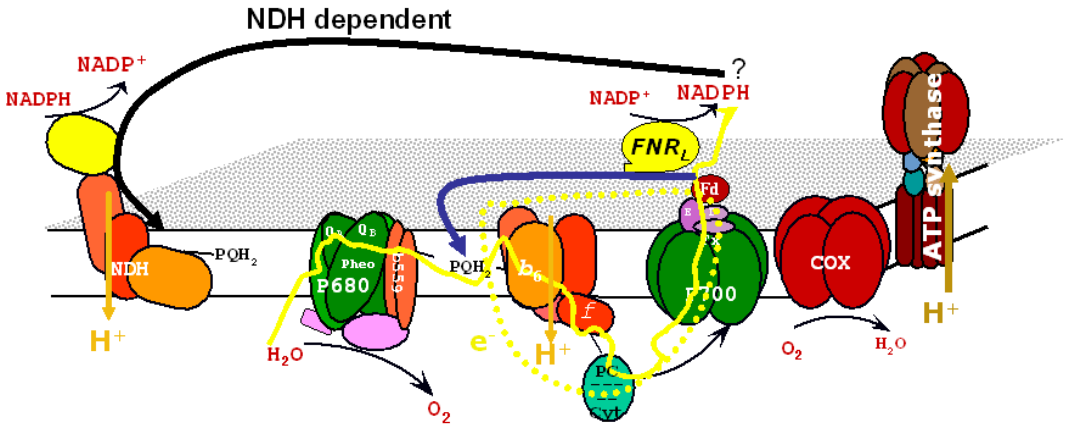

Figure 1.8 Scheme of the thylakoid membrane. The different electron and proton translocating complexes are shown. The two major pathways for cycling of electrons are indicated with a blue and a black arrow. They involve the respiratory NDH-1 complex (NDH dependent; from NADPH) and a non-identified Ferredoxin:Quinone reductase (FQR; from Ferredoxin).

Photophosphorylation requires a redox poise - a balance in its input and output of electrons. Hence, photosynthetic systems try to maintain a poised plastoquinone pool. Over-reduction of the plastoquinone pool is expected when the Calvin cycle is unable to use NADPH, and one reason for this is insufficient ATP [Allen, 2003]. It was suggested that linear ET alone would not be sufficient to generate the ATP required for CO_2 fixation and an obligatory role for cyclic ET was proposed [Golding et al., 2004]. Another role that has been postulated for cyclic ET in plants is to generate a trans-thylakoid pH gradient (ΔpH) [Heber and Walker, 1992]. The debate about the role of cyclic ET is fuelled by the difficulty of measuring it directly. Two approaches have been commonly used - $P700^+$ steady-state measurements and $P700^+$ relaxation following far-red illumination.

What is for sure is the fact that cyclic electron transfer is triggered under excess of NADPH - for example under high light or low CO_2 [Miyake et al., 2005]. High light leads to a fast accumulation of electrons on the acceptor side of PSI and the utilization of these reducing equivalents can be limited through the Calvin cycle. Under low CO_2 conditions, the Calvin cycle is limited by

substrate availability and NADPH accumulates. In addition to that, pseudocyclic ET involving the Mehler-reaction is triggered under low CO_2 [Hackenberg et al., 2009].

What is already known about the pathways of cyclic electron flow? According to Joliot [Joliot and Joliot, 2005], it is generally believed that the pathway starting from ferredoxin, the ferredoxin:quinone reductase (FQR) dependent pathway, constitutes the major pathway for cycling of electrons in plants (shown by the blue arrow in Figure 1.8). This pathway was originally found by inhibiting cyclic electron transfer using the cyt bc_1 specific inhibitor antimycin A and no biochemical evidence for the FQR pathway was obtained so far. However, Pgr5 and Pgrl1 ([DalCorso et al., 2008] and references therein) were found to participate in this cyclic electron transfer. In plants, there are two partially redundant pathways taken by electrons in PSI cyclic ET [Shikanai, 2007, Munekage et al., 2002, 2004, 2008].

In cyanobacteria, the FQR pathway is generally considered to be a minor pathway for cycling of electrons whereas the NDH dependent pathway (Figure 1.8 black arrow) is believed to constitute the major pathway.

In *Synechocystis*, a mutant called M55 was constructed, defective in *ndhB* which is the single gene coding for the subunit NdhB of the NDH-1 complex. Due to this mutant the various functions of NDH-1 complexes were discovered. M55 is characterized by impaired cyclic ET [Mi et al., 1992b, 1994, 1995], impaired respiration and presents an impaired CO_2 uptake [Ogawa, 1991]. Due to multiple copies of genes *ndhD* and *ndhF*, distinct NDH-1 complexes with distinct functions were identified [Ohkawa et al., 2000].

NDH-1 is expressed only in low levels under high CO_2 photoautotrophic growth. Two distinct NDH-1 complexes are implicated in the carbon concentrating mechanism (CCM) and the expression of one of these complexes is induced under low CO_2 [Battchikova and Aro, 2007].

In addition to the major pathways, several other pathways have been proposed. In chloroplasts, association of FNR to PSI and/or cyt b_6f has sometimes been taken as a structural evidence for different pathways of cyclic ET [DalCorso et al., 2008]. Supercomplex formation - e.g. PSI/cyt b_6f/Fd - has also been proposed to support cyclic ET [Joliot and Joliot, 2005] but there is no clear biochemical evidence yet for such supercomplexes in cyanobacteria (see [Peng et al., 2008] for chloroplasts). During our study we wanted to address the issue of FNR involvement in these different cycling routes.

1.1.4 Cyanobacteria

Cyanobacteria constitute a large and diverse group of photosynthetic prokaryotes. They inhabit almost any illuminated environment (freshwater, marine or terrestrial). All cyanobacteria are photoautotrophs and some species can grow as well photoheterotrophically.

All oxygen-evolving photosynthetic bacteria are cyanobacteria. Many species of cyanobacteria can fix nitrogen although the enzyme responsible for N_2 fixation (nitrogenase) is sensitive to O_2. All cyanobacteria contain chlorophylls and carotenoids as photosynthetic pigments. They generally use chlorophyll *a* and lack chlorophyll *b*.

Synechocystis sp. strain PCC6803

The unicellular, non-nitrogen-fixing cyanobacterium *Synechocystis* sp. strain PCC6803, hereafter referred to as *Synechocystis*, was the first photosynthetic organism and the second bacterium to have its genome fully sequenced [Kaneko et al., 1996]. The strain was originally isolated from a freshwater lake in California (Figure 1.9) [Zhang, 2006].

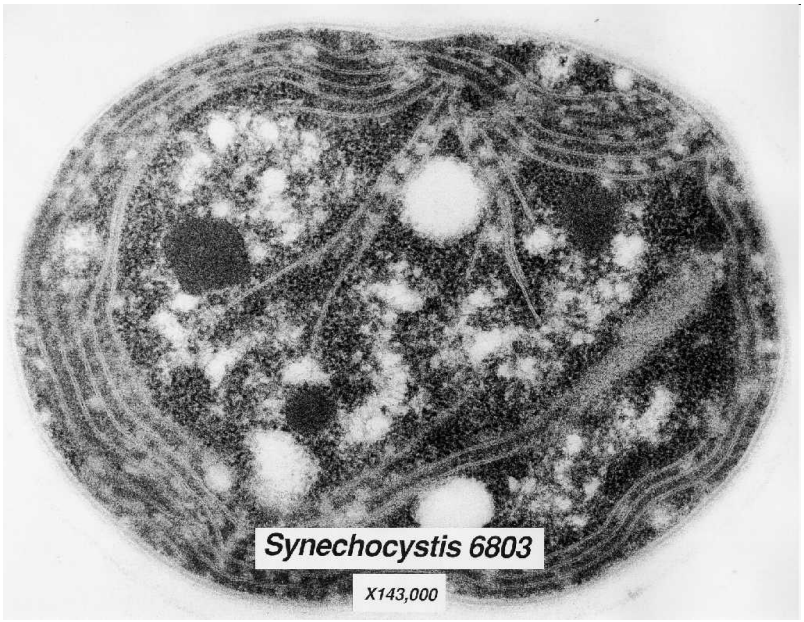

Figure 1.9 Electron micrograph of a thin section through a *Synechocystis* 6803 cell. Taken from www.nsf.gov/news/mmg/media/images/.

In addition to the cell envelope, these organisms have an internal system of thylakoid membranes (closely spaced membranes in Figure 1.9) where the electron transfer reactions of photosynthesis and respiration occur. The three-dimensional organization of the cytoplasm has been investigated using standard transmission electron microscopy and electron tomography. On one hand, it was shown that the thylakoid membranes are physically discontinuous from the plasma membrane [Liberton et al., 2006]. On the other hand, close connections between thylakoids and cytoplasmic membrane systems were observed [van de Meene et al., 2006]. Therefore, this debate is not closed yet.

We will now introduce the differences between cyanobacteria and chloroplasts that are important for the following study. We will start by a detailed description of the light-harvesting

complex - the phycobilisome - in cyanobacteria followed by an introduction on structure and function of FNR isoforms and the acceptor side of PSI in general.

1.2 Light-harvesting antenna

Prior to charge separation, a photon is absorbed by a pigment-protein (antenna) complex. The resulting excitation energy is transferred using radiationless steps to the chlorophylls involved in primary charge separation. These chlorophylls are generally associated to several hundred pigment molecules serving as light harvesting. This is necessary so that photosynthesis is less light-limited [Blankenship, 2002, Glazer, 1989].

Light-harvesting complexes can be divided into integral and external membrane complexes. Furthermore, they can be classified into seven families. These families include the core antenna complexes (*e.g.* CP47 and CP43 for PSII), the proteobacterial antenna complexes (*e.g.* LH1, LH2 and LH3 of purple bacteria), the eucaryotic LHC superfamily (*e.g.* LHC1 associated to PSI in algae and plants), the peridinin-Chl a protein (in Dinoflagellate algae), the chlorosome (in green sulfur bacteria and green filamentous bacteria) and the phycobilisome (in cyanobacteria and red algae) [Ughy, 2005]. The major difference between cyanobacteria/red-algae and green algae/brown algae/plants is the presence of a giant antenna complex, the phycobilisome (PBS; [Adir, 2005]).

1.2.1 Phycobilisome

The phycobilisome is an external membrane complex that is attached to the stromal side of the photosynthetic membrane and constitutes an accessory antenna. It allows species bearing these antennas to harvest light in the spectral gap (500-660 nm) between the major chlorophyll absorbing bands and thus to utilize the entire visible range of sunlight [Glazer, 1989, Adir, 2005].

In the following, we will further detail some advances in (ultra)structure determination and function of these large macromolecular protein complexes (7 to 15 Megadaltons).

Phycobilisome structure

Different types of PBS exist. We will focus on the hemidiscoidal PBS because they are present in *Synechocystis*. They are composed of a core subdomain and peripheral rods. The hemidiscoidal PBS are divided in three types (shown in Figure 1.10). They include bicylindrical, tricylindrical and pentacylindrical PBS (Figure 1.10; [MacColl, 1998]). In *Synechocystis*, the common tricylindrical hemidiscoidal PBS is present (Figure 1.10b). In addition to these classical PBS, minor PBS were identified in *Synechocystis* that do not contain core subunits [Kondo et al., 2005, 2007, 2009].

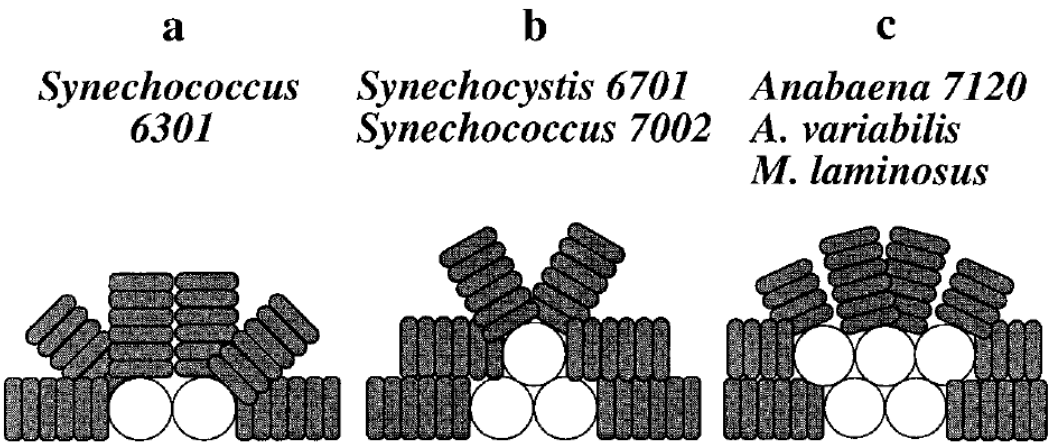

Figure 1.10 Schematic representation of the three types of hemidiscoidal PBS. a, bicylindrical; b, tricylindrical; c, pentacylindrical. Taken from [Ducret et al., 1998].

Phycobiliproteins The PBS is composed of phycobiliproteins (PBP) and mostly colorless linker polypeptides. Four major subgroups of PBP are found. They include the allophycocyanin of the core (AP, λ_A^{max}=652 nm), phycocyanin that is always present close (proximal) to the core in the rods (PC, λ_A^{max}=620 nm), phycoerythrin (PE, λ_A^{max}=560 nm) and phycoerythrocyanin (PEC, λ_A^{max}=575 nm) far away (distal) to the core in the rods when present. The PBPs are physically arranged to favor an energy gradient from PE (or PEC) through PC to AP and finally to the reaction center (λ=670-680 nm).

The smallest PBP unit are α and β ($\approx$ 17 and 18 kDa) subunits that form a heterodimer - the "($\alpha\beta$) monomer (protomer)". Each subunit contains one or more covalently attached bilins. Bilins are linear tetrapyrrole prosthetic groups. The covalent attachment of the bilins in the amino acid sequence is conserved, α84 in the α monomer, β84 and β155 in the β monomer. An α subunit of PC with the phycocyanobilin (PCB) covalently attached to a cysteinyl residue (ring A) is shown in Figure 1.11. In *Synechocystis*, only AP and PC are present in the core and rod subdomains, respectively. They are both composed of subunits that contain exclusively PCB.

Linker polypeptides In addition to the PBP, a variety of linker polypeptides are present. Except for the L_{CM}, these do not contain any chromophore. Different linkers are specifically responsible for each level of PBP assembly and function to stabilize the PBS and optimize its absorption and energy transfer characteristics. There exist linkers that anchor the core to the photosynthetic membrane (L_{CM}), linkers that connect the rods to the core (L_{RC}) and linkers that are only present in the core and the rods: L_C and L_R, respectively. *CpcC2*, *cpcC1* and *cpcD* encode the rod linkers L_R^{30}, L_R^{33} and L_R^{10} (Figure 1.13). Two independent genes (*cpcG1* and *cpcG2*) encode the rod-core linker (L_{RC}) [Ughy and Ajlani, 2004].

The core-membrane linker L_{CM} is a high molecular weight polypeptide. This major linker is

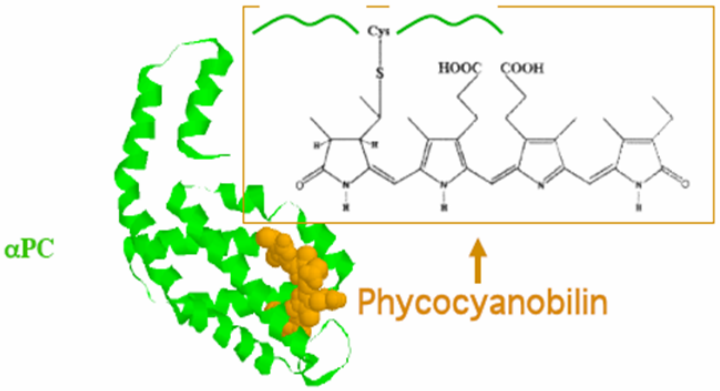

Figure 1.11 α subunit of phycocyanin (PC) with its chromophore phycocyanobilin (PCB).

responsible for the assembly of AP discs into cylinders and core formation. L_{CM} also plays a key role in anchoring the PBS to the photosynthetic membrane and in tuning the properties of the bound pigment cofactors such that absorbed light is funnelled towards the photosystems. Two copies of this multifunctional polypeptide (mass 75-125 kDa) are present per PBS core [Capuano et al., 1991, Arteni et al., 2009].

Phycobilisome Assembly PBS substructures are built up from stacked PBP discs made either of trimers (AP) or of hexamers (PC) of PBP subunits. X-ray crystallography was used to determine the structure of PBP discs. The crystal structure of allophycocyanin showed two loosely stacked trimers [Liu et al., 1999]. C-phycocyanin is a hexameric disc of 110Å diameter and 60Å thickness (Figure 1.12 and [Nield et al., 2003]). In many structures of PC, the two $(\alpha\beta)_3$ trimers that form a hexameric disk $(\alpha\beta)_6$ were positioned face to face. The hexamer is easily disassembled in $(\alpha\beta)$ monomer in diluted solutions, indicating that just a limited number of salt-bridges and/or hydrogen bonds are involved in monomer stability. Except in one case [Reuter et al., 1999], the available structures do not contain any linker.

Each of the cylinders in the tri-cylindrical core is composed of four trimeric AP discs. These discs have slightly different compositions. They involve simple AP trimers, L_C-containing AP trimers, trimers containing an alternative AP-B α subunit and trimers that possess a red-shifted β isoform and an α subunit provided by the L_{CM}. As indicated above, L_{CM} together with the L_C assemble the AP discs into cylinders and into a core substructure.

The rod-core linkage position is always occupied by a PC hexamer that is attached due to

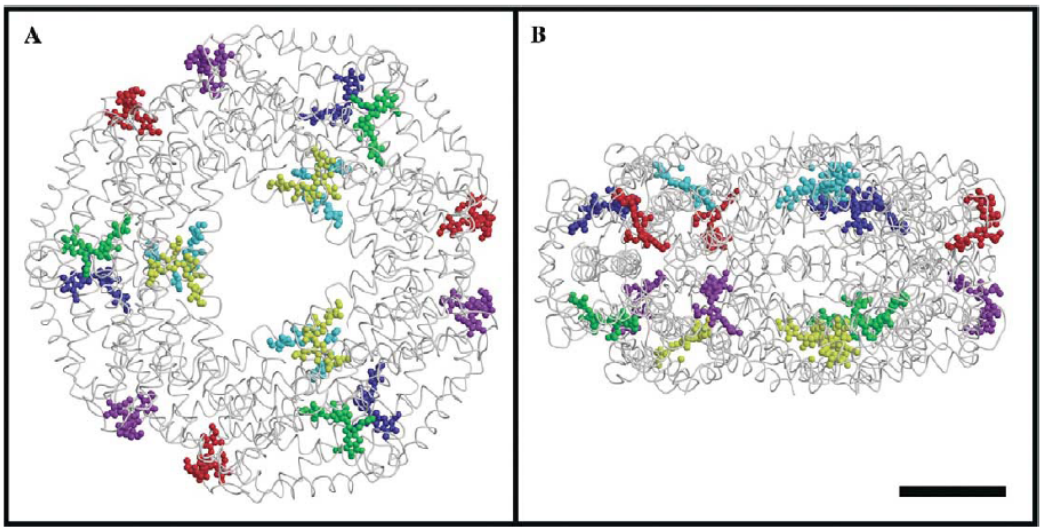

Figure 1.12 *S. elongatus* C-PC hexameric cluster. The 3 chromophores of each αβ heterodimer are depicted in the same color. Three αβ heterodimers form a disk around the three-fold axis. Bar represents 25 Å. A, projection parallel to the three-fold axis; B, projection normal to the three-fold axis. Taken from [Nield et al., 2003].

L_{RC}. For each disc at a particular rod location there exists a specific linker. Six rods radiate in a hemidiscoidal array from the core. In *Synechocystis*, rods are composed of three stacked PC hexamers. The position of the rod linkers L_R^{10}, L_R^{30}, L_R^{33} and L_{RC} in the PC hexamers is indicated in Figure 1.13.

Although many isolated components of different PBSs were crystallized, the structure of the entire PBS and its association to PSII is only studied by electron microscopy [Arteni et al., 2009].

Phycobilisome function

Attached primarily to reaction centers of PSII, the PBS can functionally link more than 600 energy-absorbing pigments to a single PSII dimer in addition to the PSII integral antenna subunits CP43 and CP47. On one side, direct measurements of fluorescence recovery after photobleaching [Mullineaux, 2004] indicated that the 10 Megadalton PBS is quite mobile *in vivo*, much more than the photosystems. On the other side, ultrastructures of the *Synechocystis* photosynthetic membranes indicated that the width of the stromal space between two membranes matches the PBS height (see Figure 1.9). Therefore, it seems difficult to imagine highly mobile PBS between the closely spaced thylakoids.

In addition to light absorption, the PBS can function as a source of nutrients under starvation conditions. There exists a mechanism of ordered PBS disassembly that requires the presence of a number of gene products. Keeping in mind that the PBS can account for up to 30 % of the total protein mass in a cyanobacterial cell, it constitutes a significant reservoir.

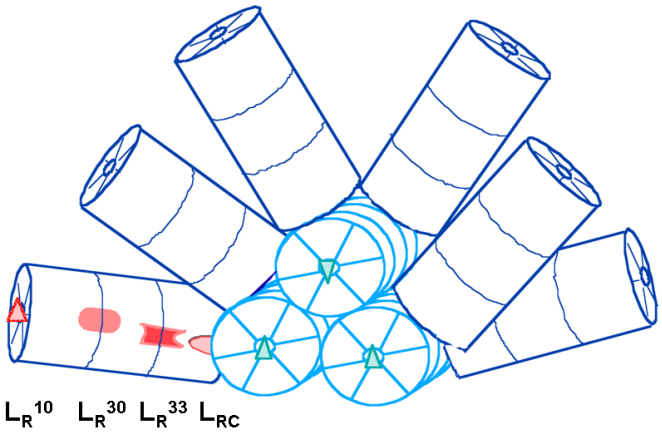

Figure 1.13 Representation of a hemi-discoidal PBS, as seen from the side. Kindly provided by Dr. Ajlani.

Energy transfer within the PBS The absorbed light energy harvested at the periphery of the PBS is transferred to the PSII reaction center complex by radiationless excitation energy transfer with an efficiency of > 95%. This implies that the energy-transfer mechanism must proceed rapidly in order to avoid energy losses by competing radiative or non-radiative decay processes. Light energy is absorbed mainly by the peripheral rods, where the shortest wavelength absorbing PBP (PE or PEC) are located. The excitation energy is then transferred by a radiationless resonance energy transfer to C-PC and then to AP. Energy is finally transmitted to PSII and partially to PSI reaction centers through the terminal emitters of the PBS (Figure 1.14) [Sidler, 1994].

The spectroscopic properties of the bilins are modified by the protein in two ways which are critical for their role in light absorption and energy transfer:

1. the bilins in all PBP are held rigidly in extended conformations,
2. the excited state lifetime of the pigment in the protein is long (*vs.* the isolated pigment).

The extended conformations allows the strong absorption in the visible part of the light spectrum. The long excited-state lifetime avoids the loss of excitation energy by radiationless de-excitation pathways. The absorption and transfer of light energy is performed by chromophores that are called donors. Acceptors can both absorb excitation energy and fluoresce. Thus, the steady state fluorescence emission originates almost exclusively from the acceptors.

In C-PC, the bilins at α84 and β155 are donors and the bilin at β84 is the acceptor. PCB β84 extends into the center of the trimeric disc, whereas those at α84 and β155 lie toward the

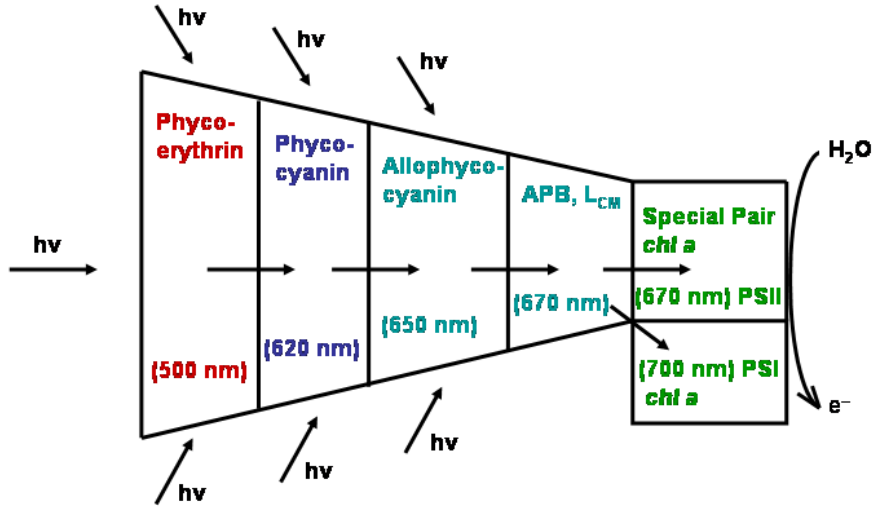

Figure 1.14 Energy flow in PBS of cyanobacteria and red algae. Radiationless excitation energy transfer from short-wavelength (PE) to long-wavelength-absorbing pigment-protein complexes (AP). Energy is finally transferred to and distributed between PSII and PSI. Adapted from [Sidler, 1994].

periphery. In the face-to-face arrangement of double discs in the rods, the consecutive discs are arranged to favor rapid energy transfer. Picosecond energy transfer measurements showed that the excitation energy absorbed by any bilin at the periphery is rapidly localized on the centrally located acceptor bilins (yellow and light blue chromophores in Figure 1.12A) [Glazer, 1989].

Directional energy transfer is promoted through the PBS. Between the PC discs, interaction with different linker polypeptides confer distinctive spectroscopic properties to the acceptor bilins. The absorption and emission spectra of the $(\alpha^{PC}\beta^{PC})_6L_{RC}$ complex are shifted towards the red relative to those of $(\alpha^{PC}\beta^{PC})_6L_R^{33}$. In consequence, the favored direction of transfer is from the distal disc to the PC disc proximal to the core.

In summary, the energy absorbed by any of the bilins in the PBS localizes rapidly (< 8 ps) on the four terminal acceptor bilins (APB and L_{CM}) in the core. The emission of these bilins overlaps precisely the absorption spectrum of the reaction center of PSII. The light-guide function of the PBS is completed when energy is transferred radiationless from the terminal acceptors in the PBS to the reaction center [Glazer, 1989].

1.2.2 Phycobilisome rod mutants

PBS mutants were constructed in three rod-linker-coding genes located in the *cpc* operon of *Synechocystis* [Ughy and Ajlani, 2004]. *CpcC1* and *cpcC2* encode L_R^{33} and L_R^{30}, respectively. L_R^{33} and L_R^{30} are linker polypeptides that attach the middle and the distal PC hexamer of the rods (Figure 1.13). During *in vitro* studies, we used a mutant called CB in which *cpcC1* and *cpcC2* were deleted. The PBS contained only one PC hexamer per rod (Figure 1.15) [Ughy and Ajlani, 2004].

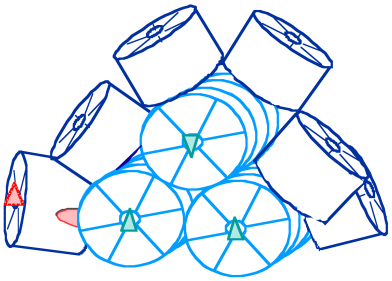

Figure 1.15 Representation of the PBS in the CB mutant. WT PBS contains 3 hexamers of PC per rod, whereas CB contains only 1 hexamer of PC per rod. Kindly provided by Dr. Ajlani.

1.3 Photosystem I and its electron acceptors

We were interested in the acceptor side of PSI. Electrons following the linear electron transfer are designated to reduce $NADP^+$, building up the reducing power NADPH. We will now further introduce PSI, Fd and FNR.

1.3.1 Photosystem I

The three-dimensional structure of cyanobacterial PSI was solved by Jordan et al. in [2001]. It provided atomic details of the 12 subunits and 127 cofactors comprising 96 chlorophylls, two phylloquinones, three [4Fe-4S] clusters, carotenoids and lipids. The cofactors involved in ET are located within the membrane subunits PsaA/PsaB and the stromal subunit PsaC (Figure 1.16). It can be seen that the chlorophyll pairs are arranged in two branches labelled A and B. There has been some controversy about whether the two branches work [Brettel and Leibl, 2001] and this issue is now settled in favor of the theory that the two branches work. The first of the three [4Fe-4S] cluster F_X is located in the middle between PsaA and PsaB. The following two [4Fe-4S] F_A and F_B are provided by the stromal subunit PsaC. We will now further introduce the ET kinetics inside PSI.

Electron transfer in PSI was reviewed [2001] by Brettel and Leibl. Standard free energy levels and kinetics of charge separation are shown in Figure 1.17. Charge recombination between $P700^+$

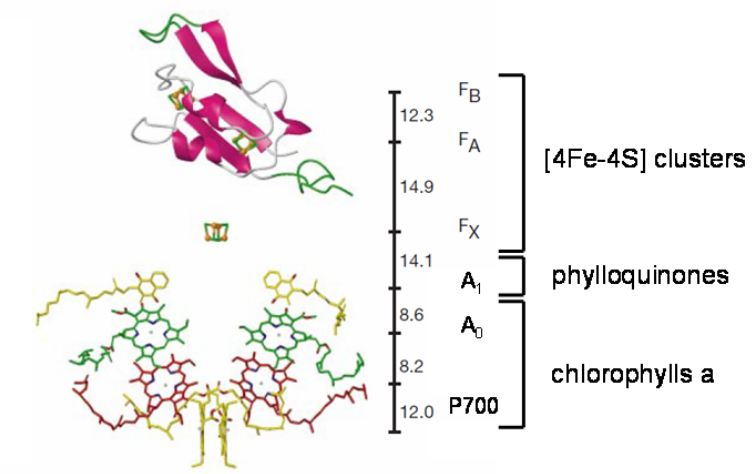

Figure 1.16 Cofactors of the electron transfer chain (ETC) and of PsaC. View parallel to the membrane plane. The pairs of chlorophylls of the ETC are arranged in two branches A and B. The chlorophylls a (P700 and A_0), the phylloquinones (A_1) and the [4Fe-4S] clusters (F_X, F_A and F_B according) are labelled to their spectroscopic terms. The center-to-center distances between the cofactors (black lines) are given in Å. Adapted from [Jordan et al., 2001].

and the reduced form of any one of the electron acceptors can be observed when forward electron transfer to the subsequent acceptor is blocked. In addition to that, reduction midpoint potentials are indicated on the right in Figure 1.17. The reduction midpoint potentials are very similar for F_A and F_B and it is generally thought that F_A and F_B undergo fast (< 1 μs) redox equilibrium [Setif, 2001]. They are both higher than the midpoint electron potential for F_X/F_X^-. We will be furthermore interested in the stromal subunits of PSI as they provide the docking site for Fd binding.

The three stromal subunits of PSI are shown in Figure 1.18. In addition to providing the two terminal electron acceptors of PSI, they provide the docking side for Fd that is shown as a dashed ellipse in Figure 1.18. This complex formation is important for efficient electron transfer. We will now further introduce Fd structure and function in plants and cyanobacteria.

1.3.2 Ferredoxin

Ferredoxin (Fd) is a soluble, low molecular weight protein (*ca.* 11 kDa) that mediates transfer of one electron from a donor to an acceptor. The redox active center is a [2Fe-2S] cluster with a highly negative redox potential (-350 to -450 mV), making reduced Fd a powerful reductant. The [2Fe-2S] cluster is ligated by four highly conserved Cys residues [Bottin and Lagoutte, 1992,

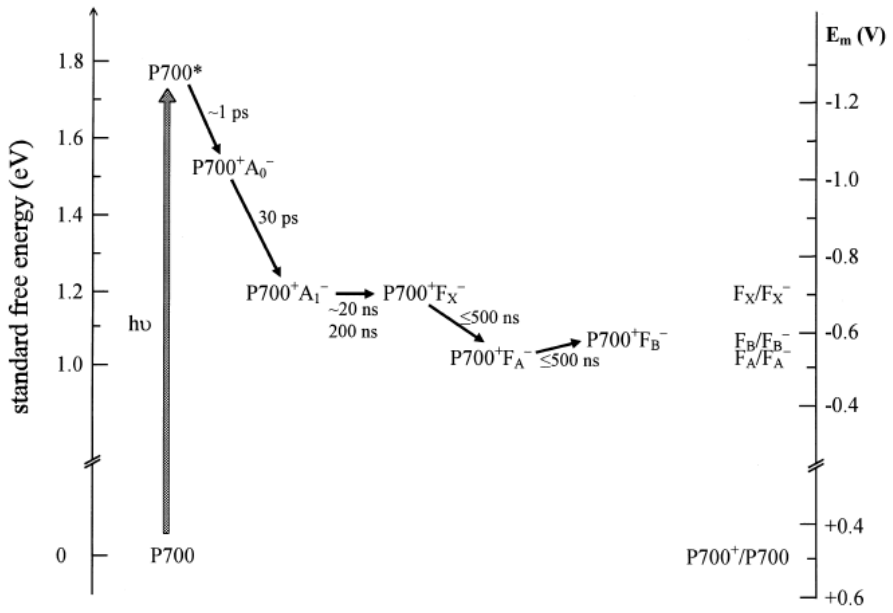

Figure 1.17 Approximate standard free energy levels and kinetics of charge separation in PSI. The standard free energy of the dark state (P700) was arbitrarily set to zero. Reduction midpoint potentials (versus NHE) obtained by redox titrations of intact PSI are indicated on the right-hand scale. Taken from Brettel and Leibl [2001].

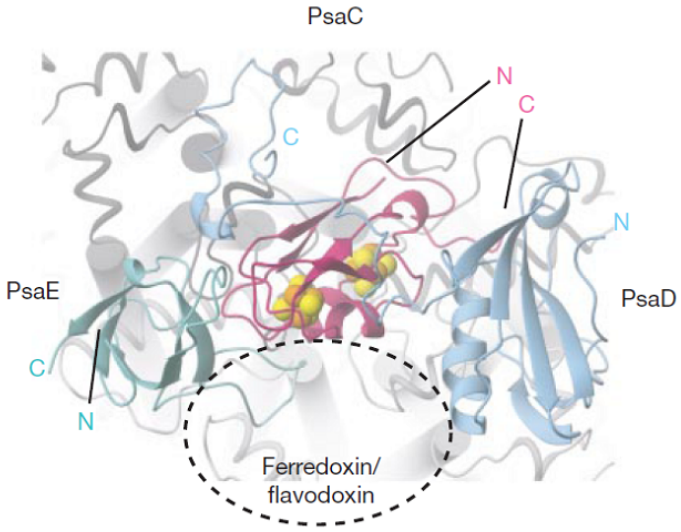

Figure 1.18 View along the membrane normal from the stromal side showing subunits PsaC, PsaD and PsaE. They cover some of the loop regions and helices of PsaA and PsaB (light grey). Dashed ellipse: putative docking site of ferredoxin, covering loops of PsaA. Taken from [Jordan et al., 2001].

Hanke et al., 2004b].

Fd is best known for its photosynthetic role by accepting electrons from PSI and donating them to the enzyme FNR for photoreduction of $NADP^+$. Donation of electrons by Fd has been demonstrated to many other enzymes essential for cellular processes including nitrogen assimilation (*e.g.* nitrite reductase), sulfur assimilation (sulfite reductase) and redox regulation (Fd:thioredoxin reductase) [Knaff, 1996]. In addition to PSI, Fd may be reduced by NADPH oxidation by FNR. Flavodoxin can substitute Fd under conditions of iron starvation in most cyanobacteria and some algae and may be efficient in reducing most or all of the soluble electron acceptors.

Fds are present as multiple isoforms in many plants and algae. We will further introduce the isoforms existing in plants and cyanobacteria.

Plant isoforms Higher plants contain distinct leaf and root Fd isoforms with conserved differences, reflecting the different electron donors to Fd in photosynthetic and non-photosynthetic tissues. Functional differences have been demonstrated between leaf and root Fds, with respect to redox potential and activity in assays of $NADP^+$ photoreduction and NADPH oxidation. These differences are highly conserved among species: Leaf Fds have a redox potential around 50 mV more negative than root Fds; during $NADP^+$ photoreduction, leaf FNR has an affinity around 10-fold higher for leaf Fds than for root Fds, and during NADPH oxidation root FNR has an affinity around five times higher for root Fds than for leaf Fds.

As the redox potential of leaf Fd is around -420 mV, a 50 mV difference may not appear dramatic, but the flux through photosynthesis is so vast that small changes in efficiency are likely to have a profound physiological impact. It was stated that the concentration of Fd in the chloroplast is of the same order as the concentration of Fd-dependent enzymes, which could therefore be in competition, giving great physiological significance to even small differences in affinity and activity [Gou et al., 2006].

Cyanobacteria isoforms Analogously to plants, cyanobacteria also possess several molecular forms of [2Fe-2S] Fd encoded by distinct genes. The most abundant protein form has been termed Fd1 (Fed1). The *fed1* gene (*ssl0020* in *Synechocystis*) was found to be strongly expressed as a light-induced transcript. The other *fed*-like genes appeared to be silent or moderately expressed. *fed1* was found to be critical to *Synechocystis* viability in spite of fed-like genes *slr0150*, *sll1382* or flavodoxin induction, even after the addition of glucose that compensates for the loss of photosynthesis [Poncelet et al., 1998]. We used during our studies only the major Fd isoform assuming that it is involved in all the metabolic pathways under our conditions. This is in

contrast to the plant isoforms, where tissue specificity ensures the function of distinct isoforms in distinct metabolic pathways.

Kinetics of ferredoxin reduction After PSI photoexcitation, several fast kinetic components (submicrosecond and microsecond) for Fd reduction have been identified *in vitro*. The rates of the fast kinetic components did not depend on the concentration of the partners. In addition to that, a slow kinetic component was also identified characterized by a rate that depends linearly on the Fd concentration. The fast and slow kinetic components are thus called first-order and second-order phases, respectively. The first-order phases are thought to correspond to ET processes which occur within PSI/Fd complexes. The second-order phase corresponds to a diffusion-limited ET which is observable in the fraction of PSI which does not bind Fd before flash excitation [Setif, 2001].

At least two or three first-order components were necessary to describe the first-order kinetics of Fd reduction. The spectra of the three phases obtained in *Synechocystis* were shown to be consistent with Fd reduction from $(F_A,F_B)^-$. At least 80% of Fd is reduced within the PSI/Fd complex at pH 8 in *Synechocystis*. The two slower first-order processes might result from some rate limitation either in ET from F_B to Fd or during intramolecular PSI ET. The distal cluster F_B is photoreduced in the submicrosecond time range in PSI. Heterogeneity of ET kinetics is an intrinsic property of Fd reduction, and was ascribed to different conformations of the PSI/Fd complex.

Fd reduction should compete efficiently with the recombination reaction between $P700^+$ and $(F_A,F_B)^-$ and this would imply a $t_{1/2}$ of several orders of magnitude faster than the recombination (30-100 ms). Furthermore, a high efficiency of Fd may be required for avoiding reduction of oxygen from $(F_A,F_B)^-$ which is potentially harmful for PSI. It has been speculated that, *in vivo*, complex formation is useful, though not critical, for promoting efficient reduction of the soluble acceptors and avoiding reduction of oxygen by $(F_A,F_B)^-$ [Karplus and Faber, 2004].

Complex formation was found to occur as well between Fd and the enzyme FNR in plants and cyanobacteria [Hanke et al., 2004b]. As stated above, FNR receives two electrons from two Fds to finally reduce $NADP^+$ to NADPH during linear electron flow. We will now introduce the structure and function of FNR that catalyzes the last step of the building up of the NADPH.

1.3.3 Ferredoxin:NADP oxidoreductase

Structure of ferredoxin:NADP oxidoreductase

From their primary sequences, the different ferredoxin:NADP oxidoreductases (FNRs) can be grouped in three major branches. The plant-leaf chloroplast FNRs are on one branch, the widely

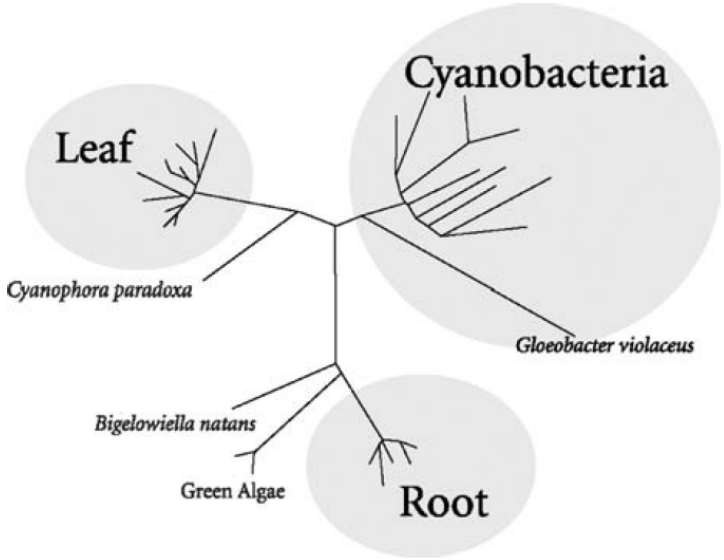

Figure 1.19 Relationships among various FNR amino-acid sequences. In the unrooted dendrogram shown, each branch represents 1 of 30 known plastid FNR sequences. The lengths of the branches are proportional to the level of sequence difference. Taken from [Karplus and Faber, 2004].

diverse cyanobacterial FNRs are on a second branch, and the root plastid enzymes together with the enzymes from green algae chloroplasts are on the third branch (Figure 1.19). All of the plastid type FNRs share sequence identities of over 40%. Crystallographic structures have been determined for six different FNRs: four leaf-type enzymes, one root-type enzyme and one cyanobacterial enzyme (*Anabaena variabilis*). These enzymes all have equivalent structures including two classical structural domains (Figure 1.20A). The amino-terminal residues (*ca.* 150) form the FAD-binding domain (blue in Figure 1.20A) and the carboxy-terminal residues (*ca.* 150) form the $NADP^+$ binding domain (pink in Figure 1.20A). The plant chloroplast enzymes are structurally similar and the root and cyanobacterial enzymes are structurally variable. One major difference in the corn root enzyme structure compared to leaf is that the amino terminus packs in a completely different position. Based on sequence comparisons, this amino-terminal packing appears to be conserved among root-type enzymes. With regard to amino-acid residue conservation, among the *ca.* 40 known FNR sequences, about 25% of the residues in the protein are conserved. It was stated that this high level of conservation over such long evolutionary distances implies a fairly stringent level of selection [Karplus and Faber, 2004].

FAD binding The FAD binding site in FNRs is quite highly conserved for the FMN half of the prosthetic group that contains the isoalloxazine (upper part in Figure 1.20A). In contrast, the adenosine portion of FAD (lower part in Figure 1.20A) shows significant variation in its position of binding. The isoalloxazine moiety is the best defined portion of the FAD and the adenosine

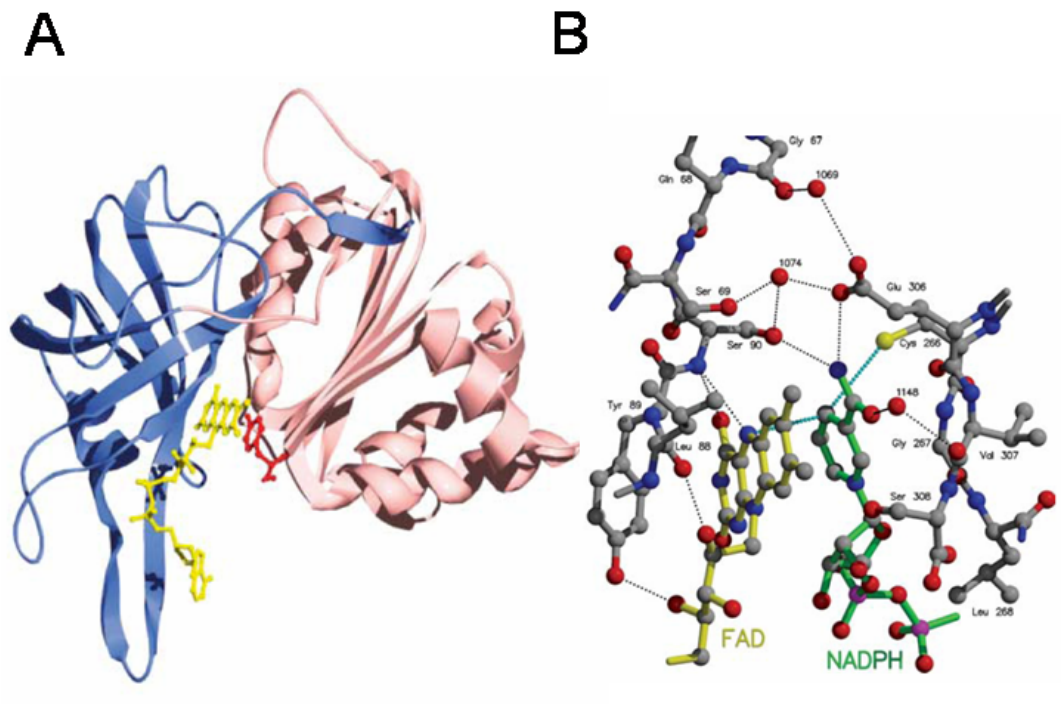

Figure 1.20 Ferredoxin:NADP oxidoreductase structure. A: The Cα polypeptide backbone of plant-type ferredoxin:NADP oxidoreductase. FNR is a two-domain flavoprotein. The computer graphic is based on X-ray diffraction data for the spinach enzyme, with the FAD binding domain shown in blue, the NADP(H) binding domain in pink, and the FAD prosthetic group in yellow. Taken from [Carrillo and Ceccarelli, 2003]. B: Geometry of the productive NADPH-FAD Michaelis charge transfer complex. A view is shown including all atoms surrounding the locus of hydride transfer, that is the nicotinamide C4- and the FAD N5-atoms. The model is that of the pea FNR Y308S-NADPH complex (pdb entry 1QFZ chain A). Taken from [Karplus and Faber, 2004].

portion is highly mobile.

NADP(H) binding The originally published structures showed that the C-terminal Tyr residue (shown in red in Figure 1.20A) was blocking nicotinamide access to the flavin. A technique of crystal soaking with $NADP^+$ had resulted only in clear density for the 2′-phospho-5′-AMP (PAMP) part of the dinucleotide. The 2′-phosphate itself has been proposed to be the primary recognition feature, with the adenine and 5′-phosphate being of secondary importance. Because of how NADP binds to FNR, we will introduce the NADP as two halves, the PAMP half and the nicotinamide-mononucleotide (NMN) half (in Figure 1.20B the NMN part is shown). From crystallographic studies, it was observed that only in a small fraction of the enzyme (15% pea FNR, [Piubelli et al., 2000]) and an even smaller fraction of cyanobacterial enzymes [Hermoso et al., 2002] the C-terminal Tyr swings out of the way so that the NMN half of NADP binds properly. A more complete understanding of nicotinamide binding was finally obtained using a mutant of pea FNR with the C-terminal Tyr converted to Ser [Deng et al., 1999, Piubelli et al., 2000]. A surprise compared to other NAD(P) dependent flavoenzymes was that the nicotinamide was not co-planar with the flavin, but made a 30° angle with it [Karplus and Faber, 2004].

Roles of active site residues were proposed by Deng et al. [1999] and involved the boat-like conformation of the nicotinamide ring to facilitate hydride transfer. In addition to that, the C-terminal Tyr does not play an active role in hydride transfer, but is primarily a placeholder for the nicotinamide that modulates the binding thermodynamics of NADP and protects the flavin from reaction with oxygen. It was also speculated that reduction of the flavin or Fd binding might promote the movement of Tyr, even if dynamics of Tyr movements may be sufficient to support catalysis [Karplus and Faber, 2004].

Ferredoxin binding Protein-protein interaction is an important determinant for electron transfer between Fd and FNR. The X-ray crystal structures of complexes formed between Fd and FNR from the cyanobacterium *Anabaena* 7120 [Morales et al., 2000], maize leaf [Kurisu et al., 2001] and maize root have been solved (see Figure 1.21 for the cyanobacterial Fd-FNR complex). In the complex structure of Fd and FNR, Fd binds to a concave region on the FAD-binding domain of FNR, bringing the [2Fe-2S] cluster into close proximity to that of FAD. Different orientations of Fd relative to FNR have been found in cyanobacteria, plant-leaf and plant-root complexes. The relative buried surface areas differ as well, the root complex having a decreased buried surface area [Hanke et al., 2004b].

The complex in general is largely electrostatic in nature. The pattern of interaction between Fd and FNR is composed of a core of hydrophobic interactions surrounding the prosthetic groups, stabilized by a series of interactions between charged side chains and through hydrogen bonds.

Hydrophobic effects originating from dehydration of water molecules in the protein-protein interface may also give a significant contribution. In *Anabaena*, a total of ten hydrogen-bonding and ionic-bridge interactions stabilize the complex [Morales et al., 2000]. The side chains involved in intermolecular charge interactions concern mainly acidic Fd residues and basic FNR residues [Hurley et al., 2002].

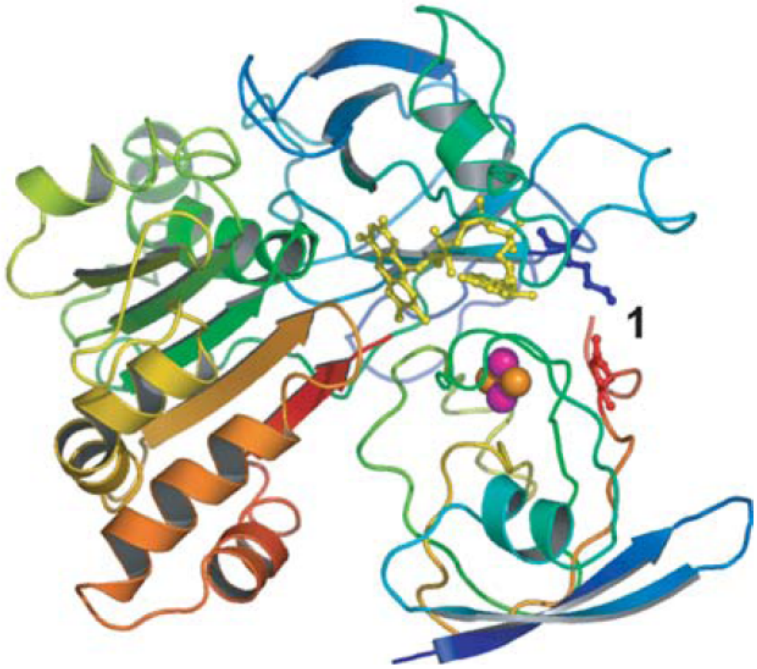

Figure 1.21 Ribbon drawing of Anabaena Fd : FNR complex (PDB code: 1EWY). One intermolecular salt bridge is shown as ball-and-stick model: 1, FNRLys75-FdGIu94. Taken from [Hanke et al., 2004b].

Redox potentials may change when binding occurs [Batie and Kamin, 1984b]. A negative redox shift in the potential of the [2Fe-2S] cluster of Fd was observed that would be advantageous to ET in the photosynthetic direction [Hanke et al., 2004b]. The more weakly binding complexes seem to yield more rapid ET and catalytic turnover. Thus, it could be that effective *in vivo* ET involves very short-lived (nearly collisional) complexes, rather than a tight, highly specific complex [Karplus and Faber, 2004].

FNR superfamily Given the early origin of photosynthesis, FNRs would be expected to be ancient proteins. Consistent with this, there exists a large and diverse family of oxidoreductases which have as a catalytic core the two-domain FNR-like module [Karplus et al., 1991]. They are diverse enough that some use FAD and others use FMN whereas some use NADP and others use NAD. Structurally known members of the family are sulfite reductase, NO synthase, NADPH: cytochrome P450 reductase, *etc.*.

Mechanism of ferredoxin:NADP oxidoreductase

Early studies [Shin and Arnon, 1965] showed that the physiological role of the chloroplast oxidoreductase was to catalyze the final step of photosynthetic electron transfer, namely, the electron transfer from the iron-sulfur protein Fd, reduced by PSI, to $NADP^+$ (Equation 1.3.1).

$$2Fd_{red}(Fe^{2+},Fe^{3+}) + NADP^+ + H^+ \rightleftharpoons 2Fd_{ox}(Fe^{3+},Fe^{3+}) + NADPH \quad (1.3.1)$$

Equation 1.3.1 shows the ability of FNR to exchange electrons between obligatory one- and two-electron carriers, which is a direct consequence of its prosthetic group. FAD and other flavins can exist in three different redox states: oxidized, one-electron reduced (semiquinone radical) and fully reduced (hydroquinone), containing 18, 19 and 20 electrons in a π orbital system, respectively. The isoalloxazine ring also provides lone electron pairs for protonation, which results in tautomers. FNR functions are not confined to photosynthesis. The backreaction of Equation 1.3.1 is actually more often found in nature in heterotrophic tissues such as plant roots, heterotrophic bacteria, animal and yeast mitochondria, *etc.*. Following the backreaction, NADPH is oxidized and reduced Fd is available for numerous metabolic pathways (detailed in paragraph on Fd).

As indicated above, FNR forms complexes with NADP(H). The enzyme actually displays a strong preference for NADP(H) and is a poor NAD(H) oxidoreductase. FNR was stated to be characterized by its plasticity as a catalyst [Ceccarelli et al., 2004] and is ubiquitous among living organisms. Steady-state and rapid kinetic measurements have resulted in a comprehensive model describing the various reactions of Equation 1.3.1 [Batie and Kamin, 1984a].

The overall reaction was interpreted as an ordered two-substrate process, with $NADP^+$ binding first (Reaction 1 in Figure 1.22). Under these assumptions, the kinetics were consistent with the formation of ternary complexes as intermediates of the catalytic mechanism (Reaction 2 and 5 in Figure 1.22). We will first introduce the individual steps of the $NADP^+$ reductase activity of FNR and discuss the NADPH oxidation later in detail.

NADP(H) binding (Reactions 1 and 9 in Figure 1.22) $NADP^+$ is probably the leading substrate during FNR turnover even if no chemistry is expected to occur between the oxidized nicotinamide and the oxidized flavin. For example, $NADP^+$ greatly accelerates the full reduction of FNR by reduced Fd [Batie and Kamin, 1984a]. Formation of the binary NADP:FNR complex was studied using differential spectroscopy. As indicated above, the C-terminal Tyr must be displaced to allow stacking of the nicotinamide ring onto the re-face of the isoalloxazine moiety. This

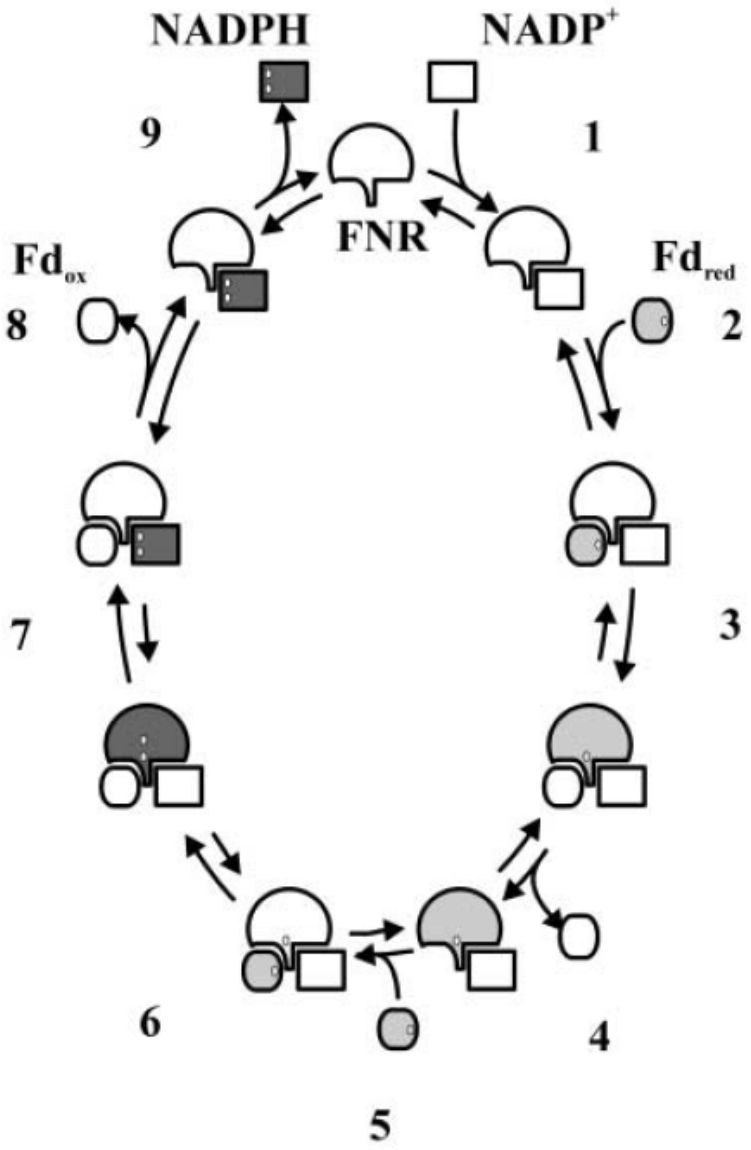

Figure 1.22 The electron transfer mechanism of ferredoxin-NADP(H) reductase. The various steps of the catalytic pathway were initially proposed by Batie and Kamin [1984a] on the basis of kinetic and binding experiments on the spinach FNR. Oxidized forms are white, one-electron reduced forms are light grey and two-electron reduced forms are dark grey. An error was found in the present scheme, between steps 5 and 6 the FNR should be in light grey as already one-electron reduced. Taken from [Carrillo and Ceccarelli, 2003].

thermodynamically unfavored process results in a decrease of the binding affinity for NADP(H) [Carrillo and Ceccarelli, 2003].

Binding of NADP(H) to FNR might thus be interpreted as a two-step binding of the nucleotide to a bipartite site. First, a strong interaction between the PAMP part and FNR is carried out and is followed by isomerization that favors NMN part stacking onto the isoalloxazine moiety to facilitate hydride transfer. The second step of NADP(H) binding is energetically costly and weakens the entire interaction to a remarkable extent [Carrillo and Ceccarelli, 2003]. Reaction 9 in Figure 1.22 also represents the initial event of the reverse reaction, the reduction of Fd due to NADPH oxidation.

ET from Fd_{red} to FNR (Reactions 2-4 in Figure 1.22) First electron reduction of FNR_{ox} by Fd_{red} to the radical semiquinone is too fast to be measured by rapid mixing techniques. The molecular association of FNR with its electron partners is steered by electrostatic interactions. This could explain the interchangeable accommodation of Fd and flavodoxin to FNR, that share very low sequence similarity. It was determined that the surface electrostatic potentials of Fd and flavodoxin overlap completely [Ullmann et al., 2000].

As shown in Figure 1.21, binary complexes of oxidized FNR and Fd have been resolved by X-ray crystallography for *Anabaena* and maize couples [Kurisu et al., 2001, Morales et al., 2000]. As indicated above, the FAD and [2Fe-2S] redox centers were sufficiently close for direct electron transfer and the relevance of complementary patches of basic and acidic residues in FNR and Fd was confirmed. It is believed that first a nonproductive complex is built up due to polar interactions. Then, several fine adjustments stabilized by hydrogen bonds, salt bridges, van der Waals interactions and hydrophobic packing forces originate from the dehydration of the protein-protein interface [Carrillo and Ceccarelli, 2003].

Differences between maize and cyanobacterial complexes were found that indicate different protein-protein interactions. Hurley et al. [2002] proposed that crucial parameters for Fd and flavodoxin binding might be proximity of the prosthetic groups in a nonpolar environment to facilitate direct electron transfer.

Building up of FNR_{red} (Reactions 5-7 in Figure 1.22) First electron reduction of FNR by Fd_{red} on one hand was too fast to be observed [Batie and Kamin, 1984a]. The second electron reduction on the other hand was too slow to be compatible with steady-state catalysis in the absence of $NADP^+$. This process actually involves various steps: dissociation of Fd_{ox} (Reaction 4 in Figure 1.22), binding of Fd_{red} (Reaction 5) and flavin reduction (Reaction 6). The reaction is inhibited by Fd_{ox} and stimulated by $NADP^+$, indicating that Reaction 4 is the rate-limiting step. In addition

to that, $NADP^+$ seems to facilitate Fd_{ox} release which allows the entire reaction to proceed at a rapid pace through Reactions 4 and 8 [Batie and Kamin, 1984a].

Furthermore, a ternary complex including Fd_{ox}, FNR_{ox} and NADPH is readily formed. A strong case of negative cooperativity for binding was observed, that decreases Fd binding in the presence of NADP(H) and *vice versa*. The reciprocal negative cooperativity is translated into positive cooperativity at the kinetic level [Batie and Kamin, 1984a, 1986]. These observations are compatible with the proposed mechanistic cycle shown in Figure 1.22.

$NADP^+$ reduction and product release (Reactions 8 and 9 in Figure 1.22) The sequence of Reactions 8 and 9 proposed in Figure 1.22 is one example. They involve $NADP^+$ reduction prior to Fd_{ox} dissociation and as the final step NADPH dissociation from the FNR_{ox}. Alternative pathways such as first Fd_{ox} dissociation before $NADP^+$ reduction might be envisaged. Again, it was Batie and Kamin [1984a] that provided evidence that $NADP^+$ reduction is faster than dissociation of Fd from FNR.

NADPH oxidation - the backward reaction Ferredoxin reduction is the most widely distributed function of FNR-type proteins. NADPH binding to oxidized FNR leads to rapid hydride exchange between the nucleotide and the oxidoreductase, resulting in a succession of charge-transfer complexes involving flavin and nicotinamide. The appearance of these species can be followed by long-wavelength absorbance signals.

In Figure 1.23 two different mechanisms for FNR catalysis are shown. The reaction mechanism in A corresponds to the mechanism discussed above during $NADP^+$ reduction. The reaction mechanism in B shows the same ordered mechanism for the NADPH oxidation (backward reaction of FNR). It was proposed that the NADPH oxidation involves the same mechanism as the $NADP^+$ reduction as all the reactions involved are in principle reversible. The reaction mechanism in C corresponds to a so-called ping-pong mechanism (two-step mechanism). No ternary complexes are involved in this reaction mechanism. First, NADPH passes two electrons on FNR, that are stored and $NADP^+$ dissociates from FNR before the first Fd_{red} is fixed. Two Fds receive two electrons and thereby reoxidize FNR (see Figure 1.23C).

To distinguish between these two mechanisms during NADPH oxidation, the velocity of the reactions are systematically plotted versus one of the two substrate concentrations in a double reciprocal plot. This plot is called a Lineweaver-Burk plot and consists in a graphical method to distinguish between mechanisms. Spinach Fd reduction was measured *in vitro* and resulted in parallel lines by increasing the inhibitor concentration, $NADP^+$. This indicates the mechanism in Figure 1.23C to operate, without formation of a ternary complex [Forti and Sturani, 1968].

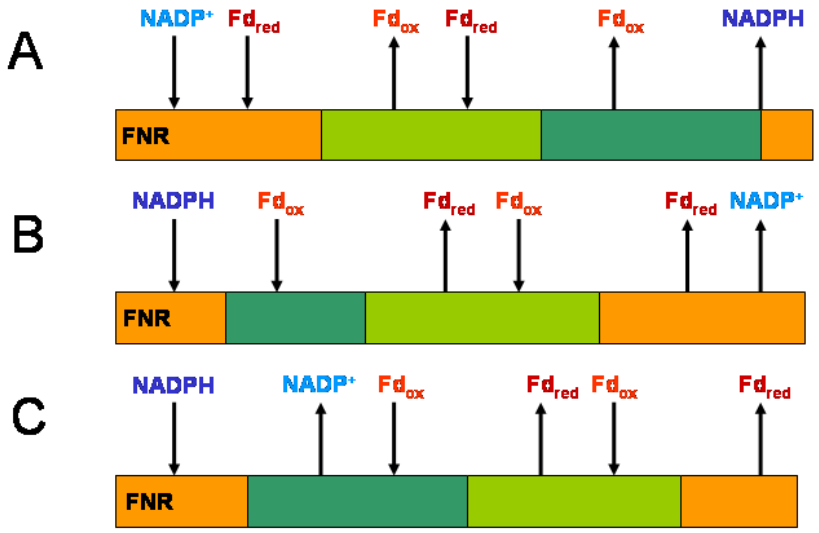

Figure 1.23 The electron transfer mechanisms of ferredoxin-NADP(H) reductase. **A**: $NADP^+$ reduction following the mechanism proposed by Batie and Kamin [1984a]. **B**: NADPH oxidation following the same reaction mechanism as $NADP^+$ reduction in reverse order. **C**: NADPH oxidation following a two-step mechanism. $NADP^+$ bright blue, NADPH dark blue, Fd_{ox} bright red, Fd_{red} dark red, FNR_{ox} orange, FNR_{sq} bright green, FNR_{red} dark green. Adapted from [Carrillo and Ceccarelli, 2003].

This was surprising, as distinct kinetic constraints must operate to justify different reaction mechanisms.

This could indeed be the case concerning Fd_{ox} release. This step may be rate-limiting during $NADP^+$ reduction. Ternary-complex formation prevents rate limitation *via* Fd_{ox} release during this reaction. It was proposed that this requirement could be relieved in the reverse reaction if Fd_{red} dissociates from FNR_{sq} and FNR_{ox} at rates compatible with steady-state catalysis [Carrillo and Ceccarelli, 2003].

Product inhibition studies could also be revealing to obtain informations concerning the kinetic mechanism of NADPH oxidation. Following an ordered pathway as determined for the $NADP^+$ reduction, a competitive inhibition by $NADP^+$ is expected during NADPH oxidation (product inhibition). If the mechanism on the other hand follows a two-step kinetic mechanism, $NADP^+$ inhibition is characterized by mixed-type inhibition (see Chapter 2).

Isoforms of ferredoxin:NADP oxidoreductase

We will first introduce the isoforms of FNR in plants and afterwards introduce similarities and differences to cyanobacterial FNRs.

Plant isoforms These isoforms are tissue-specific, *i.e.* leaf isoforms (photosynthetic; pFNR) are primarily required for the photoreduction of $NADP^+$, and root isoforms (heterotrophic; hFNR) generate reduced Fd following NADPH oxidation. Root FNR was observed in one early report on radish roots [Morigasaki et al., 1990]. In plant roots, genetically distinct, soluble, root-type FNRs were found and characterized *e.g.* from tomato [Green et al., 1991] and corn [Onda et al., 2000, Aliverti et al., 2001] roots. Similar to Fd isoforms, root FNRs were found to be shifted in the redox potential, being more adapted to provide physiological Fd_{red} in nonphotosynthetic tissues [Aliverti et al., 2001]. Best affinities were obtained between root Fd and root FNR and between leaf Fd and leaf FNR isoforms [Onda et al., 2000].

Interestingly, the redox potentials of these oxidoreductases as those of their corresponding Fds have been tuned by evolution to favor the physiological direction of electron transport. However, the four proteins can be readily exchanged *in vitro* when assayed in a variety of reactions, indicating that the major parameter driving $NADP^+$ or Fd reduction *in vivo* would be the substrate availability [Carrillo and Ceccarelli, 2003].

In addition to leaf-type and root-type FNR, different isoforms have been found in maize [Okutani et al., 2005] and wheat leaves [Gummadova et al., 2007]. They vary in localization and might be implicated in meeting changing metabolic capacity and reductant demands [Gummadova et al., 2007]. Concerning the localization, it is interesting to note that one isoenzyme

was exclusively soluble in maize, a second isoenzyme was found only attached to the thylakoid membrane and a third one had a dual location [Okutani et al., 2005].

Cyanobacterial isoforms The *petH* gene encoding FNR in the cyanobacterium *Synechococcus* sp. PCC 7002 was cloned and sequenced [Schluchter and Bryant, 1992]. An additional N-terminal domain was identified that was 78% similar to the phycocyanin associated linker protein CpcD. The resulting molecular mass was around 45 kDa for this FNR versus 35 kDa for the plant plastid FNR. Thus, the N-terminal extension of FNR serves to localize the protein on the rods of the antenna complex in cyanobacteria, the PBS [Schluchter and Bryant, 1992].

Although the binding to PBS is now established, a controversy still exists concerning the exact localization of FNR on the PBS. On one side, it was proposed that FNR attaches to the distal PC hexamer due to the highest similarity of its N-terminus to the distal rod linker L_R^{10} [Schluchter and Bryant, 1992, Gómez-Lojero et al., 2003]. On the other side, a localization close to the core on the proximal PC hexamer [Arteni et al., 2009] was proposed. It was also proposed that the N-terminal extension may help localizing the FNR directly to the thylakoid membrane, providing an anchor domain and the question was raised what may be the function of the attachment of FNR to the antenna complex [van Thor et al., 2000].

It was recently established, that a second FNR isoform is generated by an in-frame initiation of translation [Thomas et al., 2006] in *Synechocystis*. These two isoforms are encoded by a unique *petH* gene and differ in size - 34 kDa and 46 kDa - for the small and the large isoforms, respectively. The latter is the isoform identified by [Schluchter and Bryant, 1992]. The smaller isoform was previously identified as a proteolytic degradation product. However, the authors in [Thomas et al., 2006] identified the small isoform as a product of an internal ribosome entry site (IRES) within the *petH* open reading frame (ORF). We denote the small isoform as FNR_S and the large isoform as FNR_L.

As for plant-like FNR, FNR_S is composed of the two catalytic domains (green): the NADP and the FAD binding domains that are typical (Figure 1.24). In Figure 1.24, the N-terminal extension of FNR_L is shown in white and pink for the hinge- and the linker-like domain. The latter is responsible for the attachment of FNR_L to PBS.

The two isoforms are translated from distinct methionines (Met), Met1 and Met113 for FNR_L and FNR_S, respectively. Thomas et al. [2006] showed that the linker-like domain of FNR_L undergoes proteolysis in the absence of PC, just as PBS linkers are known to be highly sensitive to proteolysis when not attached to PBPs. They also showed that obligate photoautotrophic cyanobacteria expressed only FNR_L and FNR_S accumulated in *Synechocystis* and most probably in other facultatively heterotrophic cyanobacteria under conditions where heterotrophic metabolism was needed.

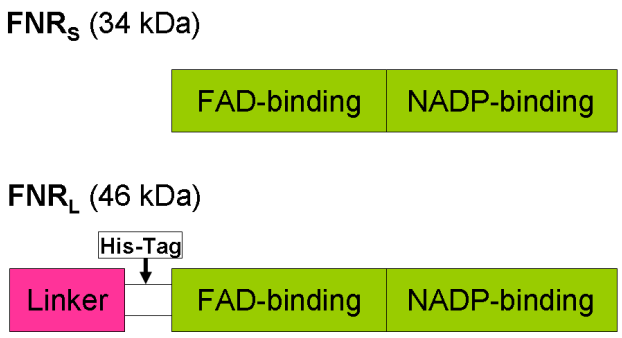

Figure 1.24 Representation of FNR_S and FNR_L primary structures highlighting their functional domains.

Therefore, Thomas et al. [2006] concluded that FNR_L probably sustains photoautotrophic growth ($NADP^+$ reduction) and FNR_S might be more adapted to provide electrons for heterotrophic growth (NADPH oxidation). Mutants were constructed in *Synechocystis* which translate either the small or the large FNR isoform only. These mutations are introduced in the next section.

Ferredoxin:NADP oxidoreductase mutants

In Figure 1.25A the representation of the FNR_L polypeptide with the linker, hinge (H), and enzymatic (FNR) domains is shown for the WT. As a consequence of the presence of the two methionines Met-1 and Met-113, in principle both isoforms can be expressed in the WT under different growth conditions. Under standard photoautotrophic conditions, the major isoform is FNR_L as indicated by the wider arrow in Figure 1.25A.

Missense and frame-shift mutations were introduced in *petH* to elucidate the function of the two isoforms in facultative heterotrophic cyanobacteria. The missense mutation in MI6 changed the Met113 into an isoleucine (see Figure 1.25B). Frame-shift mutations, created by a single base deletion or insertion, caused premature translation stops upstream and downstream of Met-113 in FS1 and FS2, respectively (see Figure 1.25C) [Thomas et al., 2006].

As shown in Figure 1.26, cell extracts from WT contained FNR_L as major isoform with only trace amounts of FNR_S. MI6 contained only FNR_L (Figure 1.26), consistent with FNR_S originating from an internal ribosome entry site (IRES) at Met-113. In cell extracts from FS1, FNR_S is present at the WT FNR_L level, whereas FNR_L is absent (Figure 1.26). It was shown in [Thomas et al., 2006], that FNR_S does not bind to the PBS due to the missing linker-like domain.

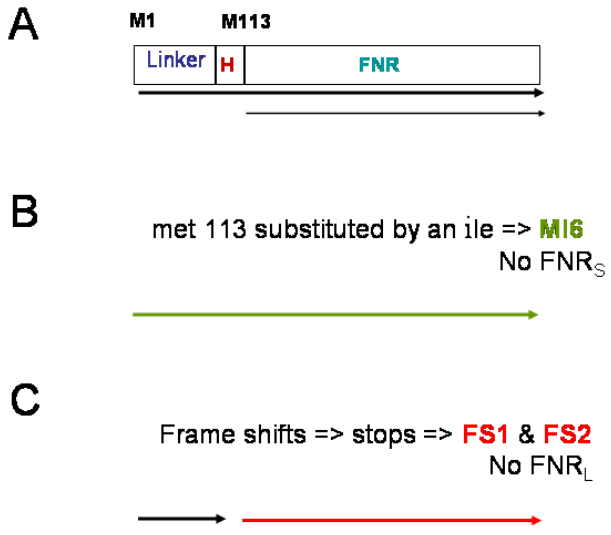

Figure 1.25 *Synechocystis* WT, FS1 (FNR_S) mutant and MI6 (FNR_L) mutant strains.

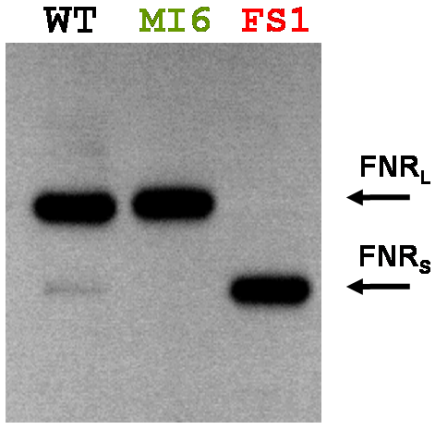

Figure 1.26 Immunoblot of total protein extracts for *Synechocystis* WT, FS1 and MI6 strains. Kindly provided by Dr. Ajlani.

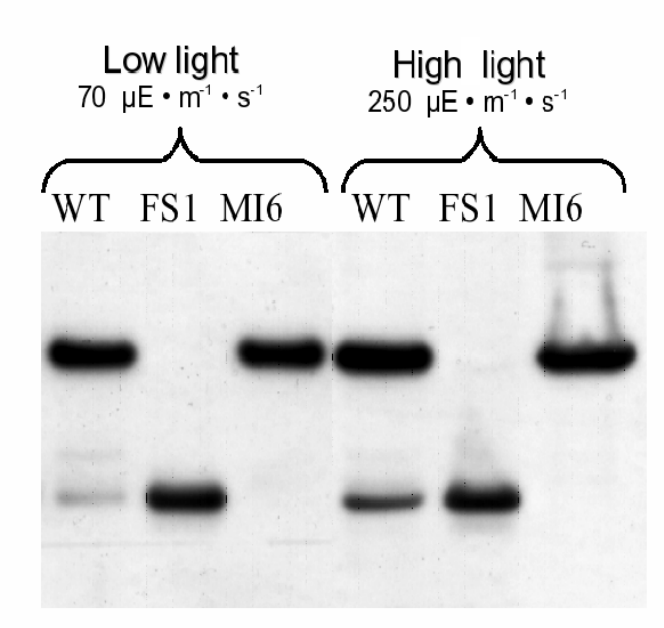

Figure 1.27 Immunoblot of total protein extracts for *Synechocystis* WT, FS1 and MI6 strains under low and high light from [Thomas et al., 2006].

Different growth conditions have been tested for the newly constructed mutants. First, under photoautotrophic growth, the light intensity was varied and WT, FS1 and MI6 strains were tested for their FNR isoforms by performing immunoblots on the total protein extracts. In Figure 1.27 are shown immunoblots for WT, FS1 and MI6 strains under low and high light. The WT exhibits accumulation of FNR_S under high light compared to low light [Thomas et al., 2006].

This may be explained by the stress conditions of high light. Normally, high light results in increased turnover of the photosynthetic machinery, thus building up increased levels of NADPH. The induction of FNR_S may help evacuate the excess of NADPH by the reverse reaction catalyzed by FNR. In this way, the excess NADPH is oxidized into $NADP^+$ and the electrons are fed back in the PQ pool by respiratory or cyclic electron flow. One interesting photoautotrophic condition may be limiting CO_2. If the main substrate for the Calvin-cycle is limiting, the electrons may accumulate at the acceptor side of PSI, probably in the form of NADPH. We will summarize the results of different growth characteristics tested by Dr. Ajlani for the WT, FS1 and MI6 strains.

Growth characteristics

Different growth conditions have been tested by Dr. Ajlani for the WT, MI6 and FS1 strains. WT can grow under photoautotrophic (light and CO_2), chemoheterotrophic (dark and glucose) as well as bleaching (under N-starvation) conditions.

Under photoautotrophic conditions, mutant FS1 is characterized by a slower growth. The

MI6 mutant grows just as the WT. This can be correlated to the FNR isoforms expressed under these conditions. Both the WT and MI6 exhibit FNR_L as the major isoform, whereas FS1 contains only FNR_S. Apparently, FNR_S cannot sustain photoautotrophic growth to the same extent as FNR_L.

Under chemoheterotrophic conditions, FS1 exhibits an increased growth compared to WT. MI6 failed to grow. Apparently, FNR_S in the FS1 mutant is better adapted to sustain heterotrophic growth which includes the oxidation of NADPH for reducing Fd just as in nonphotosynthetic tissues in plants. MI6 seems to have become an obligatory photoautotroph due to the presence of only FNR_L. However the WT strain can adapt to heterotrophic growth but not to the same extent as the FS1 mutant.

In the study of [Thomas et al., 2006], extensive studies under N-starvation have been carried out. These growth conditions are characterized by the trimming of PBS using the rods as nitrogen source. Analogously to the chemoheterotrophic growth but to a lesser extent, FS1 exhibits fast PBS degradation compared to WT whereas MI6 exhibited a limited possibility to adapt to N-starvation. Again, FNR_S in FS1 allows a better adaptation to N-starvation conditions probably due to the fact that FNR_S participates to the heterotrophic metabolism induced in the early stages of N-starvation. WT can still grow under these conditions, trimming the PBS and inducing FNR_S expression. There may be transformation of FNR_L into FNR_S due to proteolysis when the linker-like domain is not protected due to PC association. MI6 cannot induce FNR_S and thus will only after extended bleaching get proteolysed into FNR_S.

After this introduction, we can now state the objective of the PhD and briefly outline different approaches.

1.4 Objective

The objective of this PhD is to determine the function of the attachment of FNR to PBS in facultative heterotrophic cyanobacteria and the respective roles of the two FNR isoforms. First, we compared the two FNR isoforms for their intrinsic, catalytic activities (Chapter 2). To approach *in vivo* conditions, we purified an FNR_L-PBS subunit complex and compared it to FNR_S. In addition to that, preliminary reconstitution studies of PBS-FNR_L binding were carried out using biochemical techniques. Second, we compared FNR mutants to WT following *in vivo* studies (Chapter 3).

Chapter 2

In vitro studies

2.1 Results and discussion

We were interested in comparing the *in vitro* activities of the two FNR isoforms as different roles were proposed for the FNR isoforms of *Synechocystis* [Thomas et al., 2006]. The small isoform FNR_S on one hand was shown to accumulate in the WT under heterotrophic or nitrogen starvation conditions. On the other hand, the large isoform FNR_L is the major isoform under photoautotrophic conditions. It was proposed that FNR_L could be implicated in the linear photosynthetic reactions ($NADP^+$ reduction), whereas FNR_S would be implicated in cyclic photosynthetic or respiratory reactions (NADPH oxidation, see Chapter 1). This was our working hypothesis.

2.1.1 Purification of FNR_L-PC

Previous studies [Schluchter and Bryant, 1992, Nakajima et al., 2002, Thomas et al., 2006] have shown that when FNR_L is not bound to PC, its N-terminal part is easily proteolysed just as the PBS linkers. Therefore intact FNR_L is not detected *in vivo* in mutants lacking PC [Thomas et al., 2006]. One to two PC hexamers per PBS contained the native FNR_L attached to it [van Thor et al., 1999b, Gómez-Lojero et al., 2003] and we decided to purify a native complex composed of FNR_L and a PC hexamer in order to preserve the native conformation of FNR_L. In the WT, the PBS contains six rods composed of three PC hexamers each. For the purification, we used the CB mutant, which contains only one PC hexamer per rod [Ughy and Ajlani, 2004]. Additionally, six histidines were inserted between the catalytic domains (FAD- and NADP-binding domain) and the linker-like domain, in the hinge domain (Figure 1.24 in Chapter 1). In this way, neither the enzymatic activity nor the binding to PC was hindered by the His-tag insertion. This mutant is named CBH. CBH grows normally and its PBS composition is not altered.

A first step consisted in purifying sufficient amounts of homogeneous FNR_L-PC to measure the catalytic activities. The procedure, described in Chapter 5, started with PBS isolation on a sucrose step gradient (Figure 2.1A). The lower blue band corresponds to the PBS complex and an additional centrifugation was carried out to concentrate the PBS complex. The intact PBS was then selectively dissociated into AP and PC (PBS fraction, lane CBH in Figure 2.1B). The mixture was incubated with a Ni-resin where FNR_L and associated polypeptides were bound due to the His-Tag on FNR_L (unbound fraction, lane UB in Figure 2.1B). After extensive washing (lanes W1-W2), the sample was eluted *via* competitive binding of imidazole to the Ni-resin (lane E). The eluted fraction was highly enriched in FNR_L compared to entire PBS as shown in Figure 2.1B. Additionally, a linker called L_{RC} and the α and β PC were found. Contamination by a linker called L_{CM} was also detected in the eluted fraction.

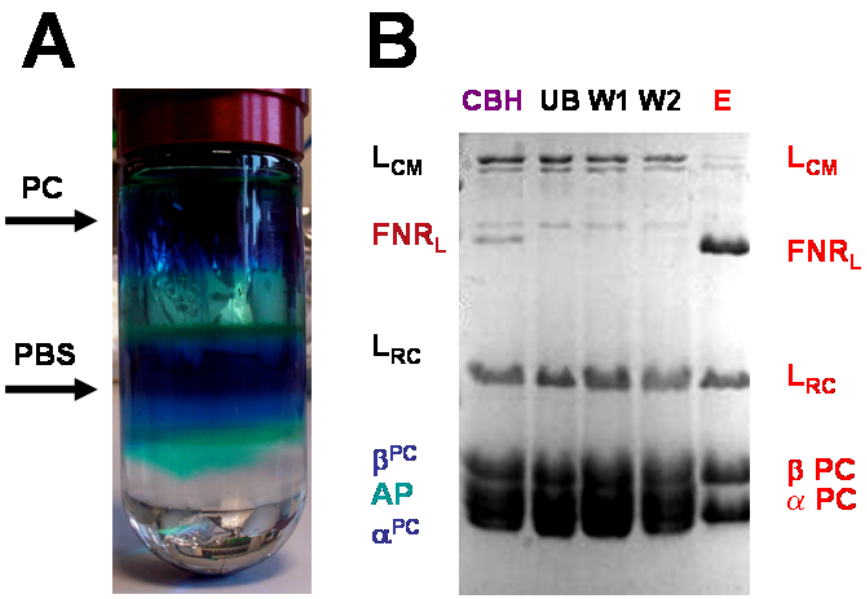

Figure 2.1 Phycobilisome isolation and IMAC purification of the FNR_L-PC complex. A: density gradient showing PC and PBS fractions. B: SDS-PAGE analysis of the different fractions. Taken from [Bordot, 2005]. CBH: entire PBS from the mutant CBH, UB: unbound fraction, W1 and W2: washing fractions, and E: elution fraction. Polypeptides in CBH are indicated on the left. Polypeptides in E are indicated on the right.

To determine the size of the complex and ensure its homogeneity, gel filtration was performed on a preparative column and three fractions were recovered (Figure 2.2). The first and major fraction F1 was recovered at 89 mL. The shape of the peak indicates a homogeneous complex. F1 had an estimated molecular mass of around 330 kDa. This is in agreement with a PC hexamer (230 kDa) with FNR_L (46 kDa) and L_{RC} (28 kDa) attached to it. Furthermore, as shown in the

inset of Figure 2.2, all three characteristic wavelengths for peptide-, FAD- and PC-absorption were present in contrast to minor fractions, F2 and F3, that were recovered at 112 and 125 mL. The inset of Figure 2.2 shows on one hand that F2 contains only a background absorption of PC and on the other hand that F3 contains no FAD-characteristic absorption. In addition, these fractions were found at a lower molecular mass. Therefore, we assigned F2 and F3 to dissociation products of the FNR_L-PC complex.

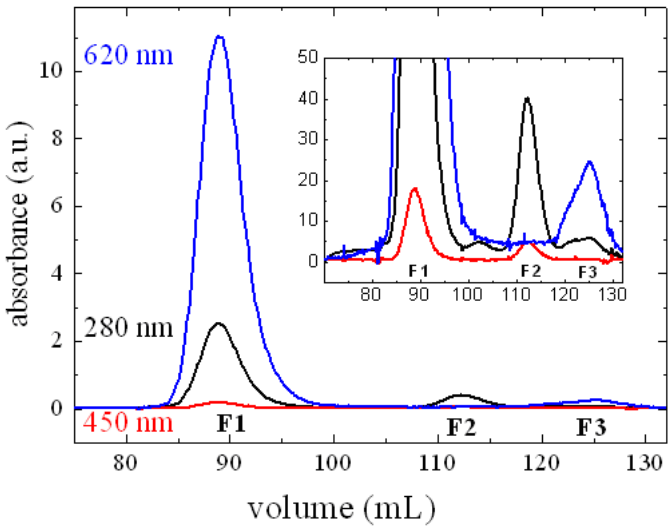

Figure 2.2 Gel filtration chromatogram. The chromatogram was followed at 620, 450 and 280 nm which corresponds to characteristic PC-, FAD-cofactor and peptide absorption. The inset shows a zoom in low absorbance region (ma.u.) of the recovered fractions F1, F2 and F3.

The different fractions were monitored *via* UV-Vis absorption spectroscopy and SDS-PAGE (Figure 2.3). The specific absorption of the CBH PBS at 650 nm corresponding to AP strongly decreased during the different purification steps. This absorption decreased significantly after Ni-affinity chromatography (E *vs.* CBH in Figure 2.3). After gel filtration, the absorption at 650 nm was completely abolished (F1 fraction in Figure 2.3). This indicates that we purified an FNR_L complex that contains PC only.

In summary, we purified a homogeneous PBS subcomplex that contains a PC hexamer and FNR_L as well as L_{RC} attached to it. Fraction F1 described above was used to carry out activity measurements.

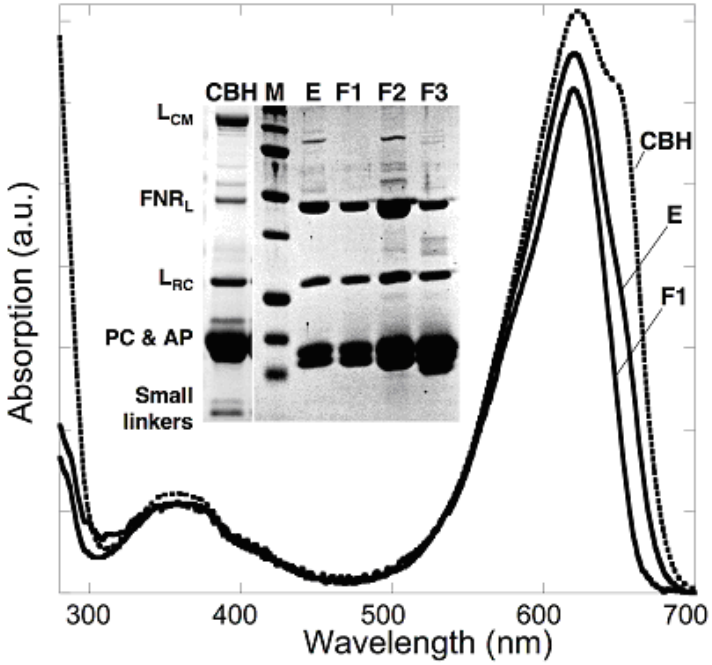

Figure 2.3 Overview of the purification of the FNR_L-PC complex. Absorption spectroscopy for the CBH PBS, E (Ni-affinity: elution fraction) and F1 (gel filtration: major fraction) are shown. In the inset, SDS-PAGE electrophoretic fractions are shown. CBH: entire PBS from this mutant, M: molecular mass marker, E: elution fraction during Ni-affinity chromatography, F1, F2 and F3: fractions obtained during gel filtration chromatography. Polypeptides are indicated on the left.

2.1.2 FNR quantification in FNR_L-PC

Before performing *in vitro* activity measurements, the FNR_L in the complex has to be quantified. First, the apoenzyme quantification was carried out (Table 2.1). The density of the different bands on SDS-PAGE was determined. A stoichiometry for the complex of about 1:1:1 for FNR_L : $(\alpha^{PC}\ \beta^{PC})_6$: L_{RC} was found.

sample	FNR_L concentration (μM)	FAD concentration (μM)	FAD/FNR_L
1	0.43 ± 0.02	0.39 ± 0.02	0.91 ± 0.09
2	0.55 ± 0.04	0.49 ± 0.05	0.89 ± 0.16
3	1.22 ± 0.03	1.19 ± 0.04	0.98 ± 0.06

Table 2.1 Quantification of FNR_L and FAD in FNR_L-PC. Each sample represents an average of three measurements.

The next step was the quantification of the holoenzyme (FAD concentration, see Table 2.1). Only the FAD-containing enzyme can perform catalysis. This is why the quantification of the holoenzyme is essential before starting *in vitro* activity measurements. For FNR_S, several methods were developed. First, a holoenzyme quantification can be determined *via* the FAD absorption at 450 nm. This method cannot be performed with the FNR_L-PC complex, as the characteristic FAD absorption is hidden behind the enormous absorption of the cyanobilin attached to PC (Table 2.2).

wavelength (nm)	ε (M^{-1} cm^{-1})
620 (PBS cofactors)	14,400,000
620 (PC cofactors)	2,370,000
450 (free FAD)	11,300

Table 2.2 Extinction coefficients for cofactors.

For the same reason, the photochemical reduction with deazaflavin/EDTA was difficult to perform [Massey et al., 1978]. We tried to obtain difference spectra under anaerobic conditions. Instead, the PC absorption was altered under the action of blue light. This made FAD quantifications in the complex difficult. Holoenzyme quantification by extraction *via* SDS was hindered for the same reason in FNR_L-PC. Finally, the TCA extraction method was combined together with standard apoprotein quantification (Micro-BCA) and absorption due to PC chromophore.

In summary, the TCA extraction method was the only holoenzyme quantification working for the purified FNR_L-PC. This is due to the covalently-linked bilins in PC and the non-covalently linked FAD in FNR_L. TCA treatment extracts selectively FAD and proteins containing bilins are precipitated. Three independent samples were treated with TCA and the non-covalently bound

FAD was extracted. The holoenzyme quantification is shown in Table 2.1. The procedure is detailed in Chapter 5. A ratio between 0.92-1.00 for [FAD]/[FNR_L-PC] was obtained (Table 2.1). The FAD release from FNR_L-PC is shown in Figure 2.4.

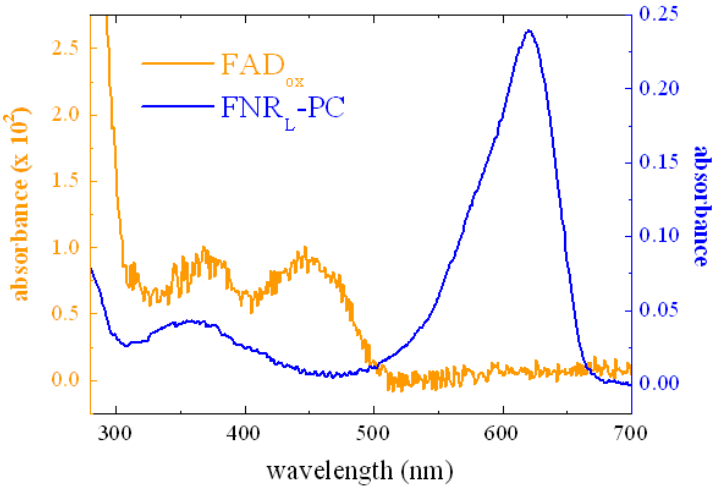

Figure 2.4 FAD release from the FNR_L-PC complex. The blue trace (right y-scale) shows the characteristic FNR_L-PC absorption, at a concentration of 0.1 µM. The PC-cofactor determines essentially the FNR_L-PC absorption with an absorption maximum at 620 nm and an extinction coefficient shown in Table 2.2. The orange trace (left y-scale) shows the FAD absorption, after extraction by TCA from FNR_L-PC, at a concentration of 0.81 µM (ε for FAD shown in Table 2.2). The characteristic FAD absorption in solution exhibits absorption maxima at 450 and 378 nm.

2.1.3 Reconstitution of PBS-FNR_L

We performed preliminary reconstitution measurements of PBS with FNR_L. These biochemical studies could provide us with higher amounts of entire PBS or subcomplexes, although not native.

To do so, we isolated and purified the PBS of two mutant strains. We used two PBS and FNR mutant strains called CBH and CBFS. CBFS contains the same mutation as CBH on the PBS and, in addition to that, a FNR mutation equivalent to the one in FS1, resulting in the absence of FNR_L. In parallel, we purified, from *E. coli*, a recombinant FNR_L and incubated FNR_L with PBS in different ratios of PBS:FNR_L (1:0, 1:2, 1:8, 1:12). The next step consisted in performing a second density step-gradient in order to purify the FNR_L bound to the PBS as in [Gómez-Lojero et al., 2003].

The authors in [Gómez-Lojero et al., 2003] studied sedimentation profiles of sucrose gradients combined with diaphorase activity profiles (FNR activity) in *Synechococcus* sp. PCC 7002. They

showed that binding of exogenously added FNR_L to PBS was possible and that a maximum of six binding sites are available for FNR_L in the WT and the mutant similar to CB PBS. In the WT PBS, one to two FNR_L per PBS were found [Gómez-Lojero et al., 2003, van Thor et al., 1999b]. We observed 1.2 FNR_L per CBH PBS (lane CBH in Figure 2.5 and Table 2.3) which was in agreement with [Gómez-Lojero et al., 2003] (1.0-1.6 FNR_L/PBS in the WT).

CBFS did not contain FNR, as the unique FNR_S isoform present in this mutant is missing the linker-like domain responsible for the attachment to PBS (lane CBFS in Figure 2.5). The latter mutant was used for reconstitution experiments with FNR_L. A control was carried out by incubating the PBS of CBFS with a 12-fold excess of FNR_S per PBS. No bound FNR_S was detected, as observed (lanes CBFS FNR_S 1:12). We observed a significant increase of FNR_L amounts from the CBFS PBS fraction of the density gradient (lanes CBFS PBS:FNR_L 1:2, 1:8 and 1:12 in Figure 2.5). The density of the FNR_L bands were analyzed and the data were normalized assuming that there are six copies of L_{RC} linker per PBS. The samples CBFS PBS:FNR_L 1:2, 1:8 and 1:12 resulted in 4.5, 6.4 and 5.9 FNR_L per PBS (Table 2.3) and indicated saturation of the binding sites. Therefore, CBFS PBS seems to incorporate around 6 FNR_L per PBS which is in agreement with 6 binding sites available for FNR_L in *Synechococcus* PCC7002 [Gómez-Lojero et al., 2003].

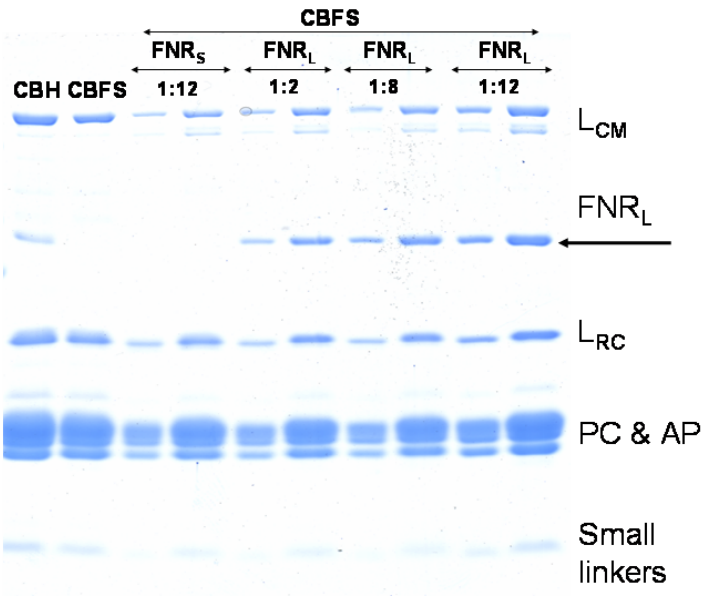

Figure 2.5 Reconstitution of PBS-FNR_L. CBH: PBS from a mutant that contains 1 PC hexamer per rod and FNR_L in natural amounts; CBFS: PBS from a mutant that in addition does not contain FNR_L; PBS:FNR_S 1:12; PBS:FNR_L 1:2, PBS:FNR_L 1:8 and PBS:FNR_L 1:12. All the reconstituted PBS:FNR samples are loaded twice in 2 different amounts.

These measurements are very promising to finally answer the question about the possible localization of FNR_L in the PBS [van Thor et al., 1999b, 2000, Gómez-Lojero et al., 2003, Arteni et al., 2009]. In the future, these reconstitution studies can be facilitated by the availability of a

Lane	FNR_L per PBS
CBH	1.19
CBFS:FNR_L 1:0	0
CBFS:FNR_L 1:2	4.5
CBFS:FNR_L 1:8	6.4
CBFS:FNR_L 1:12	5.9

Table 2.3 Calculated FNR_L stoichiometries for CBH- and CBFS PBS. The number of FNR_L was obtained by densitometric analysis of SDS-PAGE.

His-Tag containing FNR_L that can be overexpressed in *E.coli*. This would result in a facilitated and up-scaled purification of FNR_L which is needed in high amounts for such studies.

2.1.4 NADPH oxidase activity

In order to test our working hypothesis, we wanted to compare the catalytic constants of FNR_S and FNR_L-PC. For this, we were carrying out two different assays. The first assay is called ferricyanide reductase activity. The second assay is called Fd-mediated cytochrome *c* reductase activity.

Ferricyanide reductase activity

We performed the ferricyanide reductase activity assay (also called diaphorase activity) to measure the affinity to the substrate NADPH, to determine the catalytic turnover and the catalytic efficiency during NADPH oxidation. This was done in the presence of an artificial electron acceptor, potassium ferricyanide ($K_3[Fe(CN)_6]$). Ferricyanide in the oxidized state exhibits a characteristic absorption with a maximum around 420 nm (ε_{420nm}= 1020 $M^{-1}cm^{-1}$). When this external electron acceptor receives one electron, its absorption is abolished. Thus, the reaction was followed spectrophotometrically.

The reaction starts with the addition of the substrate NADPH. After a hydride transfer, the reduced FAD in the enzyme FNR reduces ferricyanide in two one-electron transfer reactions (Figure 2.6). The initial velocity of the catalyzed reaction is recorded, analyzed and plotted against the initial substrate concentration of NADPH (Figure 2.7). The only rate-limiting step is hydride transfer from NADPH to $FNR_{S/L}$ as an excess of ferricyanide was used. By varying the initial substrate concentration of NADPH, we obtained informations about the affinity to NADPH and the catalytic turnover. We obtained the catalytic efficiency as well which is calculated from these two values. The obtained Michaelis-Menten catalytic constants are listed in Table 2.4. The Michaelis-Menten constant K_m(NADPH) is shown for the two FNR isoforms. A 30% decrease

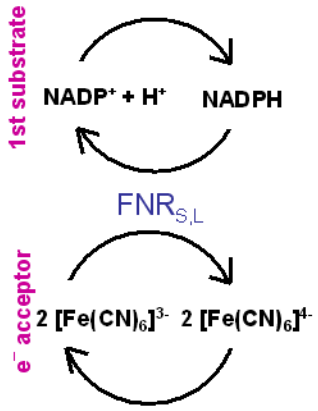

Figure 2.6 Scheme of ferricyanide reduction.

was observed for FNR_L-PC compared to FNR_S. The Michaelis-Menten constant is related to the affinity. Thus, an increase in affinity for NADPH of about 30% was observed in the FNR_L-PC complex compared to FNR_S.

We want to recall that, following our working hypothesis, FNR_S is catalyzing the NADPH oxidation under heterotrophic growth. Heterotrophic growth is accompanied at least transiently by increased NADPH concentrations where catabolism contributes to NADPH built-up. Thus, the physiological conditions may not require a high affinity of NADPH to FNR_S.

In contrast, FNR_L is catalyzing the $NADP^+$ reduction under photoautotrophic growth. These conditions may require a better $NADP^+$ affinity. If we assume that the $NADP^+$ affinity is similar to NADPH affinity, the increased affinity of FNR_L-PC for NADPH may be correlated to a faster turnover of $NADP^+$ reduction. We have seen in Chapter 1 that Fd_{ox} dissociation can be rate-limiting for $NADP^+$ reduction. This limitation is decreased by *prior* $NADP^+$ binding and by the mechanism of positive kinetic cooperativity. Increased $NADP^+$ affinity for FNR_L-PC may thus favor the physiologically catalyzed reaction, *i.e.* $NADP^+$ reduction.

Furthermore, the catalytic turnover k_{cat} is shown for the two FNR isoforms. A 30% decrease was observed for FNR_L-PC compared to FNR_S. Apparently, the increase in affinity to NADPH limits turnover. This is in agreement with the physiologically catalyzed reactions for the two FNR isoforms (see above). The ratio of the catalytic turnover over the Michaelis-Menten constant k_{cat}/K_m reflects the catalytic efficiency of the two FNR isoforms. Similar values were observed for FNR_L-PC and FNR_S.

Ferredoxin-mediated cytochrome *c* reductase activity

We performed ferredoxin-mediated cytochrome *c* reductase activity tests to measure the affinity to the second substrate Fd, to determine the catalytic turnover and the catalytic efficiency in

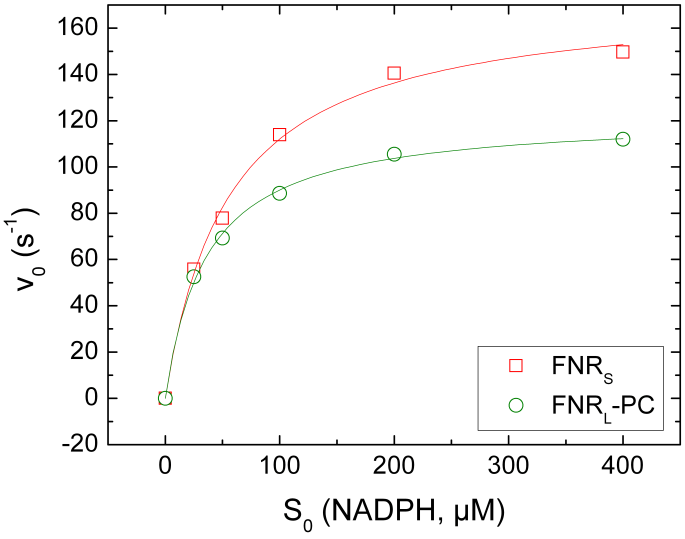

Figure 2.7 Ferricyanide reductase activities of FNR_S and FNR_L-PC.

Ferricyanide reductase activity	(unit)	FNR_L-PC	FNR_S
K_m(NADPH)	(µM)	40 ± 3	55 ± 5
k_{cat}	(s^{-1})	124 ± 3	174 ± 5
k_{cat}/K_m	(μM^{-1} s^{-1})	3.1 ± 0.3	3.2 ± 0.4

Table 2.4 Ferricyanide reductase activity of FNR_L-PC and FNR_S.

an alternative and more physiological NADPH oxidase activity using both natural substrates of FNR (Fd and NADPH).

This was achieved in the presence of Fd as an intermediate and cytochrome *c* as the final artificial electron acceptor. When cyt *c* receives an electron, a characteristic absorption maximum builds up ($\Delta\varepsilon_{550nm}$= 21.1 mM^{-1} cm^{-1}; Sigma Aldrich C2506). Thus, the absorption change permitted us to follow the reaction spectrophotometrically [Shin and Pietro, 1971, Zanetti et al., 1980].

The reaction is started by the addition of the substrate NADPH. After hydride transfer, the reduced FAD in the FNR reduces the oxidized ferredoxin and finally the cytochrome *c* in two one-electron transfer reactions (Figure 2.8).

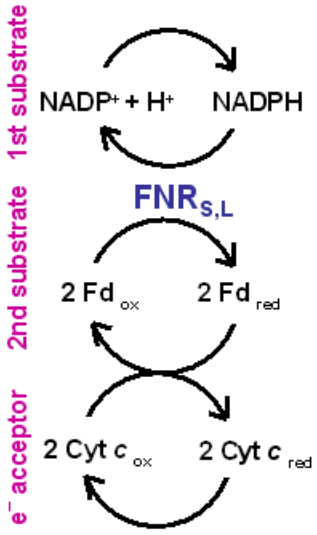

Figure 2.8 Scheme of Fd-mediated cyt *c* reduction.

The initial velocity of the catalyzed reaction is plotted against the initial Fd_{ox} concentration (Figure 2.9). The only rate-limiting step is the electron transfer from $FNR_{S/L}$ to Fd as both NADPH and cyt *c* were used in excess. By varying the initial Fd concentration, we obtained information about the affinity to Fd_{ox}, the catalytic turnover and the catalytic efficiency. The Michaelis-Menten catalytic constants are listed in Table 2.5. The Michaelis-Menten constant K_m(Fd) is shown for the two FNR isoforms. A 70% increase was observed for FNR_L-PC compared to FNR_S. Thus, a decrease of about 70% of the affinity to NADPH was observed for FNR_L-PC compared to FNR_S. Such an important decrease in the affinity for FNR_L-PC may be explained by the presence of the additional PC hexamer. Due to its considerable size (230 kDa), it may cause steric hindrance and thus complex formation of Fd_{ox}-FNR_{red} or Fd_{ox}-FNR_{sq} *prior* to electron transfer may be limited.

Furthermore, the catalytic turnover k_{cat} was determined for the two FNR isoforms. No significant decrease was observed for FNR_L-PC compared to FNR_S. Therefore, a change in

$K_m(Fd_{ox})$ is not correlated to a change in turnover, in contrast to the case of NADPH. A 44% decrease was observed for the catalytic efficiency k_{cat}/K_m of the FNR_L-PC complex compared to FNR_S . This would mean that FNR_S is slightly better in performing NADPH oxidation than FNR_L-PC. This difference in the catalytic efficiency is in agreement with our working hypothesis.

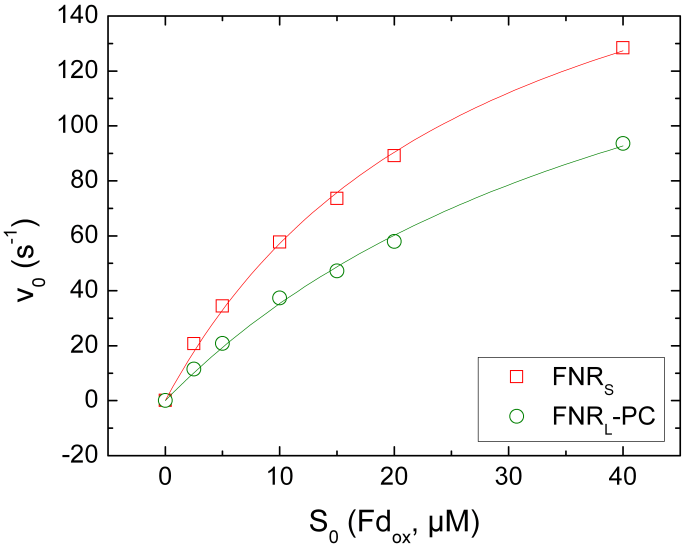

Figure 2.9 Fd-mediated cyt *c* reductase activities of FNR_S and FNR_L-PC.

Cyt *c* reductase activity	(unit)	FNR_L-PC	FNR_S
$K_m(Fd)$	(µM)	47 ± 6	28 ± 2
k_{cat}	(s^{-1})	202 ± 17	215 ± 9
k_{cat}/K_m	($\mu M^{-1}\ s^{-1}$)	4.3 ± 0.9	7.7 ± 0.8

Table 2.5 Cyt *c* reductase activity of FNR_L-PC and FNR_S.

$NADP^+$ inhibition of cyt *c* reduction

In order to get further informations about the mechanism of the catalysis, we measured the apparent inhibition constant (see Chapter 1). To measure the inhibition of NADPH oxidation, we repeated the Fd-mediated cyt *c* reductase reactions for FNR_L-PC in the presence of 50 µM $NADP^+$. The results for the FNR_L-PC are shown in Figure 2.10 together with Michaelis-Menten fits and the obtained catalytic constants are shown in Table 2.6.

On one side, the apparent Michaelis-Menten constant K_{mapp} is almost doubled in the presence of $NADP^+$. Thus, only about half the Fd_{ox} affinity is observed. On the other side, the

catalytic turnover remains constant. This decreased the catalytic efficiency to almost half of the catalytic efficiency in the absence of $NADP^+$. The apparent inhibition constant K_I for $NADP^+$ was determined (Equation 2.1.1).

$$K_I = [I] \cdot \frac{K_m}{K_{mapp} - K_m} \tag{2.1.1}$$

We did not repeat this experiment at other $NADP^+$ concentrations as these assays are very Fd-consuming. We cannot exclude that the apparent inhibition constant might vary as a function of the concentration of $NADP^+$ used in the assay.

It has been shown that *prior* $NADP^+$ binding to FNR inhibits NADPH oxidase activity [Carrillo and Ceccarelli, 2003]. As introduced in the catalytic cycle (see Chapter 1), the binding of $NADP^+$ is actually the first step of $NADP^+$ reduction and may be as well considered as the last step of the reverse reaction (NADPH oxidation). Therefore $NADP^+$ inhibition could be ascribed to product inhibition.

Cyt *c* reductase activity $NADP^+$	(unit) (μM)	FNR_L-PC 0	FNR_L-PC 50
K_m(Fd)	(μM)	47 ± 6	85 ± 32
k_{cat}	(s^{-1})	202 ± 17	207 ± 47
k_{cat}/K_m	($\mu M^{-1}\ s^{-1}$)	4.3 ± 0.9	2.4
K_I	(μM)		46.6

Table 2.6 Inhibition of cyt *c* reductase activity for FNR_L-PC.

Furthermore, we drew a Lineweaver-Burk plot of the inhibition data (Figure 2.11) which in this case meant plotting the $1/v_0$ *vs.* $1/Fd^0_{ox}$. Details of the catalyzed reaction can be obtained from such plots if different concentrations of the inhibitor result in parallel lines or intersecting lines. Parallel lines indicate a simple two-reaction pathway (also called ping-pong mechanism) if the two substrates are involved in an alternative manner (Figure 1.23). Intersecting lines indicate the involvement of a ternary complex. In our case the ternary complex would contain FNR, Fd and NADP(H). As the figure 2.11 presents intersecting lines (although for only one concentration of $NADP^+$), the involvement of a ternary complex is indicated. This is in contrast with results obtained by Forti and Sturani on spinach FNR [Forti and Sturani, 1968]. Following the same assay, they found parallel lines using different concentrations of $NADP^+$ and thus proposed a different mechanism during NADPH oxidation with no involvement of ternary complexes.

Involvement of ternary complexes have been found for FNR_S-like plant FNR during $NADP^+$ reduction [Batie and Kamin, 1984a, Carrillo and Ceccarelli, 2003]. Here, inhibition data were

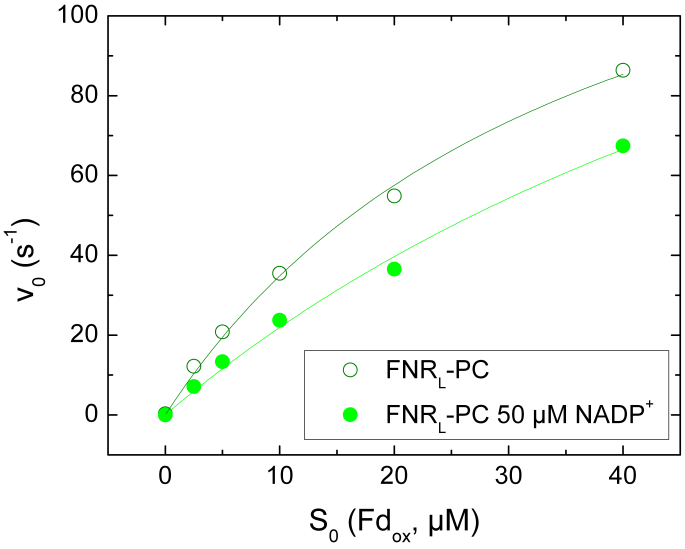

Figure 2.10 Inhibition of cyt *c* reductase activities of FNR_L-PC.

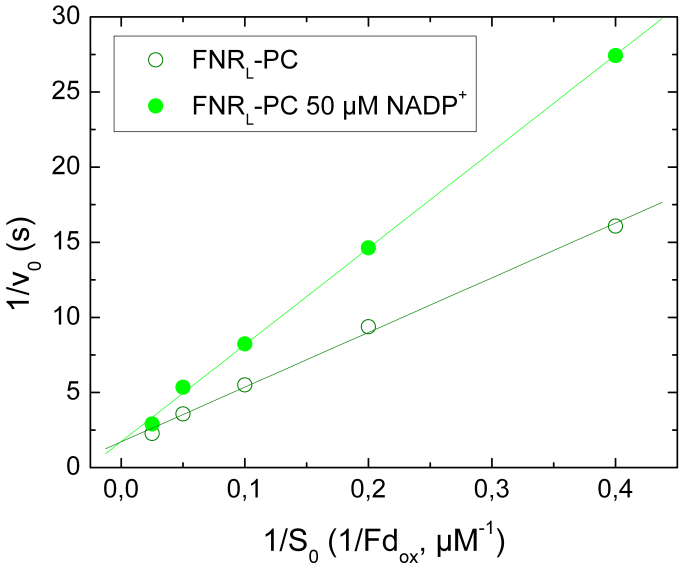

Figure 2.11 Lineweaver-Burk plot of the inhibition of FNR_L-PC cyt *c* reductase activities.

obtained for the first time for a native FNR_L attached to a PBS subunit. The result indicates the involvement of a ternary complex during NADPH oxidation. This would mean that the reaction mechanism should be the same for $NADP^+$ reduction and NADPH oxidation. Assuming that reaction mechanisms are similar, the Fd_{ox} affinity may be smaller during $NADP^+$ reduction for FNR_L-PC *vs.* FNR_S. As this reaction is limited by Fd dissociation, this would result in faster $NADP^+$ reduction and by contrast, decreased Fd_{ox} affinity correlates with slower NADPH oxidation.

2.1.5 $NADP^+$ reductase activity

$NADP^+$ reduction is the major reaction catalyzed by FNR during photoautotrophic growth. Following this FNR activity, the reducing power is built up in the form of NADPH. In order to test our working hypothesis, we wanted to compare FNR_S and FNR_L-PC catalytic constants. First, catalytic constants can be determined for the one-electron reduction of FNR. Second, multiple turnovers can be determined experimentally. Using the catalytic constants from single reduction, turnover can be calculated for the case that the first one-electron reduction is limiting the overall reaction. Experimental turnover can then be compared to the calculated turnover.

Compared to the NADPH oxidase activity, the assays for $NADP^+$ reductase activity involved an additional partner: PSI. The kinetics of FNR reduction and Fd reoxidation were measured in the ternary mixture PSI/Fd/FNR by laser flash absorption spectroscopy [Cassan et al., 2005]. First, a laser flash at 700 nm excites the reaction center of PSI. This results in oxidation of P700 and in charge separation (scheme A in Figure 2.12). We will further regard especially the acceptor side of PSI. At the end of the charge separation, the final acceptor in PSI, (F_AF_B), is reduced (PSI_{red} in Equation 2.1.2). Afterwards, a cascade of single electron transfers is occurring. The first electron transfer occurs from the reduced acceptor of PSI, $(F_AF_B)^-$, to oxidized Fd (first reaction in Equation 2.1.2 and scheme B in Figure 2.12). This results in reduced Fd and oxidizes the terminal acceptor. Electrons from reduced Fd are then transferred to FNR in single electron transfers (reaction 2 in Equation 2.1.2 and scheme C in Figure 2.12). We were performing $NADP^+$ reductase activity under two different conditions. The first condition permits only the first one-electron reduction of $FNR_{S/L}$ by Fd_{red}. The second condition is adapted for multiple turnover of $FNR_{S/L}$.

$$PSI_{red} \longrightarrow PSI_{ox} + Fd_{red} \xrightarrow{+\ FNR_{ox}} Fd_{ox} + FNR_{sq} \tag{2.1.2}$$

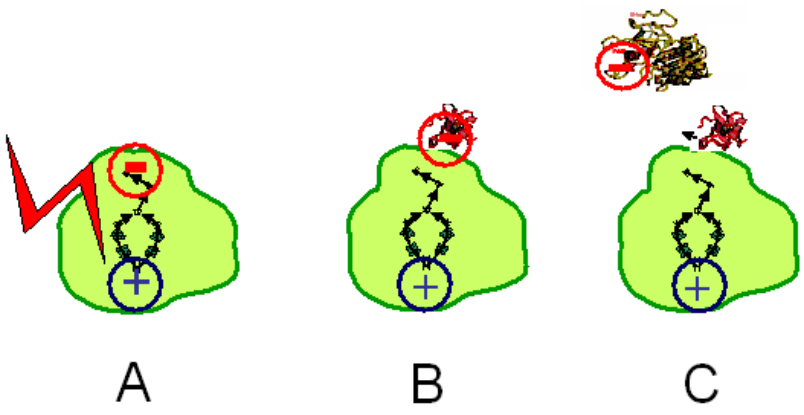

Figure 2.12 Reaction and scheme of single FNR reduction.

Single reduction by reduced Fd

We performed measurements in the presence and the absence of the second substrate $NADP^+$. After the actinic laser flash (at t=0) has triggered a charge separation in PSI, an electron transfer cascade is occurring towards FNR, *via* Fd. Concentrations of PSI (and the concentrations of photoreduced Fd) are chosen inferior to FNR to transfer only one electron per FNR and single electron transfer to FNR can be followed. The first one-electron reduction of oxidized FNR results in the build-up of a radical species called semiquinone. This radical species exhibits a differential absorption spectra with a maximum around 520 nm (Figure 5.1 in Chapter 5). We can thus follow the build-up of the semiquinone radical by following the absorption changes at 520 nm.

The kinetics in Figure 2.13 show the events due to reduction of the PSI electron acceptors, Fd and $FNR_{S/L}$. The contribution of $P700^+$ has been eliminated as explained in Chapter 5. In the absence of $FNR_{S/L}$ (black traces in Figure 2.13A and B), only a single kinetic component is observed. The reduction of the final electron acceptor of PSI, (F_AF_B), is not time-resolved on this timescale. It corresponds to the decrease in absorption that is seen just after the flash. The kinetic component that can be seen in the black trace is due to reduction of Fd. This results in a further decrease of absorption at 520 nm. Fd reduction can be further divided in a fast (submicrosecond and microsecond; small fraction) and a slower (millisecond) component (see Chapter 1). The fast component accounts for less than 10% of the full Fd reduction signal. This component corresponds to a fast electron transfer in the preformed PSI-Fd complex [Setif and Bottin, 1994]. The slower component accounts for a second-order diffusion-limited reduction of Fd.

Single reduction of FNR_S in the presence of $NADP^+$. In the presence of $NADP^+$, we observed the two isoforms acting according to the proposed catalytic cycle [Batie and Kamin, 1984a]. It

has been shown in this article, that the $NADP^+$ binds first to the FNR before binding Fd (ordered binding). The red, green, blue and purple traces in Figure 2.13A correspond to increasing concentrations of FNR_S as indicated on the right. Here, the same initial fast decay is observed but, in addition to that, an absorption increase is observed at 520 nm. This component is ascribed to the reduction of FNR_S by Fd_{red} with rate constants k_1 and k_{-1}. The rates and the final amplitudes of this absorption change increase with the FNR_S concentration. We used the following kinetic model to simulate the observed kinetics:

$$PSI_{red} + Fd_{ox} \xrightarrow{k_r} PSI_{ox} + Fd_{red} \tag{2.1.3}$$

$$Fd_{red} + FNR_{ox} \rightleftharpoons Fd_{ox} + FNR_{sq} \qquad K_{eq} = \frac{k_1}{k_{-1}} \tag{2.1.4}$$

In Equation 2.1.3, PSI_{red} stands for PSI with the reduced terminal acceptor (F_A,F_B). Reduction of this terminal acceptor of PSI is not considered on this time scale. Following Equation 2.1.3, one electron is passed to Fd. In Equation 2.1.4, the FNR is reduced once by Fd_{red}. This results in the build-up of the radical species, the semiquinone FNR. In order to solve the kinetic model analytically, it has to be further simplified. This has been done by considering all the reactions as pseudo first-order. The solution equations are shown in detail in Chapter 5. By applying these solution equations, we could perform a global fit analysis. We obtained the following values for the rate constants: k_r = 50.0 μM^{-1} s^{-1}, k_1 = 15.2 μM^{-1} s^{-1}, k_{-1} = 5.4 μM^{-1} s^{-1} for FNR_S. Furthermore, we calculated the equilibrium constant K_{eq} from Equation 2.1.4 (K_{eq} =k_1/k_{-1}) and obtained K_{eq} = 2.84. From the equilibrium constant, the midpoint redox potential E_m can be calculated in the following way:

$$\Delta E_m = E_m(FNR_{ox}/FNR_{sq}) - E_m(Fd_{ox}/Fd_{red}) = (RT/F)\ \ln(K_{eq})$$

We wanted to obtain the midpoint redox potential for the first one-electron reduction of FNR, $E_m(FNR_{ox}/FNR_{sq})$. We can assume that $E_m(Fd_{ox}/Fd_{red})$=-412 mV for *Synechocystis* Fd as obtained from [Bottin and Lagoutte, 1992]. With this, we calculated the midpoint redox potential for the first one-electron reduction of FNR. We obtained $E_m(FNR_{ox}/FNR_{sq})$=-385 mV for FNR_S. In previous studies, FNR_{sq} was only hardly observed during redox titrations [Corrado et al., 1996] because the semiquinone radical is thermodynamically unstable. The values of the rate constants, equilibrium constant and the midpoint redox potential are summarized in Table 2.7.

Single reduction of FNR_L-PC in the presence of $NADP^+$. The same experiment as for FNR_S was performed with FNR_L-PC. Due to limited amounts of this complex, the kinetics were obtained at lower concentrations of the complex. The kinetics are shown in Figure 2.13B in the absence (black trace) and the presence of FNR_L-PC (red, green, blue and purple traces).

The experimental data were fitted as for the FNR_S and the obtained rate constants, equilibrium constant and midpoint redox potential are shown in Table 2.7. On one side, a 25-30% decrease of k_1 and k_{-1} is obtained in FNR_L-PC *versus* FNR_S. This is in contradiction to our working hypothesis, that the FNR_L-PC might be more adapted to perform $NADP^+$ reductase activity. The FNR receives the electron from Fd_{red}. As discussed above in 2.1.4, the presence of the additional PC hexamer might result in steric hindrance when Fd is involved. This might explain the decrease in rate constants for our complex compared to FNR_S.

On the other side, the equilibrium constant and the midpoint redox potential for the first one-electron reduction of FNR were quite similar. This indicates that in the presence of $NADP^+$, the electrostatic environment of FAD is not modified in our complex compared to FNR_S. Deduced from first one-electron FNR reduction, both isoforms seem to be able to perform $NADP^+$ reduction.

Single reduction of $FNR_{S/L}$ in the absence of $NADP^+$ We repeated the same measurements in the absence of $NADP^+$. This is in contrast to the proposed catalytic cycle [Batie and Kamin, 1984a]. Normally, the $NADP^+$ is bound to FNR *prior* to Fd binding and electron transfer. This condition might mimic a physiological stressed state, when NADPH is in excess and hence $NADP^+$ is limiting.

The kinetics are shown in Figure 2.14 in the absence (black trace) and the presence of FNR_S (red, green, blue and purple traces) and FNR_L-PC (red, green and blue traces). It would be interesting to compare single FNR reduction +/- $NADP^+$. This is indeed possible for the k_1 rate constant. However, the rate constant k_{-1} and thus the derived values K_{eq} and E_m are obtained with a large uncertainty (data not shown). This might result from the measurement itself, favoring first one-electron reduction and thus unfavoring the back-reaction on a short timescale. This results in overlapping uncertainties for k_{-1}, K_{eq} and E_m. We will now discuss the differences that are significant in our measurements.

The rates, equilibrium constants and midpoint electron potentials are summarized in Table 2.8. Overall, the rate constants for both FNR isoforms are larger without than with $NADP^+$. This agrees with a previous study [Cassan et al., 2005]. This effect was attributed in this article to a repulsive electrostatic effect between the phosphate moiety of $NADP^+$ and the negatively charged Fd. The rates k_1(+$NADP^+$)/k_1(no $NADP^+$) are 0.77 and 0.61 for FNR_L-PC and FNR_S,

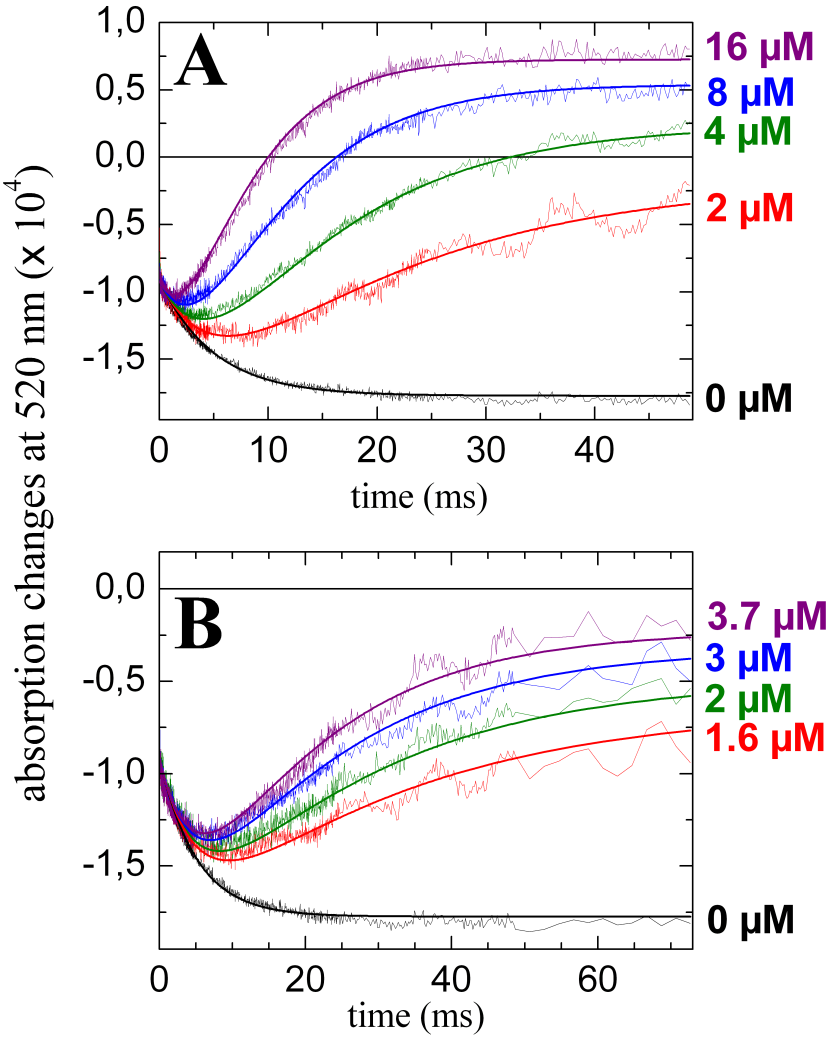

Figure 2.13 Flash titration of FNR_S (A) and FNR_L-PC (B) in the presence of $NADP^+$ under single reduction conditions. Thin line, data; bold line, fit.

respectively. Compared to FNR_S, FNR_L-PC presents a decrease for k_1 and k_{-1}. Thus, FNR_L-PC exhibits steric hindrance due to PC in the complex in the absence and presence of $NADP^+$.

As a summary, $NADP^+$ reduction measurements does not seem to favor our working hypothesis. Especially single FNR reduction may not be able to explain different growth characteristics of the FNR mutants. It has to be noted that several steps are involved during catalysis following first one-electron FNR reduction (see Chapter 1). Multiple turnover during $NADP^+$ reduction may help comparing the steps involved during catalysis after the first one-electron reduction of FNR.

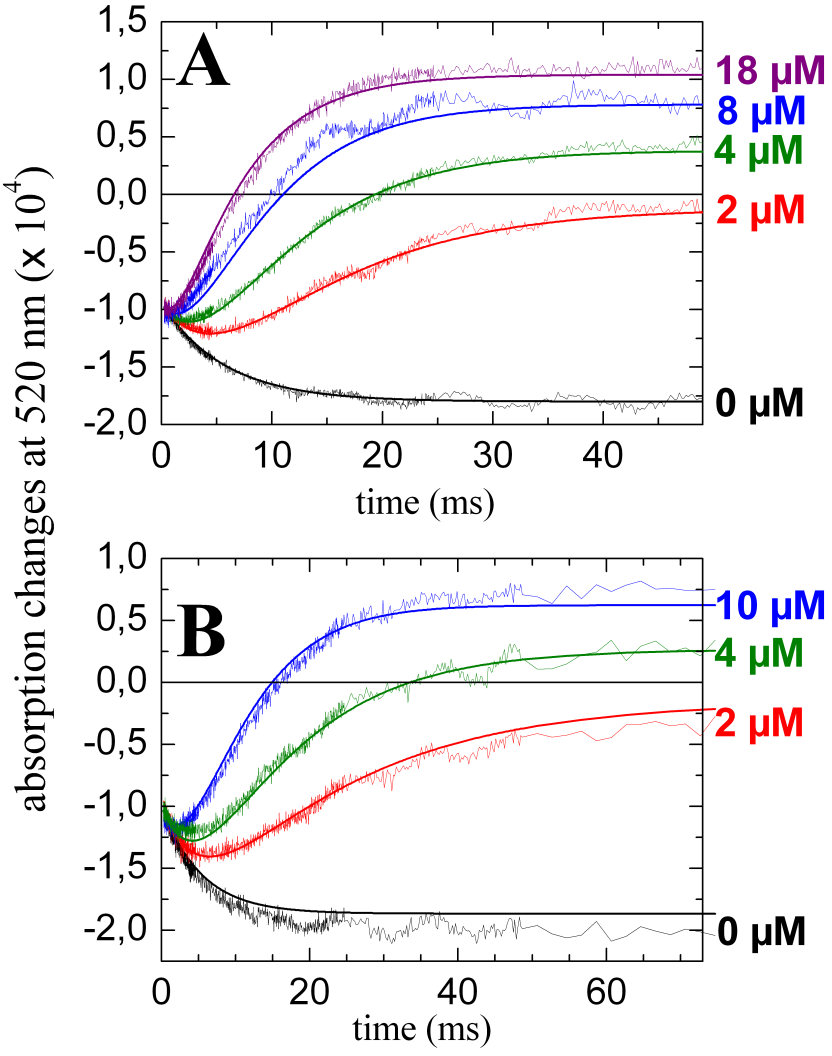

Figure 2.14 Flash titration of FNR_S (A) and FNR_L-PC (B) in the absence of $NADP^+$ under single reduction conditions. Thin line, data; bold line, fit.

	Single reduction of FNR by Fd_{red}	(unit)	FNR_L-PC	FNR_S
+ $NADP^+$	Second-order forward rate k_1	(μM^{-1} s^{-1})	10.8	15.2
	Second-order reverse rate k_{-1}	(μM^{-1} s^{-1})	4.0	5.4
	$K_{eq} = k_1/k_{-1}$	-	2.73	2.84
	$E_m(FNR_{ox}/FNR_{sq})$	(mV)	-386	-385

Table 2.7 Single reduction of FNR_L-PC and FNR_S by Fd_{red} in the presence of $NADP^+$.

	Single reduction of FNR by Fd_{red}	(unit)	FNR_L-PC	FNR_S
- $NADP^+$	Second-order forward rate k_1	(μM^{-1} s^{-1})	14.1	24.9
	Second-order reverse rate k_{-1}	(μM^{-1} s^{-1})	4.6	10.6
	$K_{eq} = k_1/k_{-1}$	-	3.06	2.35
	$E_m(FNR_{ox}/FNR_{sq})$	(mV)	-384	-390

Table 2.8 Single reduction of FNR_L-PC and FNR_S by Fd_{red} in the absence of $NADP^+$.

Catalytic turnover of FNR isoforms during $NADP^+$ reduction

We performed a second type of measurements on $NADP^+$ reduction: the catalytic turnover of the two FNR isoforms. We measured the kinetics obtained for a ternary mixture PSI/Fd/FNR in the presence of $NADP^+$. As the product of this reaction is NADPH, one might on one hand follow the build-up of NADPH. This was however not easily possible in our set-up. On the other hand, in our laboratory the redox changes of the second substrate Fd can be easily followed [Cassan et al., 2005]. Electrons flow from PSI to Fd and, under the action of FNR, NADPH build-up is followed. Alternative measurements using continuous light illumination during photoreduction were performed with FNR in excess so that FNR catalysis is not rate-limiting. On the other side our set-up is specifically adapted to determine rate-limitation due to FNR catalysis (see below).

Conditions for multiple catalytic turnover were characterized by PSI in large excess over FNR (3.75 μM *vs* 0.15/0.3 μM). In addition to that, Fd is added in excess over PSI (Fd_{ox} concentration 8 μM). The reaction starts with photoexcitation of PSI (3.75 μM). The same concentration of Fd_{ox} will get rapidly photoreduced from PSI_{red}. The large excess of reduced Fd will afterwards doubly reduce FNR. Following the catalytic cycle proposed by Batie and Kamin in [1984a], FNR reduction by Fd_{red} is involved at steps 3 and 6 (see Chapter 1). We can thus follow spectrophotometrically the reoxidation of Fd_{red}. Furthermore, we subtracted the decay rate in the absence of $FNR_{S/L}$ (k_{noFNR}) from the reoxidation in the presence of FNR (k_{FNR}). Reoxidation of Fd_{red} in the absence of FNR is mainly due to slow reduction of oxygen. We would like to point out that no maximum turnover rate (k_{cat}) is measured *via* these measurements.

Multiple turnover of FNR_S. We obtained values of 2.2 and 4.1 s^{-1} for (k_{FNR} - k_{noFNR}) with 0.15 and 0.3 µM FNR_S (Figure 2.15A). We calculated the monoexponential decay rate as indicated in Chapter 5. This results in 55 and 51 reoxidized Fd_{red} per second and per FNR_S. The average value of 53 is indicated in Table 2.9.

Multiple turnover of FNR_L-PC. The same type of measurements were performed using FNR_L-PC. We obtained similar rates of 2.14 and 3.69 s^{-1} for (k_{FNR} - k_{noFNR}) with 0.15 and 0.3 µM FNR_L-PC (Figure 2.15B). This results in the averaged value of 50 reoxidized Fd_{red} per second and FNR_L-PC (Table 2.9).

Overall, the multiple turnover rates for the two isoforms are similar. From these results, both isoforms are equally capable of catalyzing the $NADP^+$ reductase activity of FNR under multiple turnover conditions. This was in contrast to our working hypothesis.

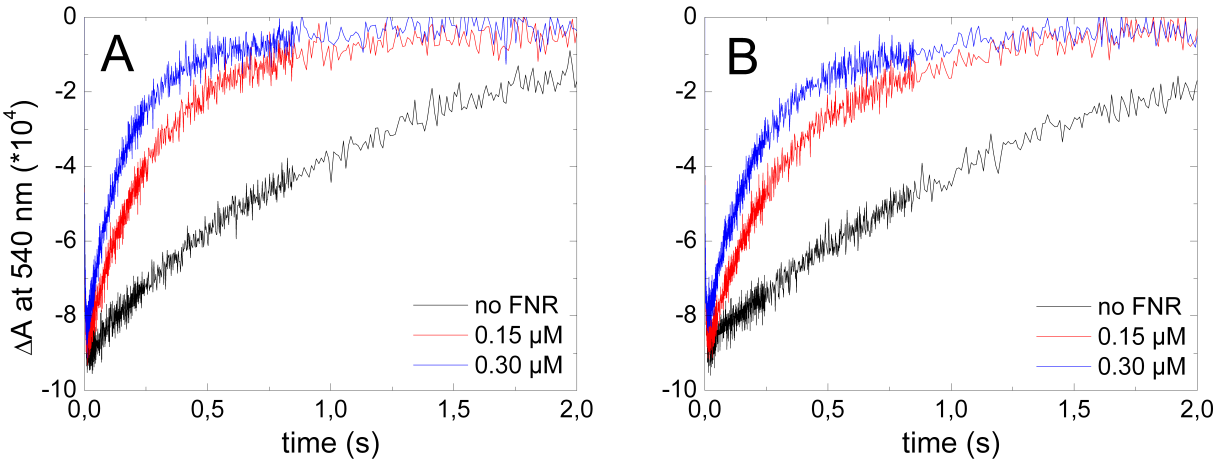

Figure 2.15 Flash titration of FNR_S (A) and FNR_L-PC (B) in the presence of $NADP^+$ under catalytic turnover conditions.

Calculated turnover rate. In the previous paragraph, we have presented experimental catalytic turnover rates for the two FNR isoforms. We have seen that these turnovers are relatively slow. Due to special conditions during the measurements (discussed below), the first one-electron reductions were observed to be slow, too. We wanted to check if the two observations might be related, that is if first one-electron reduction might limit the overall reaction.

For this, we calculated a catalytic turnover rate by using the experimental rate k_1 of single FNR reduction and by supposing that this rate limits overall turnover. This calculation was performed according to Equation 5.3.1 in Chapter 5. We obtained 40.5 and 57 reoxidized Fd per second and $FNR_{S/L}$ for FNR_S and FNR_L-PC, respectively (Table 2.9). The smaller value obtained

for FNR_L-PC results from a smaller rate k_1. These rates are in agreement with the experimental turnovers (Table 2.9).

As explained in Chapter 1, rate limiting steps during $NADP^+$ reduction were proposed to be Fd_{ox} dissociation or NADPH release [Aliverti et al., 2001, Batie and Kamin, 1984a, Carrillo and Ceccarelli, 2003] and, contrary to our results, no indications were found for a rate limitation by ET from Fd_{red} to FNR. We attribute our results to the high ionic strength which leads to a decrease in k_1 strong enough that it becomes the limiting rate.

Multiple turnover: Initial rate of reoxidation of 3.75 μM Fd_{red}	FNR_L-PC	FNR_S
(reoxidized Fd_{red} per second and per FNR)		
Observed rate	50	53
Calculated rate (with limiting k_1)	40.5	57

Table 2.9 Multiple turnover of FNR_L-PC and FNR_S.

2.1.6 Catalytic properties of cyanobacterial FNR_S

Our first objective was the *in vitro* characterization of FNR_S in comparison to FNR_L-PC. These *in vitro* activities were performed under high ionic strength (high salt) conditions that ensure the stability of the purified FNR_L-PC. The interprotein ET reactions depend on the salt concentration (see Chapter 1). This makes comparison with previously obtained rate constants and catalytic parameters not straightforward. However, comparison may be useful to understand which steps or reactions are mostly affected by ionic strength. Thus, we will compare our results with results obtained on cyanobacterial FNR_S under low salt [Medina et al., 1998, Cassan et al., 2005].

NADPH oxidase activities

Extensive NADPH oxidation measurements were carried out on *Anabaena* sp. FNR_S [Medina et al., 1998]. We will compare catalytic parameters concerning ferricyanide reduction and Fd-mediated cytochrome *c* reduction.

Ferricyanide reduction. On one hand, catalytic turnovers k_{cat} were found to be quite similar to high-salt results. On the other hand, affinities for NADPH were found to be two-fold decreased in our case (Table 2.10). This indicates that high salt is not detrimental for this oxidase activity. This also means that the affinity to NADPH is decreased in high salt.

Fd-mediated cytochrome *c* reduction. On one hand, catalytic turnovers k_{cat} were found to be similar (Table 2.10). On the other hand, affinities to Fd were found to be 3-fold decreased in our case (Table 2.10). Electrostatic interactions are known to be weakened in the presence of high salt. This might explain the strong decrease in affinity to Fd in our conditions. The important decrease in affinity to Fd might also explain the decreased catalytic efficiencies.

Ferricyanide reductase activity	(unit)	*Anabaena* FNR_S
K_m(NADPH)	(μM)	23.0 ± 1.2
k_{cat}	(s^{-1})	225 ± 3
k_{cat}/K_m	(μM^{-1} s^{-1})	9.82 ± 0.15
Cytochrome *c* reductase activity		
K_m(NADPH)	(μM)	11.0 ± 2.0
k_{cat}	(s^{-1})	200 ± 10
k_{cat}/K_m	(μM^{-1} s^{-1})	18.2 ± 1.0

Table 2.10 NADPH oxidation of the *Anabaena* FNR_S.

$NADP^+$ reductase activities

Extensive $NADP^+$ reductase activities were carried out previously in our laboratory on *Synechocystis* FNR_S [Cassan et al., 2005] in low salt. We will compare catalytic parameters concerning single FNR reduction and multiple turnover of FNR.

Single FNR reduction. Single FNR reduction by Fd_{red} was strongly inhibited in high salt. The second-order rate constant k_1 was 27-fold decreased in our case compared to low salt (15.2 *vs.* 417 $\mu M^{-1}s^{-1}$ see Table 2.11). As it has been found in NADPH oxidase activities, electrostatic interactions are known to be weakened in the presence of high salt and this results in this strong decrease in the rate of single FNR reduction.

Multiple turnover of FNR. The data concerning multiple turnover of FNR in low salt were recalculated using $\varepsilon_{461nm}(FNR_S) = 9000\ M^{-1}cm^{-1}$. This results in 330 reoxidized Fd_{red} per second and FNR. The rate of Fd_{red} reoxidation was 6 times smaller in our case (53 *vs.* 330; Table 2.11). This indicates that high salt has a strong effect on overall turnover. However, the effect is smaller than on single FNR reduction. The calculated turnover (calculated from the single FNR reduction) is 27 times smaller in our case (57 *vs.* 1564; Table 2.11).

Under low salt, catalytic turnover is increased. As can be seen in Table 2.11, single FNR reduction works at an even more increased rate (k_1 = 417 $\mu M^{-1}s^{-1}$) which results in a 4-5 times increased calculated turnover rate (1564 *vs.* 330). This indicates that in low salt, first FNR

reduction is not limiting. We have seen before that first electron reduction was limiting for both FNR isoforms under high salt conditions whereas under low salt, another first-order process is limiting. This may be Fd_{ox} dissociation, hydride transfer or NADPH release.

Single reduction of FNR by Fd_{red} (unit)	high salt	low salt
Second-order forward rate k_1 (μM^{-1} s^{-1})	15.2	417
Multiple turnover: Initial rate of reoxidation of 3.75 μM Fd_{red}		
(reoxidized Fd_{red} per second and per FNR)		
Observed rate	53	330
Calculated rate (with limiting k_1)	57	1564

Table 2.11 Multiple turnover of FNR_S under high and low salt.

2.1.7 Catalytic properties of plant FNR_S

Previous work has been performed on different FNR isoforms in plants under low salt. These FNR isoforms have a size corresponding to FNR_S. They are encoded by different genes and thus are composed of slightly different catalytic domains. They are called leaf (photosynthetic; p) FNR and root (heterotrophic; h) FNR according to their respective localization. In plants there are as well different Fd present in leaves and roots. Here we compare our results with results obtained on different plant FNR isoforms under low salt.

NADPH oxidase activities

NADPH oxidase activities have been extensively studied in maize FNR [Onda et al., 2000] and spinach and corn FNR isoforms [Aliverti et al., 2004]. The different Fd isoforms have been compared in *Arabidopsis thaliana* [Hanke et al., 2004a, Gou et al., 2006]. A review summarizes the knowledge on Fd:FNR electron transfer complexes [Hanke et al., 2004b]. We will compare catalytic parameters concerning ferricyanide reduction and Fd-mediated cytochrome *c* reduction.

Ferricyanide reduction. The leaf and root FNR isoforms from plants differ mainly in four catalytic or thermodynamic parameters. The first one implies ferricyanide reduction. The Michaelis-Menten constant K_m(NADPH) has been found 3-10 fold higher for leaf FNR compared to root FNR. This indicated a decreased affinity of NADPH to the leaf FNR. According to our working hypothesis, we will tentatively make the parallel between FNR_L-PC from cyanobacteria and leaf FNR from plants on the one hand, and between FNR_S from cyanobacteria and root FNR from plants on the other hand. We observed a 30% difference for the K_m(NADPH) between the

FNR_L-PC and FNR_S. However, the difference was observed in the direction opposite to what was expected. This indicated in our case an increased affinity of NADPH to FNR_L-PC.

Fd-mediated cytochrome *c* reduction. Two other differences between the plant isoforms have been found. They imply the Fd-mediated cytochrome *c* reductase activity. First, the Michaelis-Menten constant K_m(leaf Fd) has been found 5-10 fold smaller for leaf FNR compared to root FNR. This indicated an increased affinity of leaf Fd to the leaf FNR. We have found a 70% difference for the K_m(Fd) between the FNR_L-PC and FNR_S. Again, the difference was observed in the opposite direction. This indicated in our case a decreased affinity of Fd to FNR_L-PC. Second, the plants isoforms differ in the catalytic turnover k_{cat}. The k_{cat} of cyt *c* reduction is 3-4 fold smaller for leaf FNR compared to root FNR. In our case, we did not observe a significant difference for the catalytic turnover of cyt *c* reduction.

$NADP^+$ reductase activity

Another major difference observed between the plant isoforms concerns $NADP^+$ reductase activity. The midpoint potential $E_m(FNR_{ox}/FNR_{red})$ for the two-electron reduction has been found 20 mV higher for the corn root FNR than for spinach leaf FNR [Aliverti et al., 2001]. However, we cannot compare the midpoint potential for two plant FNR isoforms from the same organism as it is not yet available. We have obtained the midpoint potential for the first-electron reduction only. No significant difference was found for the two cyanobacterial isoforms concerning the $E_m(FNR_{ox}/FNR_{sq})$.

The differences in cyanobacterial FNR isoforms are in contrast with the differences observed in plants. In addition to the presence of leaf or photosynthetic FNR (pFNR) and root or heterotrophic FNR (hFNR) isoforms, multiple pFNR isoforms have been found e.g. in *Arabidopsis* (2 pFNR) [Hanke et al., 2005], *Oryza sativa* (2 pFNR) [Ohyanagi et al., 2006] and *Zea mays* (maize; 3 pFNR) [Okutani et al., 2005]. Another study was carried out in wheat [Gummadova et al., 2007]. This study has identified the presence of multiple forms of FNR in wheat leaves with varied expression and N-terminal processing. Two *Arabidopsis* mutant lines have been studied in detail, each lacking one of the pFNR isoforms [Lintala et al., 2009]. The deficiency of FNR affected electron transfer properties of the mutant plants, especially cyclic electron transfer around PSI. Moreover, a distinct difference in the function of FNR1 and FNR2 became evident upon low-temperature acclimation of *Arabidopsis*.

It is essential to consider different Fd isoforms that may interact with different FNR isoforms. In plants, the midpoint potential of root Fd was found to be much higher compared to leaf Fd (50-100 mV) [Hanke et al., 2004a, Gou et al., 2006, Aliverti et al., 1995, Akashi et al., 1999]. This

might be an important factor favoring NADPH oxidation in roots compared to $NADP^+$ reduction in leaves. In *Synechocystis*, 4 genes have been identified for *fed*-like genes [Poncelet et al., 1998]. It is usually considered that only one major isoform encoded by *fed1* is responsible for bioenergetic electron flows under photoautotrophic conditions. The Fd encoded by *fed1* exhibits a similar redox potential to leaf type Fd.

The differences between heterotrophic and photosynthetic plant FNR isoforms do not correspond to the differences present in cyanobacterial FNR isoforms (see above). In addition to that, there is no evidence that the two FNR isoforms present in cyanobacteria interact with different Fd partners. The different leaf isoforms should interact exclusively with photoautotrophic Fd (tissue specificity). Differences in membrane attachment were found for leaf FNR isoforms, too [Hanke et al., 2005, Okutani et al., 2005]. Maybe the differences between the cyanobacterial FNR isoforms resemble more the differences observed for different leaf FNR isoforms that are summarized above.

2.2 Conclusion

In the first part of my PhD, we were interested in determining the catalytic properties of the FNR isoforms of *Synechocystis*. Functional specificity of FNR was supported by a recent study [Thomas et al., 2006]. In this article, it was proposed that FNR_S is involved in oxidative metabolism (NADPH oxidation) and that FNR_L sustains NADPH production under reductive metabolism ($NADP^+$ reduction). This was our working hypothesis. Thus, we compared *in vitro* the two isoforms: FNR_S and FNR_L. We wanted to approach as close as possible the *in vivo* situation. FNR_L is always bound to PBS *in vivo* and is degraded when it is not attached to PBS. Thus, we purified a complex called FNR_L-PC that is stable and compatible with absorption spectroscopy studies. A first objective was to scale up the purification of FNR_L-PC and to purify the complex to homogeneity. We used a mutant that was composed only of one disk of PC hexamer per rod (CB, [Ughy and Ajlani, 2004]). On average, one to two FNR_L is found attached per PBS [van Thor et al., 1999b, Gómez-Lojero et al., 2003]. By using the CB mutant, we increased the FNR_L amount per phycocyanin (total of 6 hexamers per PBS instead of 18 in the WT) in the starting material by a factor of three. The purification was further facilitated due to a His-Tag inserted in the hinge domain. This mutant was constructed by Dr. Ajlani and called CBH. Thus, we could use IMAC (Immobilized Metal Affinity Chromatography) for the purification. Further impurities were eliminated during preparative gel filtration. Our results indicated a pure and homogeneous complex composed of a PC hexamer, FNR_L and a rod-core linker L_{RC} with a stoichiometry of the apoproteins around 1:1:1 for FNR_L:L_{RC}:$(\alpha^{PC},\beta^{PC})_6$ (complex size 330 kDa). Our complex was stable at 4°C. It can thus be concluded that the purification of FNR_L in our

complex favors protection from proteolytic degradation, as previously observed [Schluchter and Bryant, 1992, Nakajima et al., 2002]. We also carried out preliminary studies on reconstitution of PBS with FNR_L. These reconstitution studies open enormous possibilities in terms of up-scaled purification and structure determination of the FNR_L-PC complex.

Several articles discussed the exact localization of FNR_L in the PBS and different proposals of FNR_L binding to core-proximal [van Thor et al., 1999b, Arteni et al., 2009], core-distal [Gómez-Lojero et al., 2003] PC hexamers as well as attachment to the PBS core and thylakoid membrane [van Thor et al., 1999a, 2000] were proposed. Little was known about the function of FNR_L attachment to the PBS. This study deals with the roles of the FNR isoforms and contributes to determine the function of the attachment of FNR_L to the PBS.

We have identified the exact composition of the FNR_L-PC complex and quantified the holoenzyme in this complex. We wanted to elucidate the function of the selective attachment of the FNR_L isoform to the PBS. For this, we performed a detailed functional characterization and observed differences in $NADP^+$ reduction and NADPH oxidation between FNR_S and FNR_L-PC.

Catalytic properties of FNR isoforms

We have found several catalytic parameters that are similar for the two *Synechocystis* isoforms. Most of the differences we have observed can be explained by steric hindrance brought by the additional PC hexamer in the FNR_L-PC complex. However, we have also observed some differences that cannot be easily explained by steric hindrance.

The catalytic parameters that were similar for FNR_S and FNR_L-PC are as follows: During NADPH oxidation, the presence of the PC did not prevent the NADPH/ferricyanide oxidoreduction. The interaction with the second substrate Fd resulted in similar maximal velocities during Fd-mediated NADPH oxidation. During first-electron FNR reduction, the electrostatic environment of the FAD cofactor was not changed. In addition to that, the two isoforms seem to be able to perform $NADP^+$ reduction to the same extent under multiple turnover.

However, some significant differences were observed in the $NADP^+$ reductase and NADPH oxidase activities between FNR_S and FNR_L-PC. We will summarize now the catalytic parameters that were different for FNR_S and FNR_L-PC and could be explained by steric hindrance brought by the additional PC in the FNR_L-PC complex. We found a decreased affinity of Fd for FNR_L-PC compared to FNR_S during Fd-mediated NADPH oxidation. Furthermore, we obtained indications that the FNR_L-PC complex was less able to perform Fd-mediated NADPH oxidation. This was in agreement with our working hypothesis. The same effect of steric hindrance was observed during $NADP^+$ reduction during single electron reduction of FNR. The rate k_1 for FNR single

reduction by Fd_{red} was smaller for FNR_L-PC compared to FNR_S. These effects might be alternatively explained by electrostatic repulsion. However, electrostatic interactions are expected to be of limited importance at high salt. Overall, the rate k_1 for FNR single reduction is in contrast to our working hypothesis. This would mean that FNR_L is less adapted to perform $NADP^+$ reduction.

Finally, we will summarize the catalytic parameters that are different for FNR_S and FNR_L-PC and cannot be explained by steric hindrance. The K_m(NADPH) is decreased and the catalytic turnover is decreased to the same extent for FNR_L-PC compared to FNR_S during NADPH oxidation. The size of the substrate NADPH excludes the effect of steric hindrance brought by PC. We propose that increased $NADP^+$/NADPH affinity for FNR_L-PC might favor the physiological reaction. Following the working hypothesis, FNR_L is catalyzing $NADP^+$ reduction under photoautotrophic growth. We have seen in Chapter 1 that Fd_{ox} dissociation can be rate-limiting for $NADP^+$ reduction. This limitation is decreased by *prior* $NADP^+$ binding and by the mechanism of positive kinetic cooperativity. Following the working hypothesis, the isoform FNR_S is catalyzing the NADPH oxidation under heterotrophic growth, starvation or high-light conditions. These conditions are probably accompanied by an increased NADPH concentration. Therefore, a higher affinity of NADPH to FNR_S may not be necessary under physiological conditions.

To summarize, the results obtained for the Fd-mediated NADPH oxidation are in agreement with the working hypothesis. In addition, the results for the ferricyanide-mediated NADPH oxidation indicate adaptation to physiological conditions. Furthermore, both isoforms are capable of catalyzing the $NADP^+$ reduction under multiple turnover conditions to the same extent. Finally, by comparing calculated and experimental turnover for $NADP^+$ reduction, we found evidence, that under our conditions, the first electron reduction is rate-limiting.

The extent of the observed differences contrast with large differences between leaf and root FNR isoforms in plants. The situation of the cyanobacterial isoforms might resemble more the case of different leaf FNR isoforms present in plants. We propose that the main photosynthetic Fd [Poncelet et al., 1998] is involved *in vivo* in electron transfer with both isoforms. Thus, the observed *in vitro* differences of the two *Synechocystis* FNR isoforms might not fully explain the *in vivo* properties of the mutants expressing only one of the isoforms. We have seen in Chapter 1 that FNR mutants that express only FNR_L or FNR_S show large differences in growth under photoautotrophic and heterotrophic growth. These differences were explained by the hypothesis of function specificity of FNR isoforms [Thomas et al., 2006]. This study proposed that FNR_L could be implicated in the photosynthetic reaction ($NADP^+$ reduction), whereas the FNR_S could be implicated in the reverse reaction (NADPH oxidation).

Instead of their intrinsic catalytic properties, it would then be necessary to invoke their localization and their association to other complexes. It can be *e.g.* speculated that FNR_S is

involved in cyclic/respiratory electron flow because it is free to bind to other membrane complexes such as NADPH dehydrogenase (NDH-1) or cytochrome b_6f. By contrast, PBS-bound FNR_L would not be able to play such a role but would be dedicated only to $NADP^+$ photoreduction. For both types of activities, substrate availability (Fd_{red}/Fd_{ox} and $NADP^+$/NADPH) might also be key *in vivo* characteristics for the activity of the two isoforms. This situation would be reminiscent of what has been described recently for the different plant leaf isoforms, where catalytic activities appear to depend upon their variable attachment to the thylakoid membrane [Palatnik et al., 1997, Hanke et al., 2008].

Chapter 3

In vivo studies

3.1 Results and discussion

We studied the implication of the FNR isoforms in linear-, cyclic-, pseudocyclic and respiratory ET that are present in thylakoid membranes. In addition to that, recombination reactions involving $P700^+$ can occur under conditions where electrons cannot be evacuated on the acceptor side of PSI.

As discussed in Chapter 2, substrate (Fd, NADP(H)) availability and enzyme localization might well be important for the FNR isoforms to perform different roles *in vivo*. On one hand, the localization of FNR_L is always close to the thylakoid membrane because of the attachment to the PBS. FNR_S on the other hand may be mobile or attached to other complexes. Growth characteristics of the mutants expressing only one FNR isoform (see Chapter 1) indicates specific roles for each isoform: FNR_L could be implicated in $NADP^+$ reduction, whereas FNR_S could be implicated in NADPH oxidation (see Chapter 1) [Thomas et al., 2006]. However, from a detailed functional characterization *in vitro*, we observed small differences in the $NADP^+$ reductase and NADPH oxidase activities of FNR_S and FNR_L-PC [Korn et al., 2009]. Thus, *in vivo* studies of the FNR mutants compared to the WT should help to determine their respective roles *in vivo*.

We studied mutants containing either FNR_L (MI6) or FNR_S (FS1). We determined the phenotypes for these mutants by comparing P700 oxidation kinetics (purple in Figure 3.1) where various ET processes in the FNR mutants and WT are analyzed. We also determined the redox state of the NADP pool (green in Figure 3.1) where we obtained informations about the output of PSI ET. Furthermore, NADPH can be reoxidized *via* the NDH-dependent cyclic ET (black arrow in Figure 3.1). Finally, we measured in collaboration with D. Kirilovsky the PQ pool reduction in the dark. The PQ pool (red arrow in Figure 3.1) is reduced by different cyclic electron transfer pathways besides PSII. Reduced PQ represents the input to PSI electron transfer *via* the cyt b_6f complex.

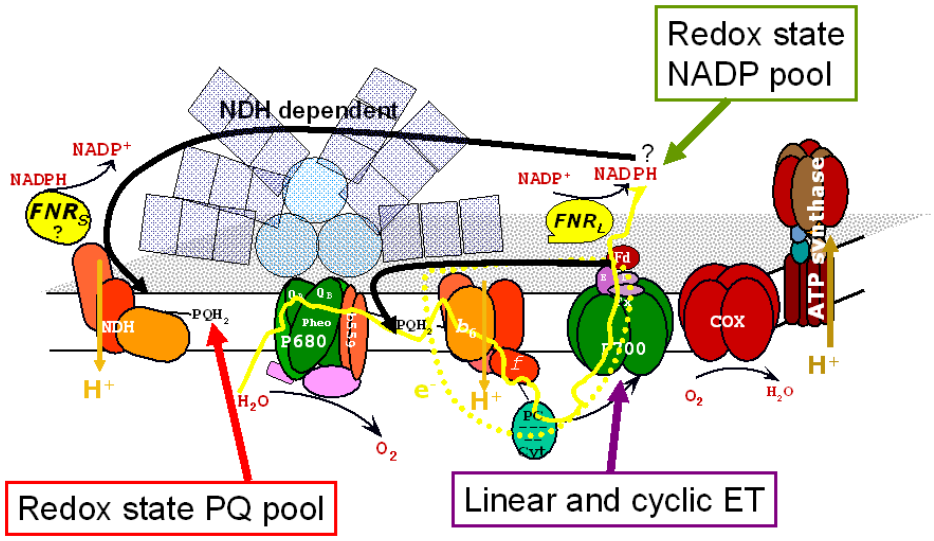

Figure 3.1 Scheme of the situation *in vivo*. Possible measurements are indicated. Adapted from G. Ajlani.

The FNR mutants and WT have been analyzed under different growth conditions. First, they were analyzed under standard photoautotrophic growth conditions. *Synechocystis* is usually grown under high CO_2 conditions (air enriched in CO_2 and HCO_3^- in the medium, detailed in Chapter 5) in the presence of light, oxygen and minimal medium. Several reports suggest a significant contribution of cyclic and pseudocyclic ET in the normal operation of photosynthesis in plants and cyanobacteria [Badger et al., 2000, Rumeau et al., 2007, Mi et al., 1992a,b]. The contribution of cyclic and pseudocyclic ET to overall ET was furthermore shown to be enhanced in conditions such as low CO_2 and high light in plants and cyanobacteria [Harbinson and Foyer, 1991, Miyake et al., 2005, Battchikova and Aro, 2007, Hackenberg et al., 2009, Eisenhut et al., 2007]. We compared the FNR mutants and WT under high- (HC) and low-CO_2 (LC) conditions.

3.1.1 NADP$^+$/NADPH ratio

The NADP pool redox state was the first phenotype that we characterized for the FS1 and MI6 mutants, that contain only FNR_S and FNR_L, respectively. NADPH build-up represents the output of PSI ET. A method has been previously used to determine NADPH fluorescence in *Synechocystis* [Mi et al., 2000]. We used the quantification of the cellular NADP$^+$ and NADPH to determine the NADP pool redox state because no blue fluorescence device was available.

We adapted a commercial kit to carry out separate extraction of NADP$^+$ and NADPH. Once extracted, the concentration of NADP$^+$ and NADPH were determined *via* colorimetric cycling and the NADP$^+$/NADPH ratio was calculated (see Chapter 5). We compared NADP$^+$/NADPH ratios in FS1 and MI6 mutants to WT.

The $NADP^+$/NADPH ratio in the WT was found to be 2.6 (see Table 3.1). This is in agreement with previously published values of 3 [Mi et al., 2000]. FS1 showed an increased $NADP^+$/NADPH ratio (4.3) compared to WT while MI6 showed a slight decreased $NADP^+$/NADPH ratio (2.0) compared to WT (Table 3.1).

These results are in agreement with our working hypothesis that is based on previously published results [Thomas et al., 2006]. On one side, FS1 showed a decreased growth under photoautotrophic conditions. The increased $NADP^+$/NADPH ratio indicates an insufficient build-up of NADPH during photoautotrophic growth. On the other side, MI6 showed a similar growth compared to WT.

Interestingly, previous work on mutant M55 in *Synechocystis* showed a lower redox state of the NADP pool. Values from 80%- [Mi et al., 2000] to up to 100%-reduced NADP pool [Cooley and Vermaas, 2001] were previously observed which corresponds to $NADP^+$/NADPH ratios of 0.25 and < 0.01. This can be correlated to the absence of the NDH-1 complexes in the M55 mutant. The authors in [Mi et al., 2000] concluded that the NDH-1 is one major site of NADPH reoxidation by respiratory or cyclic ETs. For FS1, we obtained differences in the redox state of the NADP pool that are opposite to that of M55 compared to WT. This indicates that FS1 is characterized by an increased level of NADPH reoxidation *via* respiratory or cyclic ETs. The increased $NADP^+$/NADPH ratio in FS1 may also be the result of an increased pseudocyclic ET involving the Mehler-reaction. This pathway involves Flv1 and Flv3 that are NAD(P)H dependent flavoproteins responsible for the light-dependent O_2 reduction (Chapter 1).

	$NADP^+$/NADPH
WT	2.6 ± 0.2
FS1	4.3 ± 0.8
MI6	2.0 ± 0.4

Table 3.1 Averaged $NADP^+$/NADPH molar ratios for WT, FS1 and MI6.

These measurements strengthen our working hypothesis assigning a specific role for each of the isoforms. In MI6 on one hand, FNR_L ensures a redox state of the NADP pool similar to that of the WT. We have seen in Chapter 1 that under photoautotrophic conditions, FNR_L is the major isoform in the WT. In FS1 on the other hand, FNR_S is unable of building up a similar $NADP^+$/NADPH ratio.

3.1.2 P700 oxidation kinetics using white light

Different actinic light qualities such as white light [Golding et al., 2004] and far-red (FR) light [Mi et al., 1992b] are applied to drive photosynthesis and to follow P700 oxidation and reduction kinetics. Also light quantities change from moderate continuous light to intense laser flashes.

Here, we present results obtained with continuous light illumination. First, we performed preliminary measurements on WT under white actinic light (white AL; Figure 3.2), which excites both PSI and PSII and drives linear ET. Figure 3.2 shows the kinetics of $P700^+$ formation and decay. After switching on the light, the P700 oxidation kinetics is characterized by a first fast rise which is followed by a dip phase and then a second slow rise results eventually in a steady-state. In Figure 3.2 the reduction kinetics of $P700^+$ is also shown. When the light is switched off, the oxidized P700 is reduced back to P700 rather quickly and the initial level of absorption is recovered. A second light-induced P700 oxidation is shown which exhibits a much less-pronounced dip phase.

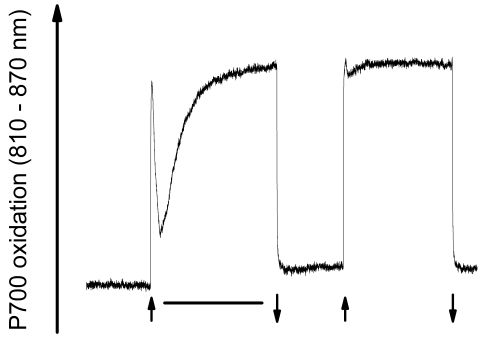

Figure 3.2 P700 oxidation and $P700^+$ reduction kinetics of WT strain under high CO_2. Characteristic curves for white light illumination are shown. Arrows under the trace indicate the light switch-on and switch-off. Horizontal bar represents 10 s.

Our observed complex kinetics of WT are in agreement with previously obtained traces of P700 oxidation [Trubitsin et al., 2005] and with blue-green fluorescence kinetics [Mi et al., 2000]. The latter authors identified the changes in blue-green fluorescence as changes in the redox state of the NADP pool. Dark-light-dark induction transients of blue-green fluorescence for *Synechocystis* WT and the *ndhB*-defective mutant M55 are shown in Figure 3.3A. This represents changes in the output of PSI ET and constitutes a complementary view to previous studies on the NADP pool redox state (see above).

WT exhibited the same two different fast and slow rising phases separated by the dip phase. The studies of [Mi et al., 2000] were carried out after repetitive dark-light-dark induction transients. This would explain why the amplitude of the dip resembles more the amplitude seen in the second P700 oxidation kinetics in Figure 3.2. The authors in [Mi et al., 2000] proposed the following explanations for the different phases upon onset of AL:

- First rapid rise: light driven accumulation of NADPH;
- Dip phase: oxidation of NADPH *via* Calvin cycle activity;

- Secondary rise phase: accumulation of NADPH as its oxidation in the Calvin cycle becomes limited, possibly going along with a limitation in ATP-supply;
- Stationary phase: matched rates of light-driven $NADP^+$ reduction and NADPH oxidation via the Calvin cycle.

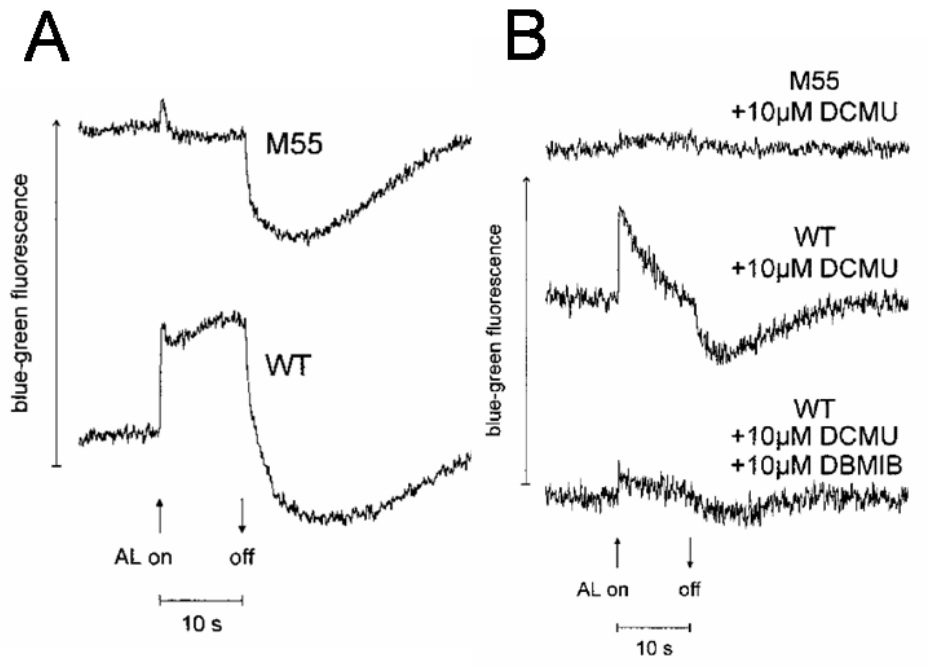

Figure 3.3 Dark-light-dark induction transients of blue-green fluorescence of *Synechocystis* WT and its *ndhB*-defective mutant M55. A: blue-green fluorescence of WT and M55. B: blue-green fluorescence of WT and M55 in the presence of inhibitors DCMU and DBMIB. Taken from [Mi et al., 2000].

P700 oxidation kinetics under white light observed in our study could also be explained in a similar way. The different phases would then correspond to P700 oxidation events as followed:

- First rapid rise: oxidation of P700 resulting in accumulation of NADPH;
- Dip phase: reduction of $P700^+$ results in decrease in light-driven $NADP^+$ reduction;
- Secondary rise: further oxidation of P700 resulting in accumulation of NADPH; Calvin cycle is limited by ATP;
- Stationary phase: matched rates of light-driven PSI oxidation and PSI reduction *via* lumenal (Pc/cyt c_6) and membrane (PQ) donors.

In Figure 3.3B dark-light-dark induction transients are shown in the presence of DCMU and DBMIB for WT and M55 mutant. These inhibitors of PSII and cyt b_6f, respectively, are widely

used as control measurements. The authors proposed that, in the WT, the transient reduction of NADPH in the presence of DCMU showed high capacity of cyclic electron flow around PSI *via* the NDH-1 which ensured reduction of the intersystem electron chain even when electron donation by PSII was abolished [Mi et al., 1992a,b]. The M55 mutant did not present a transient reduction of NADPH due to deletion of all NDH-1. The transient NADPH build-up may also be explained by the presence of prereduced donors of PSI. This reduced donor pool may be less important in the M55 mutant.

Another approach for observing P700 oxidation kinetics consists in exciting preferentially PSI. This can be achieved either by adding the PSII inhibitor DCMU or by changing the light quality to FR (> 695 nm). These approaches are regularly performed for measuring P700 oxidation and reduction kinetics in oxygen-evolving organisms [Mi et al., 1992b, Breyton et al., 2006, Ivanov et al., 2007, Lintala et al., 2007, DalCorso et al., 2008, Lintala et al., 2009]. We have chosen the FR light continuous illumination to characterize the WT and the FNR mutants.

3.1.3 P700 oxidation kinetics using far-red light

We have seen a clear increase in the $NADP^+$/NADPH ratio for the FS1 mutant. Here, we determined if the oxidized NADP pool in FS1 is due to an increase of an alternative electron transfer. We performed P700 oxidation and reduction kinetics on cells grown under standard photoautotrophic conditions. Under these conditions, the WT expresses FNR_L as the major isoform. The WT behavior should then be close to MI6, which can only express the FNR_L whereas FS1 may present differences in the kinetics as it contains only FNR_S.

Characteristic curves for FNR-mutant- and WT strains under HC are shown in Figure 3.4. Cells were dark adapted for 5′ and FR light was applied for 10 s. A very fast P700 oxidation rate with a half time of less than 0.1 s was observed for WT (Figure 3.4, black trace). In comparison with white-light illumination, no dip phase followed by a secondary slow rise were observed. This gives indications that the participation of PSII in ET is negligible under these conditions. This is explained by the use of FR light as actinic light source and the elevated PSI/PSII ratio in *Synechocystis* (PSI/PSII = 3) in comparison with *e.g.* plants. The oxidized P700 under steady-state conditions was around 80% in WT under HC, the WT exhibited the maximum amount of oxidized P700 under steady-state conditions compared to both FNR mutants. The WT under standard photoautotrophic growth is expected to perform linear ET as the major ET (see above). However, up to 20% of oxidized P700 that are missing for the WT under steady state may represent the contribution of cyclic and/or respiratory ET. We will in the following consider the WT as a reference for mainly linear ET compared to FNR mutants.

MI6, that contains only FNR_L, exhibits a similar P700 oxidation rate with a half-time of

around 0.1 s (see Figure 3.4A and B). The oxidized P700 under steady-state conditions was slightly decreased compared to wild type, around 75%. As MI6 is close to WT, we can conclude that this mutant probably performs linear electron transfer as the major electron transfer. Note that both strains contain FNR_L as the major or only FNR isoform under these conditions. Linear electron transfer is cartooned in Figure 3.5. We observed a quick rise in the signal corresponding to oxidized P700 for WT and MI6. This is represented with a positive charge on P700 in Figure 3.5. The electrons flow from P700 to $NADP^+$ *via* Fd and FNR_L. We will consider this flow of electrons as the output of PSI ET. Electrons are further evacuated *via* NADPH to the major electron sink: the Calvin cycle. We attribute this behavior to linear ET (Figure 3.5) but pseudocyclic ET may be present. WT and MI6 may perform alternative ETs as respiratory or cyclic ET that account for the difference with 100% oxidized P700 in the presence of DBMIB.

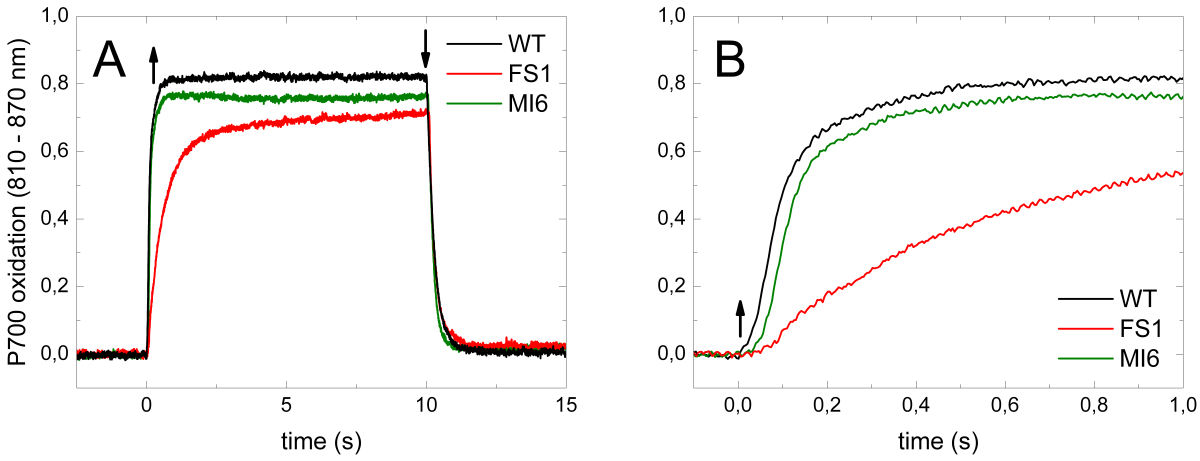

Figure 3.4 P700 oxidation and $P700^+$ reduction kinetics in high CO_2 of WT (black), FS1 (red) and MI6 (green) mutant strains. A: overall P700 oxidation and reduction kinetics. B: zoom on P700 oxidation kinetics. The three strains were shifted for their onset of illumination with WT being the first, MI6 the second and FS1 the last strain. The arrows indicate the FR light that was switched on and off. Switch-on and -off of the light could not be determined precisely (see Chapter 5).

FS1, that contains only FNR_S, showed very different P700 oxidation kinetics (Figure 3.4A and B). First, a much smaller P700 oxidation rate was observed with a half time of around 0.6 s -6 times increased compared to WT. Second, a decrease in the maximal $P700^+$ signal on the same time scale was observed. After 10 s of FR light, no real steady state was reached in this mutant under HC (around 65% at a pseudo-steady state). P700 oxidation and reduction in FS1 are depicted in Figure 3.6. In addition to the output of electrons by linear ET, $P700^+$ may be rapidly reduced or the output of PSI may be perturbed, leading to slowed P700 oxidation kinetics.

The P700 oxidation kinetics of WT, MI6 and FS1 are in agreement with the NADP pool redox states found for the three strains. These measurements revealed a striking difference in the P700

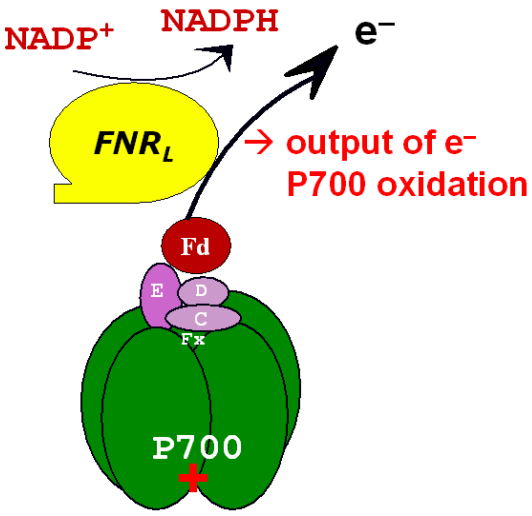

Figure 3.5 Representation of P700 oxidation by linear ET in WT and MI6.

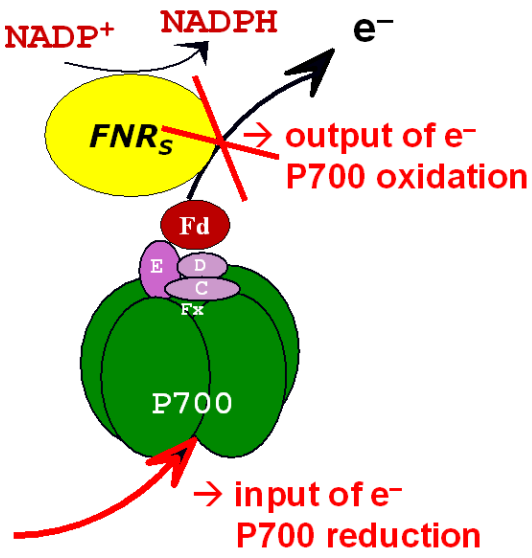

Figure 3.6 Representation of P700 oxidation and reduction in FS1.

oxidation kinetics of FS1 that has to be further studied by P700 oxidation measurements in the presence of inhibitors and complementary *in vivo* measurements as PQ pool redox state and immunoblots to determine the metabolic pathways involved.

P700 oxidation kinetics in the presence of inhibitors

The difference in the phenotype of FS1 compared to WT and MI6 was further investigated during control measurements. This consisted in adding inhibitors of electron flow. Measurements with sequential addition of DCMU, MV and finally DBMIB are shown in Figure 3.7 for WT. DCMU, MV and DBMIB are known to inhibit PSII activity (PQ reduction), recombination reactions involving $P700^+$ and cyt b_6f activity (PQ oxidation), respectively. In the presence of DCMU, the WT was characterized by a small rate increase of P700 oxidation and similar $P700^+$ reduction kinetics. We concluded that the contribution of PSII photochemistry was very small under HC (FR light, high PSI/PSII ratio in *Synechocystis*).

In the presence of DCMU and MV, the WT was characterized by a small rate increase in the P700 oxidation kinetics and a significant rate decrease in the $P700^+$ reduction kinetics (Figure 3.7). On one hand, we concluded that the contribution of recombination reactions involving $P700^+$ was rather small. On the other hand, the contribution of pseudocyclic and cyclic ET with this control measurement was not possible (see Chapter 5). We focused on the P700 oxidation kinetics as this step was especially affected in FS1.

In the presence of DCMU, MV and DBMIB, once the available reduced donors are exhausted, a very fast P700 oxidation is observed. In addition, all oxidizable P700 should be observable in the presence of DBMIB. Surprisingly, the WT was characterized by a somewhat lower steady-state of the $P700^+$ signal. We have no plausible explanation for this decrease in steady-state of $P700^+$. There may be some interference of the three different inhibitors. However, the P700 oxidation kinetics was further accelerated and the $P700^+$ reduction kinetics was slowed down (Figure 3.7).

The P700 oxidation kinetics for MI6 are shown in Figure 3.7. Overall, the kinetics in the presence of DCMU, MV and DBMIB were similar for MI6 *vs.* WT. Only small increases in the rate of P700 oxidation were observed in the presence of DCMU and MV. This indicated a small contribution of PSII photochemistry and recombination reactions involving $P700^+$ in this mutant. In the presence of DBMIB, a further significant though small increase in the rate of P700 oxidation was observed. We have obtained evidence that WT and MI6 exhibit mainly linear ET as the contribution of recombination reactions involving $P700^+$ was rather small and the kinetics in the presence of MV and DBMIB did not show much difference. The difference between MV and DBMIB traces indicated that alternative ET such as cyclic and respiratory ET were poorly inhibited in the presence of MV (see Chapter 5).

The P700 oxidation kinetics for FS1 are shown in Figure 3.7. The sequential addition of inhibitors (DCMU/MV/DBMIB) resulted in a sequential increase in the rate of P700 oxidation. Thus a small contribution of PSII photochemistry is apparent in the FS1 P700 oxidation. Addition of MV resulted in a significant increase of P700 oxidation kinetics (Figure 3.7). This increase can be attributed to inhibition of recombination reactions and/or to partial inhibition of cyclic/respiratory ET. The addition of DBMIB resulted in a strong increase in the rate of P700 oxidation (Figure 3.7). The cyt b_6f complex is involved in respiratory and cyclic ETs. The addition of DBMIB eliminates all these ETs and thus very fast P700 oxidation kinetics were obtained. The difference between MV and DBMIB indicated a major contribution of cyclic and/or respiratory ET in FS1.

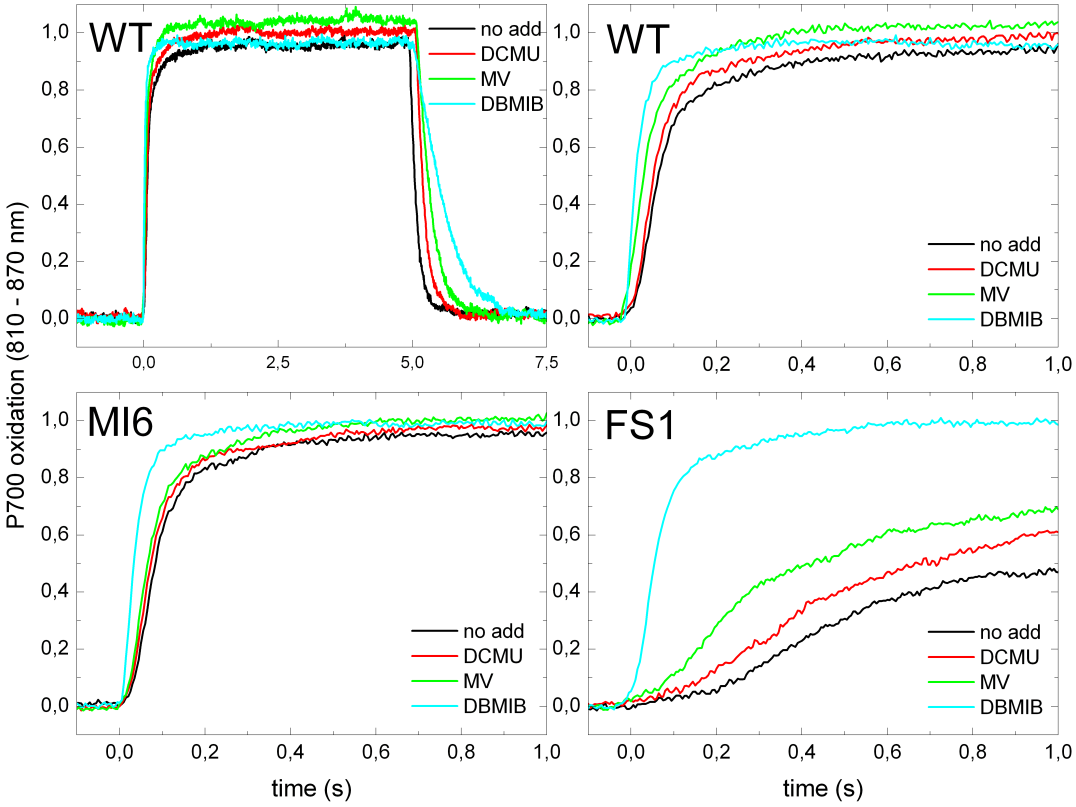

Figure 3.7 P700 oxidation and $P700^+$ reduction in the presence of inhibitors. WT left: overall P700 oxidation and reduction kinetics shown. WT right: zoom on P700 oxidation kinetics. MI6 and FS1: zoom on P700 oxidation kinetics. Traces in black, red, green and cyan correspond to no addition and sequential additions in the order of DCMU, MV and DBMIB, respectively.

Induction of cyclic ET under low CO_2

We have obtained strong indications that FS1 may present increased respiratory or cyclic electron flows. To further test this hypothesis, we repeated some of the measurements under LC. Several reports presented evidence that LC induces cyclic and pseudocyclic ET [Harbinson and Foyer, 1991, Miyake et al., 2005, Hackenberg et al., 2009]. We may be able to confirm the involvement of FNR_S in the reoxidation of NADPH under LC.

LC decreases growth dramatically. We first checked the impact of LC on the pigments composition and confirmed the expected phenotype of decrease in PBP content in the three strains (Chapter 5). We will present detailed comparison of WT and mutant strains under LC concerning the P700 oxidation kinetics. If cyclic/respiratory ET was observed under HC for the FS1 mutant, we may be able to observe the same effect on WT under conditions of induced cyclic and pseudocyclic ETs (LC).

We repeated the P700 oxidation and reduction kinetics under LC. First, we will present the overall P700 oxidation and reduction kinetics and then focus on the P700 oxidation kinetics for WT, FS1 and MI6. In Figure 3.8, characteristic curves for the WT and mutant strains are shown after growth under LC for 24 hours. WT exhibited a rate decrease in P700 oxidation kinetics. Furthermore, the steady-state of oxidized P700 was also significantly smaller. MI6 on the contrary did not exhibit significant changes. Under LC, MI6 exhibited the largest steady-state amount of oxidized P700. FS1 under LC exhibited enhancement of the phenotype present in HC, the half time for the P700 oxidation rate almost doubled and kinetics had clearly two phases. The steady-state oxidized P700 was slightly smaller and similar to that of the WT under the same conditions. The oxidation kinetics for WT, MI6 and FS1 are now compared separately under HC and LC.

WT was adapted to LC for 24 hours or for entire growth (8-9 days). Figure 3.9 shows WT kinetics under HC and LC on a 1 s time scale. As a function of duration in CO_2 limitation, the rate of P700 oxidation decreased. The half time for P700 oxidation increased from 0.09 s to 0.12 s and finally 0.29 s for HC, LC for 24h and entire growth, respectively (Table 3.2). The steady state of oxidizable P700 decreased in the same way. The steady state decreased from initially 80% to 65% and finally to 45% (Table 3.2).

Under LC the WT P700 oxidation resembles that of FS1. Linear ET was hindered due to CO_2 limitation. Alternative electron sinks may operate to evacuate the electrons accumulated on the PSI acceptor side. If cyclic/respiratory ET was observed under HC in FS1, the WT may be able to induce the same alternative ET under LC. We hypothesize that the induction of that behavior in the WT correlates with FNR_S accumulation in the WT. This would be in agreement with an increased FNR_S expression under high light [Thomas et al., 2006].

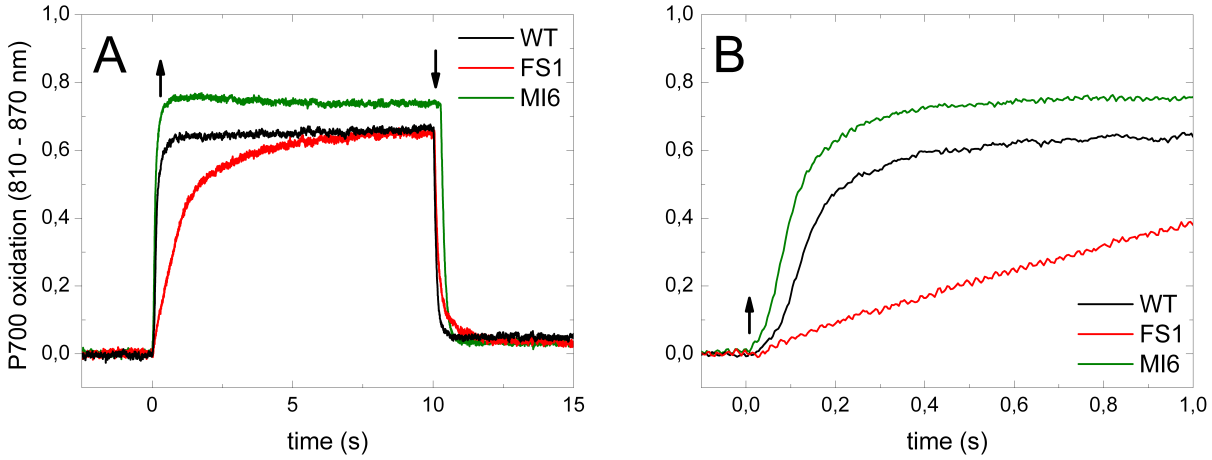

Figure 3.8 P700 oxidation and reduction kinetics in low CO_2 of WT (black), FS1 (red) and MI6 (green) mutant strains.

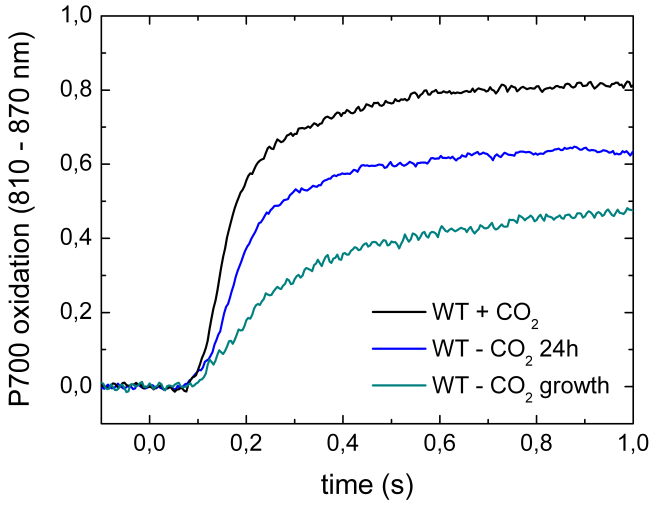

Figure 3.9 P700 oxidation kinetics under high and low CO_2 for WT. WT kinetics in high CO_2 (black), low CO_2 for 24h (blue) and in low CO_2 for 8 days (dark cyan) are shown.

For the two mutants, we compared the P700 oxidation kinetics on a shorter time scale (1 s) after 24 hours in LC to those in HC. Contrary to the WT, MI6 did not exhibit changes in the P700 oxidation rate under LC (Figure 3.10A). The half time for the P700 oxidation rate did not change significantly and was 0.12 s and 0.104 s for HC and LC, respectively (Table 3.2). The steady state of oxidized P700 was as well unmodified (75% under both conditions; Table 3.2). Overall, the P700 oxidation kinetics of MI6 did not change under LC for 24 hours.

It is interesting to note that the mutant unable to produce FNR_S (MI6) was unable to induce the LC behavior as the WT. MI6 was still characterized by a major linear ET under LC. An alternative electron sink may be pseudocyclic ET in the MI6 mutant. Under HC, only a small contribution of pseudocyclic ET must occur in MI6 and WT. Flv3, that is responsible for the Mehler-reaction in *Synechocystis*, is induced under LC [Eisenhut et al., 2007]. The pseudocyclic ET involving the Mehler-reaction can thus result in fast P700 oxidation kinetics under CO_2 limitation eventually involving FNR_L.

For FS1, oxidation kinetics are shown on a 1 s time scale in Figure 3.10B. Similar phenotypes were observed for FS1 under HC and LC but the phenotype was more pronounced in LC. The half time for the P700 oxidation rate increased about two-fold from 0.56 s to 1.1 s after 24 hours under LC (Table 3.2). The oxidized P700 after 10 s of FR light under quasi-steady state was decreased but to a lower extent than in the WT. In HC, the oxidized P700 under quasi-steady state was about 70%, and decreased to about 65% in LC for 24 hours (Table 3.2).

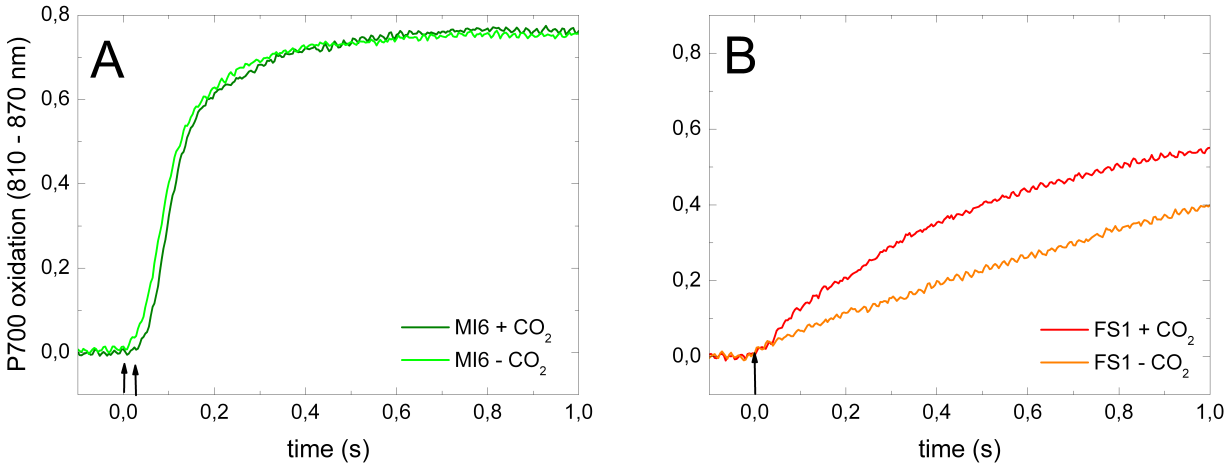

Figure 3.10 P700 oxidation kinetics under high and low CO_2 of MI6 (A) and FS1 (B) mutant strains. A: MI6 in high CO_2 (olive) and in low CO_2 for 24h (green). B: FS1 in high CO_2 (red) and in low CO_2 for 24h (orange).

We identified a clear phenotype for FS1 under HC which is accentuated under LC. FS1 is characterized by a decreased rate of P700 oxidation and a decrease of the quasi-steady state of oxidized P700. Under LC, the WT, contrary to MI6, exhibited a behavior similar to that of FS1.

oxidation	WT		MI6		FS1	
	$t_{1/2}$ (s)	$P700^+$ (%)	$t_{1/2}$ (s)	$P700^+$ (%)	$t_{1/2}$ (s)	$P700^+$ (%)
$+CO_2$	0.09 ± 0.02	80	0.12 ± 0.01	75	0.56 ± 0.08	70
$-CO_2$ 24h	0.12 ± 0.02	65	0.104 ± 0.001	75	1.1 ± 0.23	65
$-CO_2$ growth	0.29 ± 0.14	45	-	-	-	-

Table 3.2 P700 oxidation kinetics and steady state of $P700^+$ under high and low CO_2 for WT, MI6 and FS1.

These results could correlate with the accumulation of the two FNR isoforms in the three different strains. MI6 does not contain FNR_S. WT is expected to induce significant amounts of FNR_S under stress conditions as was observed under N-starvation and high-light conditions. Further immunoblotting experiments are necessary to confirm this hypothesis. FS1 does not contain FNR_L and FNR_S will be either mobile or attached to other complexes (cyt b_6f or NDH-1). Attachment to these membrane complexes may promote respiratory/cyclic ET *via* NADPH oxidation with NADPH being accumulated by linear ET or catabolism.

3.1.4 PQ reduction in the dark

We compared ET from the stromal donors to PQ pool in the WT and FNR mutants. The electron flow was monitored by the transient increase in chlorophyll fluorescence (apparent F_0) which occurs in darkness after a period of AL illumination [Schreiber et al., 1986]. This transient F_0 rise is attributed to reduction of the PQ pool by the stromal reductants accumulated during illumination period. The WT and MI6 showed similar transient F_0 increase with a maximum between 20-30 s after AL was switched off but FS1 showed significantly larger transient F_0 increases (Figure 3.11).

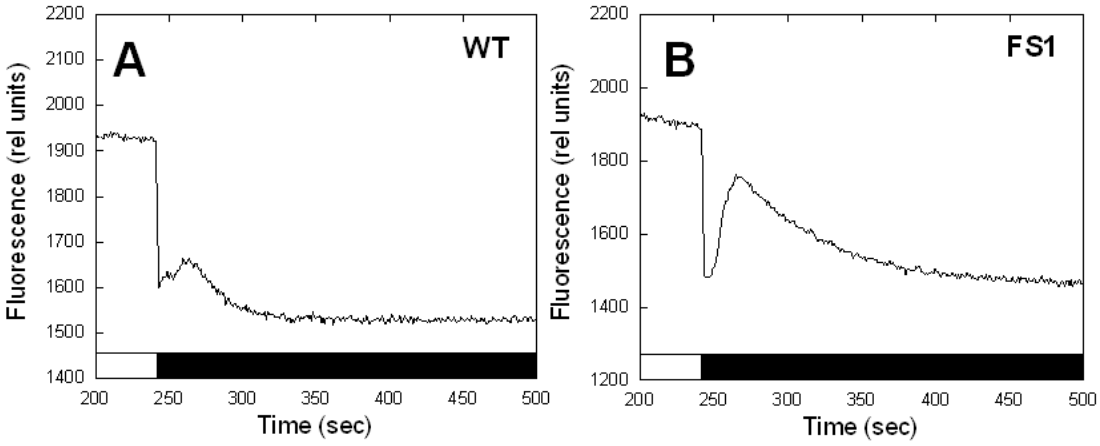

Figure 3.11 Transient PQ reduction for WT (A) and FS1 (B). Kindly provided by Dr. Kirilovsky.

This transient F_0 increase was previously observed in cyanobacteria and plants [Shikanai et al., 1998, Deng et al., 2003, Ma and Mi, 2005, Lintala et al., 2009]. It was also shown that this transient increase was significantly reduced in M55 and in the *ndhB*-deficient *Arabidopsis* mutant [Shikanai et al., 1998]. The authors concluded that the NDH-mediated cyclic ET was missing but that Fd-mediated cyclic ET may contribute to remaining F_0 increase. Thus, the increased PQ pool reduction in the dark in FS1 may well be due to an increased NDH-mediated cyclic ET.

3.2 Conclusion

Different ET pathways are operating in WT, MI6 and FS1 and we will present a model for the association of FNR_L and FNR_S in view of our *in vivo* results. We obtained evidence that cyclic or respiratory ET is induced when FNR_S accumulates. We propose that FNR_S transfers electrons to NDH-1 acting as the dehydrogenase module (Figure 3.12A). Binding of FNR to NDH-1 was proposed previously [Vara and Gómez-Lojero, 1986, Guedeney et al., 1996, Matsuo et al., 1998] and the NDH-1 dependent pathway is expected to be the major cyclic ET in cyanobacteria [Mi et al., 1992a,b]. We propose that this cyclic/respiratory ET is NDH-1 dependent and involves FNR_S.

The increase of such an alternative electron flow will result in a reduced PQ pool, a slow-down of the rate of P700 oxidation and an oxidized NADP pool. The NADP pool redox state gave indications that the mutant lacking FNR_L (FS1) presents an increased reoxidation of NADPH. Slower P700 oxidation excluded a large contribution of pseudocyclic ET and our control measurements in the presence of inhibitors showed that recombination reactions involving $P700^+$ are also not a major contributor in the FS1 P700 oxidation phenotype. Studies on PQ pool reduction in the dark resulted in an increased PQ pool reduction in FS1 compared to WT and MI6. These observations strongly indicate an increase of NADPH oxidation and subsequent injection of electrons to the PQ pool *via* NDH-1.

FNR_L is known to be attached to the PBS and is probably tuned to perform $NADP^+$ reduction involved in linear ET (Figure 3.12B). WT under HC and MI6 that contain FNR_L as the major and the only isoform, respectively, performed essentially linear ET and maybe some pseudocyclic ET.

We analyzed the FNR mutants and the WT for their phenotypes under LC conditions that are known to induce cyclic ET [Harbinson and Foyer, 1991, Miyake et al., 2005]. FS1 showed under LC an enhancement of the phenotype present under HC thus indicating an induction of the respiratory or cyclic ET. The WT under LC behaved like FS1 under HC and LC conditions and we propose that the WT P700 oxidation correlates with FNR_S accumulation under LC which would be in agreement with previous results under other stress conditions (high light and N-starvation) [Thomas et al., 2006].

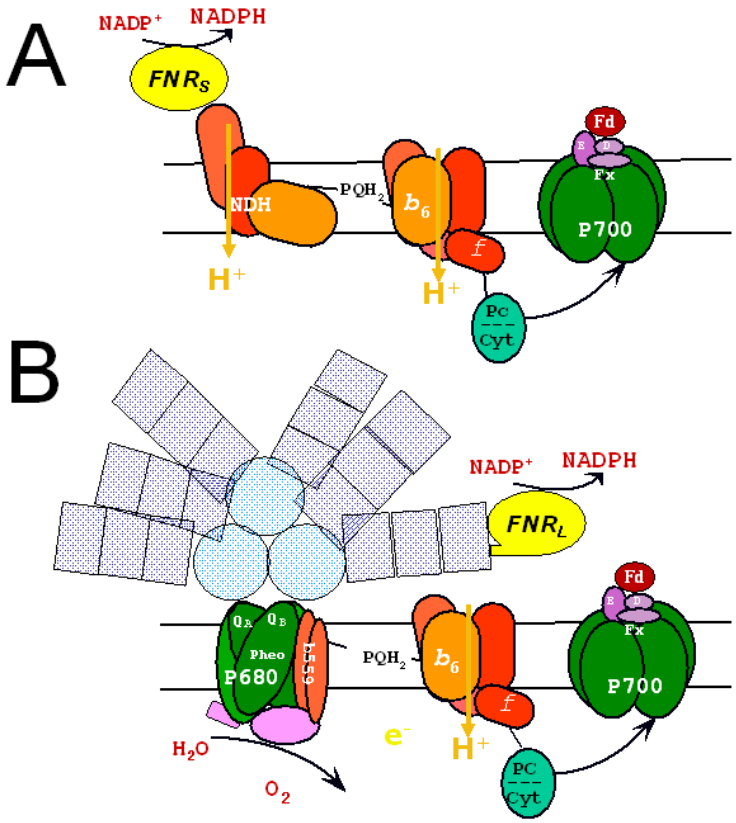

Figure 3.12 Representation of the possible association of FNR_S with NDH-1 (A) and the known association of FNR_L with PBS (B).

LC conditions also lead to Flv3 accumulation [Eisenhut et al., 2007] which promotes pseudocyclic ET and we found evidence that, under LC conditions, MI6 presents pseudocyclic ET. The absence of the LC behavior in MI6 further confirmed the involvement of FNR_S in this alternative ET present in FS1 and WT under LC.

To summarize, we obtained promising results from the *in vivo* studies indicating respiratory or cyclic ET that is dependent on NDH-1 and involves FNR_S. Further studies are necessary to establish the mechanism of the backflow of electrons into the PQ pool and the exact partners involved in addition to FNR_S. First, we will perform immunoblotting on cells grown under LC in order to confirm the accumulation of FNR_S and of NDH-1 complexes in the WT. Second, fluorescence induction measurements can confirm informations previously obtained about the PQ pool redox state. These measurements are needed to compare the WT and the FNR mutant strains. This will result in a more complete *in vivo* view and should help us understand the mechanism of respiratory/cyclic ET.

Chapter 4

Conclusions and Perspectives

4.1 Conclusions

We are interested in determining the respective roles of the two FNR isoforms in *Synechocystis*. FNR_L is attached to the PBS [Schluchter and Bryant, 1992] due to the linker-like domain that FNR_S is lacking [Thomas et al., 2006]. We wanted to determine the function of FNR_L attachment to the PBS. Previous studies strongly indicated that FNR_L sustains photoautotrophic growth ($NADP^+$ reduction) and FNR_S is expressed under stress conditions and during heterotrophic growth (NADPH oxidation; working hypothesis) [Thomas et al., 2006].

We performed *in vitro* and *in vivo* studies to determine differences due to intrinsic activities and differences due to *e.g.* enzyme localization. As FNR catalysis involves intermolecular ETs involving various steps that are concentration-dependent, it is not straightforward to compare the results obtained during *in vitro* and *in vivo* studies.

In vitro studies resulted in three major differences between FNR_S and the purified FNR_L-phycobilisome subcomplex (FNR_L-PC) beside overall similar enzymologic properties. The strongest effect was observed for the affinity of Fd_{ox} to FNR_L-PC *vs.* FNR_S during NADPH oxidation, with a decreased affinity for FNR_L-PC. This effect was attributed to steric hindrance in FNR_L-PC. As the dissociation of Fd_{ox} can be rate-limiting for $NADP^+$ reduction [Batie and Kamin, 1984a, Carrillo and Ceccarelli, 2003], this difference may result in an increased $NADP^+$ reduction for FNR_L-PC. Fd affinities are in agreement with the growth characteristics of the FNR mutants.

Steric hindrance was also observed during single FNR reduction involved in $NADP^+$ reduction for FNR_L-PC which was in contradiction with our working hypothesis. The third major difference was a larger NADPH affinity for FNR_L-PC. An increased NADPH affinity may result

in an enhanced $NADP^+$ reduction by FNR_L whereas FNR_S may still perform NADPH oxidation under heterotrophic or stress conditions, when NADPH concentration is higher.

The differences we obtained for cyanobacterial FNR isoforms do not parallel the differences obtained for plant root and leaf isoforms. In addition to different gene products that are present in different tissues, several plant FNR isoforms were found that are present in the same tissues [Okutani et al., 2005, Gummadova et al., 2007, Lintala et al., 2009]. These plant leaf isoforms may parallel the situation in cyanobacteria as they are present in the same tissues and may catalyze the different FNR reactions.

In parallel to the *in vitro* studies, we performed *in vivo* studies of the WT and FNR mutants expressing only one isoform. It is clear that FNR localization is different for FNR_S and FNR_L. FNR_L is known to be attached to the PBS but FNR_S may be soluble, membrane-attached [Palatnik et al., 1997], attached to cyt b_6f [Zhang et al., 2001] or NDH-1 [Vara and Gómez-Lojero, 1986, Guedeney et al., 1996, Matsuo et al., 1998]. In addition to that, substrate availability (Fd_{ox}/Fd_{red} and $NADP^+$/NADPH) is probably important for the catalyzed reaction. *In vivo* studies are characterized by the presence of various metabolic pathways that interact with each other (cyt b_6f, PQ pool, NADP pool etc.).

Under photoautotrophic growth, the NADP pool was found to be more oxidized in the mutant lacking FNR_L (FS1) than in the mutant lacking FNR_S (MI6) and the WT. We envisaged increased NADPH oxidation by alternative electron flows in FS1 (cyclic, pseudocyclic or respiratory ET), we excluded pseudocyclic ET and recombination reactions involving $P700^+$ and found further evidence for an increase of respiratory/cyclic ET by measuring P700 oxidation and PQ pool reduction in the dark.

If the FS1 phenotype is FNR_S-dependent, the WT should under conditions of FNR_S induction present the same phenotype. WT is known to induce FNR_S under stress conditions as N-starvation and high light [Thomas et al., 2006]. High light and LC are conditions known to induce pseudocyclic and cyclic ET [Harbinson and Foyer, 1991, Miyake et al., 2005, Hackenberg et al., 2009]. Thus we analyzed the P700 oxidation kinetics for WT, MI6 and FS1 under LC.

WT presented under LC a similar phenotype as FS1 under HC and LC. FS1 presents thus an LC-phenotype. This indicates that the FS1 phenotype is due to the presence of FNR_S. We proposed the involvement of FNR_S in the NDH-1-dependent NADPH oxidation that was previously accumulated from reductive (photosynthesis) or oxidative (carbohydrate) metabolism. MI6 mutant under LC may present an increase of pseudocyclic ET.

We clarified the issue of intrinsic activities *in vitro* of the two isoforms and obtained promising results from the *in vivo* studies indicating respiratory or cyclic ET that is dependent on NDH-1 and involves FNR_S. Further studies are necessary in order to determine the mechanism of the backflow of electrons into the PQ pool and the exact partners involved.

4.2 Perspectives

Both *in vitro* and *in vivo* studies have perspectives. First of all, product inhibition of NADPH oxidation and the corresponding K_I may be measured for FNR_S. The affinities for $NADP^+$ and NADPH are thought to be similar, but inhibition can provide more detailed informations on this issue. Another idea for the *in vitro* studies is based on reconstitution studies. A scaled-up purification of FNR_L could be obtained using a His-tagged FNR_L overexpressed in *E.coli* for further biochemical and biophysical studies, *e.g.* crystallography. Crystallography may give answers to the issue of conformation changes upon complex formation. This may validate differences observed between the two isoforms. In Figure 4.1, the crystal structures for the separately obtained subunit of phycobilisome - PC hexamer - and the oxidoreductase - FNR_S - are shown.

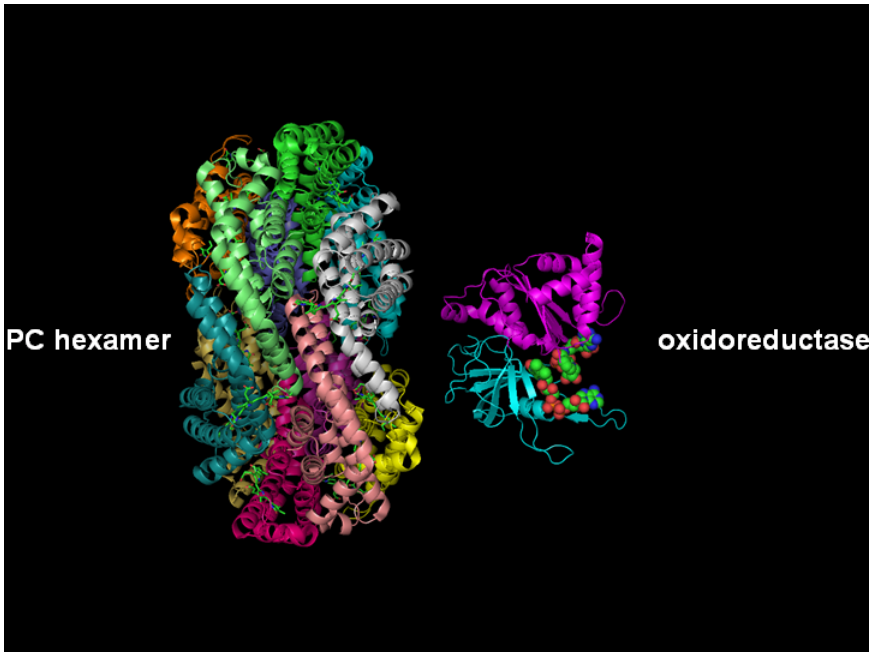

Figure 4.1 Crystal structures of FNR_S and the PC hexamer are shown side by side for size comparison and for giving a possible suggestion for the orientation of the FNR-PC complex. This Figure was created by P. Sétif using available structural data for PC hexamer and *Anabaena* FNR in the pdb.

Further *in vivo* studies are needed to determine the respective roles of the FNR isoforms present in facultative heterotrophic cyanobacteria. To determine the mechanism of the NADPH-dependent cyclic ET and the exact partners involved, several complementary studies might be useful. First, we need to confirm the accumulation of FNR_S in the WT under LC *via* immunoblotting. Second, we must confirm the informations previously obtained about the PQ pool redox state in the WT and mutants under HC and LC *via* chlorophyll fluorescence induction measurements. Third, the NADP pool redox state under low CO_2 conditions is expected to exhibit a

more oxidized NADP pool in the WT and FS1 that can be determined using the commercial kit. In addition, a module is now commercially available for the PAM spectrometer for real-time measurements of NADPH fluorescence [Schreiber and Klughammer, 2009]. This would give insights in the $NADP^+$ reduction kinetics *in vivo*.

Finally, control measurements need to be carried out under LC *via* P700 absorption. In addition, a saturating pulse method was developed to distinguish donor and acceptor side limitation in PSI [Klughammer and Schreiber, 2008]. Thus, we may obtain further informations to explain the phenotype of FS1.

In addition to the presented *in vitro* and *in vivo* perspectives, other techniques may be carried out to study the role of the FNR isoforms. Approaches such as transcriptomic studies with DNA microarrays may be used to determine differences between the mutants and WT. A genetic approach is currently underway to determine the role of the 5′ region of the mRNA of the gene *petH* for the accumulation of FNR_S.

These studies would result in a more complete *in vivo* view and clarify the important issue of the NADPH-dependent cyclic ET into the PQ pool that seems to be enhanced in FS1.

Chapter 5

Materials and Methods

5.1 Bacterial growth conditions

The cyanobacterium *Synechocystis* sp. PCC6803 was grown photoautotrophically in an orbital incubator at 34°C in a CO_2-enriched atmosphere (5 L min^{-1}) and under continuous light (60 $\mu E\ m^{-2}s^{-1}$). Allen's medium [Allen, 1968] was modified as follows: 30 μM ferric citrate, 3 μM disodium EDTA, 30 mM sodium nitrate, 250 μM potassium phosphate, 250 μM sodium carbonate, 10 mM sodium bicarbonate and microelements as in Allen's medium [Ughy and Ajlani, 2004]. All chemicals were purchased from Sigma-Aldrich.

For $NADP^+$/NADPH quantification, 50 mL were harvested during midexponential phase at OD_{580nm}=1.3. The growth conditions were photoautotrophic in the presence of high CO_2 (HC) or low CO_2 (LC) (HC: bicarbonate 10 mM in the medium and 5 L min^{-1} in the incubator) which resulted in doubling times of 8 or around 24 hours, respectively.

Complete growth under HC, LC for 24 hours and entire growth under LC was carried out. For 24 hours under LC, cells were grown under HC until OD_{580nm}(1 cm)=1.7. The cells were harvested and transferred in LC conditions about 24 hours before P700 oxidation measurements. After 8 to 9 days of exponential growth, the 50 mL cell cultures reached the OD needed to perform P700 oxidation measurements. For all three conditions, 25-50 mL were harvested during mid-exponential phase. They were transferred to fresh medium prior to *in vivo* P700 oxidation measurements. The chlorophyll concentration was adjusted to 10 μg chlorophyll * mL^{-1}.

5.2 Biochemical techniques

5.2.1 Chlorophyll quantification

No difference in the chlorophyll *a* content per cell was found between the mutants and the WT strain. This is why the calibration to a similar chlorophyll content permits a correct comparison between mutant and WT strains.

10 to 50 µL culture was harvested in 1.5 mL eppendorff tubes and resuspended in 1 mL 100% methanol. Once in methanol, excess light should be avoided in order to avoid chlorophyll to pheophytin conversion. Vortexing for a few seconds extracted 100% of the chlorophylls. One minute of centrifugation at 21,400 g was performed to remove insoluble materials. The supernatant was transferred into cuvettes and the absorbance was measured at 666 nm. The absorbance was divided by 76 (extinction coefficient chlorophyll in 100% methanol in mL mg^{-1} cm^{-1}) to obtain the chlorophyll concentration (mg/mL).

5.2.2 Purification of photosystem I, ferredoxin and short FNR isoform

Photosystem I (PSI) was purified according to [Rogner et al., 1990]. Thylakoid membranes were obtained from French press broken cells after extensive washing with ice-cold 20 mM Tricine, 1 mM EDTA, pH 7.8. PSI was obtained after solubilization with 1% (w/v) β-DM and purified on a sucrose density gradient. The upper green band consisting of highly-enriched monomeric PSI particles was dialyzed against 20 mM Tricine/NaOH, pH 7.8, and 0.03% β-DM and concentrated by ultracentrifugation. The last step of the purification procedure was anion-exchange chromatography on a Mono Q column. One modification to [Rogner et al., 1990] was the substitution of ammonium sulfate for magnesium sulfate as eluting salt.

Synechocystis recombinant ferredoxin (Fd) was overexpressed in *Escherichia coli* according to [Barth et al., 2000]. Ferredoxin was supplied thanks to Dr. B. Lagoutte and Ms. V. Mary. A Fd-rich soluble fraction from *Thermosynechococcus elongatus* was a gift from Dr. A. Boussac. Fd from this soluble fraction was purified to homogeneity using the same procedure as for *Synechocystis* Fd.

Recombinant Ferredoxin:NADP oxidoreductase (FNR) was overexpressed in *Escherichia coli* according to [Cassan et al., 2005]. A construct with deletion was designed in a pQE 60 expression vector for overproducing a 34-kDa FNR (corresponding to FNR_S). Overexpressed FNR_S was precipitated between 50 and 70% ammonium sulfate saturation. The recovered pellet was solubilized in 20 mM Tricine, pH 7.8, first roughly purified on DE52 (Whatman), and the FNR fraction was further purified by anion exchange chromatography on a Hitrap Q-Sepharose (Amersham Biosciences). The last purification step was performed by hydrophobic chromatography on a

phenyl-Sepharose matrix (HiLoad phenyl-Sepharose 16/10 from Amersham Biosciences). The reverse salt gradient was from 1.6 to 0 M ammonium sulfate in 80 mM Tricine, pH 7.8. FNR fractions were extensively dialyzed against 10 mM Hepes buffer, pH 7.0.

5.2.3 Purification of FNR_L-PC

Phycobilisome isolation

Phycobilisome (PBS) complexes were isolated [Elmorjani et al., 1986, Ajlani et al., 1995] from CBH under conditions that are known to preserve inter-subunit interactions [Gantt and Lipschultz, 1972], *i.e.* high KP (potassium phosphate pH 8) concentrations. All steps were carried out at room temperature except breaking of cells. An antiprotease cocktail (Complete, Roche) was used during the isolation of FNR_L-PC. The procedure was as follows.

18 L cultures of CBH were harvested at late exponential phase and washed twice in 0.5 M KP buffer and resulted in more than 20 mg cells and about 5-6 g of cells were used as starting material for each purification. The cells were resuspended in 15 mL 0.8 M KP, then vortexed 5-6 times for 40 s in an ice-cooled bead beater (Biospec) with half the volume of glass beads (0.1 mm diameter). Triton X-100 was added to the broken cells to a final concentration of 2% (v/v). After incubation for 30 min in the dark, unbroken cells and debris were removed by centrifugation at 25,000 g for 30 min at 18°C. If necessary, a second cycle of Triton X-100 treatment was performed to reduce chlorophyll contamination. 4-8 mL of supernatant were loaded onto sucrose step-gradients prepared as follows in 35 mL ultracentrifuge tubes: 6 mL of 1.0 M, 9 mL of 0.75 M, 9 mL of 0.5 M, and 3 mL of 0.25 M sucrose in 0.9 M KP buffer. The gradients were spun for 12-16 h in a Beckman SW-27 rotor at 26,000 rpm at 20°C. The PBS complex was collected in the 0.75 M zone.

For reconstitution assays the purified PBS complex was mixed with a molar excess of purified FNR_L (c(PBS)=0.08 µM; 0.95 µM FNR_S; 0, 0.16, 0.32, 0.64 and 0.95 µM FNR_L) and incubated for 1-2 hours. After this, a second run of sucrose step-gradients was performed overnight and the fractions were analyzed for their contents in PBS complex and FNR enzyme *via* SDS-PAGE. Densitometric analysis of SDS-PAGE were calibrated to L_{RC}, assuming that each PBS contains 6 L_{RC}.

An additional step to resuspend the PBS in a different buffer and to concentrate the sample was performed. Harvested PBSs from the 0.75 M zone of sucrose were diluted four times with 0.9 M KP buffer and ultracentrifuged at 44,000 rpm for 6-12 h at 18°C. The PBS complex, that sedimented at the bottom of the tubes, was resuspended in 150 mM KP.

IMAC purification of FNR_L-PC

Thanks to previous work a His-tag was inserted between the enzymatic domain and the linker-like domain of FNR_L (between Gly 98 and Ser 99). Thus, the FNR_L-PC complex could be purified simply following an IMAC (Immobilized Metal Affinity Chromatography) on a Ni-resin column in low phosphate conditions in order to separate PC from the PBS complex. All the following steps were performed at 4°C on ice.

The PBS complex was resuspended in 150 mM KP buffer in order to dissociate the complex in its subunits: allophycocyanin from the core and phycocyanin from the rods. This dissociation was performed overnight at 4°C in the presence of a protease inhibitor without EDTA (Roche). After preparation of the Ni-resin (ProBond, Invitrogen, France) by washing with milliQ water and 250 mM KP, the Ni-resin was added to the sample. After 1h incubation (for binding), 2 steps of washing in batch with 250 mM KP were performed. Then, the mixture of sample and Ni-resin was transferred to a column and the resin was allowed to settle. Up to 20 times the bed volume of the resin was used to wash. The elution was performed with 150 mM KP buffer containing 150 mM imidazole.

The eluted fractions were concentrated using Vivaspin concentrators (100 kDa cutoff). A first estimation of the concentration was performed by UV-Vis spectroscopy. An absorption coefficient ε_{620nm} of 2,370,000 $M^{-1}cm^{-1}$ was used for the phycocyanin hexamer [Glazer, 1989]. SDS-PAGE was performed according to [Ughy and Ajlani, 2004] to control the purification. 12% of acrylamide was used in a Tris/Tricine gel. The following fractions were loaded at 0.3 OD_{620nm} · mL except the elution fraction which was loaded at about 0.03 OD_{620nm} · mL: entire PBS complex (CBH), not-bound (NB), wash 1 (W1), wash 2 (W2), elution (E). The samples were concentrated by TCA precipitation (10% w/v) prior to loading. Proteins were visualized using Coomassie Blue stain (see Figure 2.1B in Chapter 2).

Gel filtration of FNR_L-PC

A final step consisted in checking the size of the PC complex with FNR_L bound to it and eliminating smaller complexes on a Superdex 200 preparative grade (26/85, bed volume 165 mL, void volume 64 mL) gel filtration column (GE Healthcare) with optimal separation of molecular mass between 10 and 600 kDa.

The column was washed with 3 bed volumes of ethanol and distilled water at a flow rate of 0.2 and 0.1 mL/min respectively. After this, the column was equilibrated with about 5 bed volumes of 250 mM KP buffer at a flow rate of 0.5 mL/min. The sample was injected at a maximal volume of 300 µL and was run at a flow rate of 0.5 mL/min. The peak was eluted with the same buffer after 2 hours.

The molecular mass of the purified FNR_L-PC complex was determined using calibration of the column by Vitamin B_{12} (1.35 kDa), myoglobin (17.0 kDa), ovalbumin (44.0 kDa), γ globulin (158 kDa) and thyroglobulin (670 kDa) as standards. Gel filtration was followed at three wavelengths to check total protein, FAD and PC absorptions at 280 nm, 460 nm and 620 nm, respectively and was further analyzed by SDS-PAGE and UV-Vis. The major fraction was pooled, concentrated with Vivaspin (100 kDa cutoff) and used as the enzyme preparation. All the other fractions were concentrated using Centricon (30 kDa cutoff) and analyzed on SDS-PAGE. Polypeptide quantifications were achieved by measuring the Coomassie blue density of the different bands using an Image scanner II (GE Healthcare). As a further control, different molar amounts of FNR_L-PC were loaded on an SDS-PAGE and the optical density of the FNR_L polypeptide was quantified with known concentrations of recombinant FNR_L that were loaded in neighboring lanes.

5.2.4 Quantification of apoprotein and active protein

FNR apoprotein quantification

Two samples of recombinant FNR_S and recombinant FNR_L were calibrated on the basis of the absorption maximum of the FAD (ε_{461nm}=9,000 $M^{-1}cm^{-1}$; see below) and analyzed for their protein content using the micro-BCA protein assay (Pierce Biotechnology). The protein amounts were found to be smaller than expected (92% and 91% of the calculated values for FNR_S and FNR_L, respectively), which must be ascribed to some underestimation by the micro-BCA assay. From these measurements, we conclude that there is practically no FAD-free protein in our FNR samples. 461/280 nm absorbance ratios of 0.128 and 0.122 were measured for FNR_S and FNR_L, respectively.

FNR holoenzyme quantification

Biochemical extraction is one approach to release the FAD from the holoenzyme using SDS for denaturating the enzyme [Aliverti et al., 1999]. First, the concentration of the $FNR_{S/L}$ sample was determined with an extinction coefficient of 10,500 $M^{-1}cm^{-1}$ at 461 nm [Forti, 1966, Foust et al., 1969]. Then, a minimal volume of concentrated SDS was added directly in the spectrometer cuvette (final concentration 0.2%). The molar extinction coefficient and the maximal wavelength of the cofactor FAD was altered during denaturation. Released FAD after denaturation of the protein is characterized by an extinction coefficient of 11,300 $M^{-1}cm^{-1}$ at 450 nm. A direct comparison between native and denatured protein can be established in this way. Six different

measurements on six different FNR_S preparations have resulted in a corrected extinction coefficient in the native enzyme. Instead of 10,500 $M^{-1}cm^{-1}$ at 461 nm from [Forti, 1966][Foust et al., 1969], a lower value of 9,000 ± 100 $M^{-1}cm^{-1}$ at 461 nm has been obtained.

The FAD can also be extracted by TCA precipitation of the proteins. First, the enzyme concentration was determined using the same extinction coefficient as for the SDS denaturation. Then, TCA was added to a final concentration of 5% (w/v) and the pellet was washed at the same concentration of TCA. The collected supernatants were extracted three times with diethylether to eliminate TCA. The sample was further neutralized by adding 0.1 M Na phosphate pH 7 [Engel and Massey, 1971]. Released FAD in the buffered solution was characterized by an extinction coefficient of 11,300 $M^{-1}cm^{-1}$ at 450 nm. The obtained molar extinction coefficient of 9,070 $M^{-1}cm^{-1}$ at 461 nm was similar to that obtained by SDS denaturation. Therefore, SDS denaturation and TCA extraction give identical results.

5.3 *In vitro* studies

5.3.1 NADPH oxidase activities

NADPH and horse-heart cytochrome *c* (cyt *c*) were purchased from Sigma-Aldrich. The enzymatic reactions were monitored with an Uvikon-XL spectrophotometer. The initial velocities were fitted with Origin 7.5 (OriginLab Corp., Northampton, MA) to obtain Michaelis-Menten curves.

Ferricyanide reduction was measured at room temperature (RT) in duplicate with NADPH and potassium ferricyanide ($K_3[Fe(CN)_6]$) as the electron donor and acceptor molecules, respectively [Zanetti et al., 1980]. A range of different $FNR_{S/L}$ concentrations (0.025-0.1 μM) was mixed with an excess of potassium ferricyanide (0.7 M) and 5 mM $MgCl_2$ in 150 mM KP. The reactions were initiated by the addition of a range of different NADPH concentrations (25-400 μM). The absorption decrease at 420 nm (reduction of ferricyanide) was recorded to determine the steady-state kinetic parameters. Reduction of two ferricyanide corresponds to oxidation of one NADPH. This factor of two was taken into account for determining the rate of NADPH oxidation. This rate of oxidized μM NADPH/(s × μM FNR; [s^{-1}]) was plotted against the initial substrate concentration of NADPH (μM).

The Fd-mediated cyt *c* reduction of FNR_L-PC was measured at 25°C in triplicate with Fd and cyt *c* acting as intermediate and terminal electron acceptors [Shin and Pietro, 1971, Zanetti et al., 1980]. Fd from *Thermosynechococcus elongatus* was used for these experiments as it was available in large quantities. A few control measurements were performed with *Synechocystis* Fd giving results identical to those obtained with *Th. elongatus* Fd. The reaction was started by the addition

of an excess of NADPH (400 μM final concentration). Kinetic parameters for the Fd-dependent cyt *c* reductase activity were determined. This was achieved by varying the concentrations of Fd (2.5-40 μM) in the reaction mixtures and monitoring the resulting absorption increase at 550 nm, corresponding to the reduction of cyt *c* used in excess (40 μM final concentration). The same type of measurements were performed in the presence of the inhibitor $NADP^+$ in triplicates. A concentration of 50 μM $NADP^+$ was used and the Lineweaver-Burk plots of $1/v_0$ *vs.* $1/Fd^0_{ox}$ were analyzed for the FNR_L-PC isoform.

5.3.2 $NADP^+$ reductase activities

Flash-absorption measurements with a time resolution of 10 μs were performed as described previously [Cassan et al., 2005] at 22°C. Laser excitation (700 nm) was provided by a dye laser (Continuum, Excel Technology, Villebon sur Yvette, France) pumped by a frequency-doubled Nd-Yag laser and was saturating for P700 photochemistry. Conditions were chosen to eliminate any actinic effect of measuring light.

All the spectroscopic measurements were performed under aerobic conditions in 150 mM KP containing 30 mM NaCl and 0.03% (w/v) β-dodecyl maltoside (Biomol, Hamburg, Germany). Sodium ascorbate (2 mM) and 2.6-dichlorophenolindophenol (5-25 μM) were used to reduce the oxidized P700 between two consecutive flashes. The PSI concentration was estimated using the absorption coefficient ε_{800nm}=7,740 $M^{-1}cm^{-1}$ for $P700^+$ [Cassan et al., 2005]. For all flash experiments, the kinetics are shown after substraction of the $P700^+$ contribution. This was done by measuring, in the absence of Fd, the differential absorption coefficients of $P700^+$ at 520/540 nm and at 800 nm, using methyl viologen (MV) as an electron acceptor that results in fast reoxidation of the terminal PSI acceptor $(F_A,F_B)^-$. Using this procedure, the differential absorption coefficient of $P700^+$ at 520/540 nm was found to be 50 %/34 % that of $P700^+$ at 800 nm ($\Delta\varepsilon_{520nm}$=3.9 $mM^{-1}cm^{-1}$ ≈ 7.74 $mM^{-1}cm^{-1}$ x 0.50; $\Delta\varepsilon_{540nm}$= 2.6 $mM^{-1}cm^{-1}$ ≈ 7.74 $mM^{-1}cm^{-1}$ x 0.34). The kinetics probed at 800 nm were substracted, after multiplication by the normalization factor of 0.50/0.34. In this way, all absorption changes are associated with the reduction of the electron acceptors, *i.e.* those due to (F_A,F_B), Fd and FNR.

Single reduction of FNR

Single reduction of FNR by reduced Fd was triggered by flash excitation of PSI. These experiments were performed in the presence/absence of $NADP^+$ with FNR in excess over PSI. Under this condition, a single reduction event is favored where the neutral protonated semiquinone is produced. These measurements were performed at 520 nm, which corresponds to an absorption minimum of the PSI/FNR_L-mixture (Fd absorbance is small compared to those of PSI and PC).

Moreover, a large signal is expected at 520 nm for formation of the FNR semireduced form FNR_{sq} as shown in the calculated differential absorption spectrum for FNR single reduction by Fd (Figure 5.1) [Cassan et al., 2005].

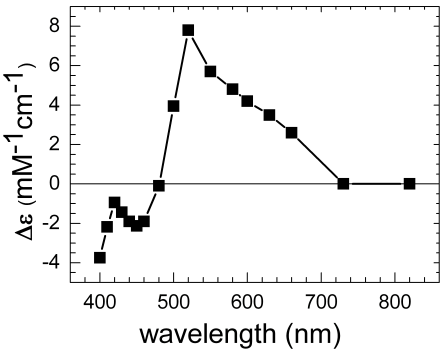

Figure 5.1 Calculated differential absorption spectrum for FNR single reduction by Fd.

Multiple catalytic turnover

In order to promote multiple catalytic turnover, the PSI concentration was more than 10-fold greater than the enzyme under investigation ($FNR_{S/L}$). Under these conditions FNR receives two electrons from Fd and NADPH is formed via hydride transfer. This multiple turnover reaction was monitored by the reoxidation of Fd_{red} at 540 nm. This wavelength was chosen because of the minimal PSI absorption, which allows actinic effects of the measuring light to be minimized in these measurements made on a long time scale [Cassan et al., 2005].

5.3.3 Fittings and calculations

Single reduction of FNR

The kinetic model used to interpret the experiments of single FNR reduction is shown in Chapter 2. It involves two reactions, the first one describes Fd reduction by PSI and the second one corresponds to the redox equilibrium of the first reduction of FNR by Fd_{red}. Such a model does not take into account complex formation and dissociation, because of the large ionic strength of the medium, which impedes formation of complexes [Hurley et al., 2002, Setif et al., 2002] and hence only considers second-order processes. We assume also that the PSI charge separation leading to the formation of $(F_A,F_B)^-$ is much faster than the subsequent steps since it occurs in the submicrosecond range [Brettel and Leibl, 2001]. The kinetic analysis is further simplified as the

experiments were performed under conditions where one partner is in large excess over the other one for each of the reactions: $Fd_{ox} > PSI_{red}$, $FNR_{ox} > Fd_{red}$, $Fd_{ox} > FNR_{sq}$. This allows the system of time-differential equations corresponding to the model to be solved analytically, using the three following first-order rates: $k_{rFd}=k_r \cdot [Fd]$ with [Fd] being the total Fd concentration ($[Fd_{red}] < [Fd_{ox}]$), $k_{red}=k_1 \cdot [FNR]$ with [FNR] being the total FNR concentration ($[FNR_{sq}] < [FNR_{ox}]$), $k_{ox}=k_{-1} \cdot [Fd]$. The solution is then the following:

$$[PSI_{red}](t)=[PSI] \cdot e^{-k_{rFd}t}$$

$$[Fd_{red}](t)=[PSI] \cdot \left[\frac{k_{rFd}-k_{ox}}{k_{ox}+k_{red}-k_{rFd}} \cdot e^{-k_{rFd}t} - \frac{k_{red}k_{rFd}}{(k_{ox}+k_{red}-k_{rFd})(k_{ox}+k_{red})} \cdot e^{-(k_{ox}+k_{red})t} + \frac{k_{ox}}{k_{ox}+k_{red}}\right]$$

$$[FNR_{sq}](t)=[PSI] \cdot \left[\frac{-k_{red}}{k_{ox}+k_{red}-k_{rFd}} \cdot e^{-k_{rFd}t} + \frac{k_{red}k_{rFd}}{(k_{ox}+k_{red}-k_{rFd})(k_{ox}+k_{red})} \cdot e^{-(k_{ox}+k_{red})t} + \frac{k_{red}}{k_{ox}+k_{red}}\right]$$

with [PSI] being the total PSI concentration. The Excel solver (V. 2003, Microsoft, USA) was used to fit the experimental results with the above equations.

Multiple catalytic turnover

When measuring multiple turnover event from reoxidation of Fd_{red}, the decay kinetics were able to be fitted with a single exponential component [Cassan et al., 2005]:

$$[Fd_{red}(t)]= [Fd_{red}]_{t=0} \cdot e^{-k_{FNR}t}$$

$$\left(\frac{d[Fd_{red}(t)]}{dt}\right) = -k_{FNR}\,[Fd_{red}(t=0)] \cdot e^{-k_{FNR}t}$$

Initial rate: $-\left(\frac{d[Fd_{red}]_{t=0}}{dt}\right) = +k_{FNR}\,[Fd_{red}]_{t=0}$

Without FNR: $-\left(\frac{d[Fd_{red}]_{t=0}}{dt}\right) = +k_{noFNR}\,[Fd_{red}]_{t=0}$

The initial decay rate k_{noFNR} in the absence of FNR was substracted from the exponential rates k_{FNR} in its presence. The initial turnover rate was then calculated from the equation:

$$-\frac{\left(\frac{d[Fd_{red}]}{dt}\right)_{t=0}}{[FNR]} = (k_{FNR} - k_{noFNR}) \cdot \frac{[PSI]}{[FNR]} \text{ as } [PSI] = [Fd_{red}]_{t=0}$$

This rate can also be calculated from rate k_1 of Equation 2.1.4 (Chapter 2) when this reaction is rate-limiting. From Equation 2.1.4, the decay rate of Fd_{red} is:

$$\frac{dFd_{red}}{dt} = -k_1\,[Fd_{red}]\,[FNR_{ox}] + k_{-1}\,[Fd_{ox}]\,[FNR_{sq}]$$

which gives for t=0:

$(d\,[Fd_{red}]/dt)_{t=0} = -k_1\,[Fd_{red}]_{t=0}\,[FNR]$ with [FNR] being the total concentration of FNR. With $[PSI] = [Fd_{red}]_{t=0}$, one gets:

$$-\frac{\left(\frac{d[Fd_{red}]}{dt}\right)_{t=0}}{[FNR]} = k_1[PSI] \qquad (5.3.1)$$

5.4 *In vivo* studies

5.4.1 $NADP^+$/NADPH quantification

The Enzychrom^{TM} $NADP^+$/NADPH assay kit (Gentaur, France) was used to quantify the $NADP^+$/NADPH ratio. $NADP^+$ is transformed into NADPH by the enzyme glucose dehydrogenase (GDH) in the presence of an excess of glucose (electron donor; Reaction 5.4.1). Two samples are used for separate extraction of $NADP^+$ or NADPH. NADPH will reduce 5-methylphenazinium methosulfate (PMS, electron transferring system; Reaction 5.4.2) and then 3- (4,5-dimethylthiazol-2-yl) -2,5-diphenyl-2/H/ -tetrazolium bromide (tetrazolium salt MTT) as final electron acceptor (absorbing at 565 nm; Reaction 5.4.3). The oxidation of NADPH into $NADP^+$ is the only rate-limiting step (**rls**; Reaction 5.4.2).

$$NADP^+ + H^+ \xrightarrow{\text{GDH, glucose}} NADPH \tag{5.4.1}$$

$$NADPH + PMS_{ox} \xrightarrow[\textbf{rls}]{} NADP^+ + H^+ + PMS_{red} \tag{5.4.2}$$

$$PMS_{red} + MTT_{ox} \longrightarrow PMS_{ox} + MTT_{red} \quad \textbf{(565 nm)} \tag{5.4.3}$$

The different steps for the calibration curve, the reconstitution of the working reagent and the sample preparation were performed as indicated by the supplier. We first tried to optimize the assay for cuvette based measurements. Then we calibrated the assay using $NADP^+$. Finally, we measured the $NADP^+$ and NADPH. From these values we could calculate the respective $NADP^+$/NADPH ratio for WT and the mutants. Ratios were calculated for five independent measurements, averaged and standard deviations were calculated.

The calibration curve was done using a $NADP^+$ standard from 0-10 µM in duplicates. The difference in optical density at 565 nm t=30' - t=0' was linear up to 10 µM (ΔOD_{565nm}=0.2-1.6) and up to 6 µM, the best linearity was obtained. This corresponded to ΔOD=1.1 (Figure 5.2). Values for [$NADP^+$] above 10 μM ($\Delta OD_{565nm} > 1.73$) led to saturation and could not be fitted.

In this way, the mutants and the WT were quantified for their NADP pool redox state. These measurements were performed with cells in their mid-exponential growth phase.

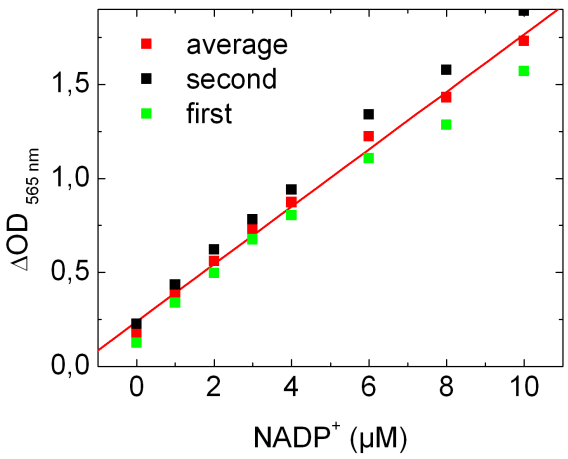

Figure 5.2 Calibration curve of $NADP^+$ quantification.

5.4.2 Absorption spectra +/- CO_2

The phycobiliprotein-antenna (PBP-antenna) -, chlorophyll- and carotenoid-content in the cells can be determined by their characteristic absorbance maxima. Whole cell absorption spectra were recorded for two different growth conditions. In order to limit scattering, several precautions were taken. First, cells were harvested and suspended carefully in a solution of 2 M sucrose in 0.9 M KP. Second, the spectra were recorded on a Aminco^{TM} DW 2 spectrometer (OLIS INC., Bogart, Georgia, USA). Here, the detector is very close to the sample in order to minimize light scattering. We measured absorption spectra of HC- and LC grown cells for the WT, MI6 and FS1 strains. Absorption spectra give us informations on the impact of the CO_2 limitation on the cell pigment composition in the WT and the mutants.

Spectra were normalized as follows. First, the absorbance of 750 nm was set to zero. Second, the spectra of the mutant and WT strains were normalized at 680 nm to the same chlorophyll *a* absorption maximum. In this way, we determined the difference in absorbance at 620 nm, characteristic for PBP in the PBS antenna.

Absorption spectra under high and low CO_2 For WT, the absorption spectra under HC and LC are shown in Figure 5.3. The absorbance at 620 nm was found to be 86% under LC compared to HC. This means that LC conditions result in a decrease in PBP content.

For MI6 and FS1, the absorption spectra under HC and LC are shown in Figure 5.4A and B. Compared to HC, the absorbance at 620 nm under LC was found to be 87% and 80% for MI6 and FS1, respectively. These values are very close to WT. Thus, all the three strains exhibit a similar

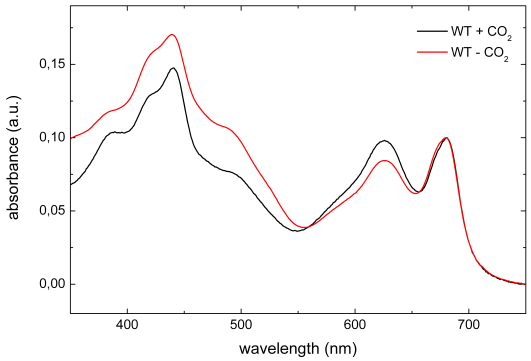

Figure 5.3 Normalized absorbance spectra of WT in high (black) and low (red) CO_2.

decrease in PBP content under LC. No significant difference is thus expected concerning PBP degradation and the strains seem to be equally stressed. They can be further compared in their P700 oxidation phenotypes under LC.

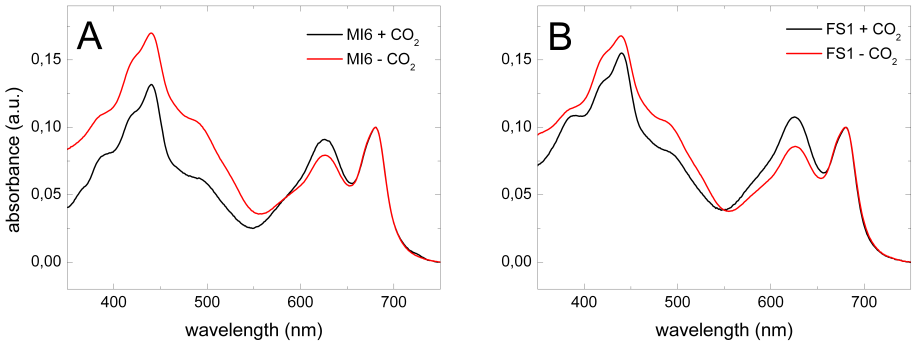

Figure 5.4 Normalized absorbance spectra of MI6 (A) and FS1 (B) in high (black) and low (red) CO_2.

5.4.3 P700 oxidation and reduction kinetics

FS1, MI6 and WT were characterized by measuring *in vivo* P700 oxidation and $P700^+$ reduction. The $P700^+$ absorption changes around 810 nm were measured with a pulse amplitude modulated fluorometer [Schreiber, 1986, Schreiber et al., 1986].

The pulse amplitude modulated system (PAM 101, 102, 103 chlorophyll fluorometer, H. Walz, Effeltrich, Germany) is equipped with fiber-optics connecting a suspension cuvette with a LED emitter, a photodiode detector and a source for continuous actinic light [Schreiber, 1986, Schreiber et al., 1986]. A modulate measuring beam (1 µs intense pulses from LED applied repetitively at 1.6/100 kHz) was used in addition to the non-modulated actinic light. The amplifier system selected the modulated signal, so that actinic illumination can be varied within wide ranges without corresponding artefactual signal changes. The obtained signal reflects relative

fluorescence yield (fluorescence intensity/light intensity). Figure 5.5 taken from [Schreiber, 1986] shows a schematic diagram of the measuring system.

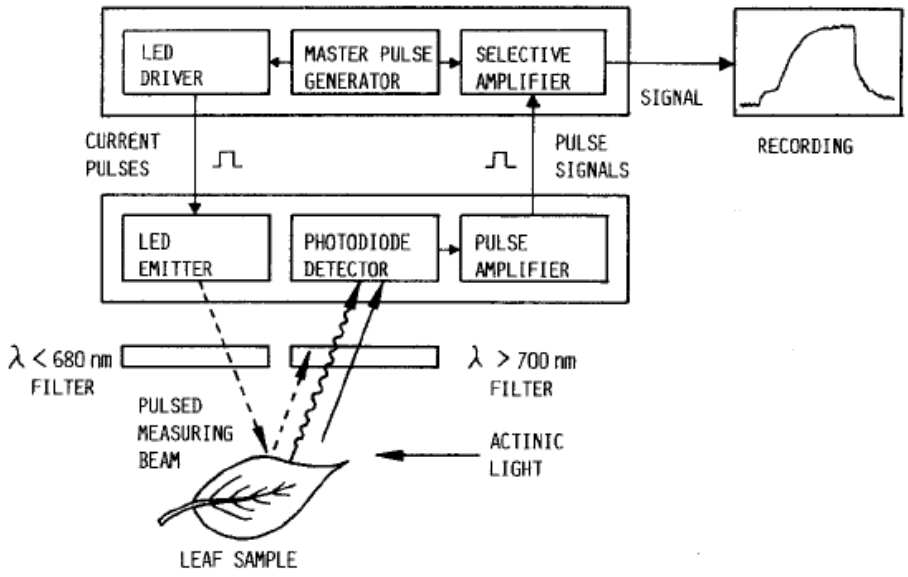

Figure 5.5 Schematic diagram of the pulse amplitude modulation (PAM) chlorophyll fluorometer

The only unit that needs to be exchanged when changing from fluorescence to absorbance measurements is the emitter-detector unit of the fluorometer [Schreiber et al., 1988]. The redox changes of P700 were measured *via* the broad band increase in absorbance caused by the $P700^+$ cation-radical at 810 nm.

In detail, the changes concern:

- 650 nm LED for fluorescence excitation is substituted by a 830 nm LED (Type HE 8811, Hitachi)
- Short-pass filter in front of the LED is exchanged with a high-pass filter (RG 780, Schott). This filter eliminates the short wavelength tail emission of the 830 nm LED
- The RG 9 filter in front of the photodiode is exchanged with a RG 780 filter. With this filter, the photodetector is protected against all visible and photosynthetically active light.

Sample preparation and analysis Measurements were performed with dark-adapted (5') cells. The cell suspensions were stirred and thermostated at 32°C. Actinic light illumination used was white light (2800 µmol s^{-1} m^{-2}) and FR light (100 µmol s^{-1} m^{-2}; about 25 photons absorbed per PSI and per s). P700 oxidation kinetics were carried out under HC and LC. Control measurements

were carried out by sequential addition of inhibitors DCMU (20 μM), MV (2 mM) and DBMIB (20 μM).

$P700^+$ exhibits an absorption around 800 nm. The contribution of plastocyanin (Pc) is expected to be the same between 810 and 870 nm. By substracting the 870 nm signal from the 810 nm signal, Pc contribution at 810 nm should be efficiently substracted by the set-up. Curves were analyzed and normalized to the maximum amount of oxidizable P700 in the presence of DBMIB. The set-up used for our measurements did not permit to define exactly the starting point. Thus, short lags before rising signals occurred could not be identified between mutant and WT strains. We will assume that addition of MV in our experiments fully inhibits the recombination processes involving $P700^+$. Moreover, our experiments with MV addition on FS1 show that, in that case, MV does not or only partially inhibits cyclic ET.

5.4.4 Monitoring of the transient increase in chlorophyll fluorescence

Cyclic ET around PSI was monitored by the transient increase of dark-level chlorophyll fluorescence after actinic light (AL) [Shikanai et al., 1998]. The PAM spectrometer introduced above was used in the chlorophyll fluorescence mode (repetitive pulses at 1.6 kHz). The saturation pulse method of chlorophyll fluorescence was used for these studies. Cell suspensions were calibrated to 3 μg chlorophyll mL^{-1}.

After 5′ dark adaptation, strong white AL was applied for around 2′ and NADPH was accumulated [Schreiber et al., 1986]. After switching off AL, a transient PQ pool reduction in the dark was observed in the mutants and WT.

Bibliography

J. P. Abrahams, A. G. W. Leslie, R. Lutter, and J. E. Walker. Structure at 2.8 a resolution of F1-ATPase from bovine heart mitochondria. *Nature*, 370(6491):621–628, 1994.

N. Adir. Elucidation of the molecular structures of components of the phycobilisome: reconstructing a giant. *Photosynthesis Research*, 85(1):15–32, July 2005.

G. Ajlani, C. Vernotte, L. DiMagno, and R. Haselkorn. Phycobilisome core mutants of synechocystis PCC 6803. *Biochimica et Biophysica Acta (BBA) - Bioenergetics*, 1231(2):189–196, Sept. 1995.

T. Akashi, T. Matsumura, T. Ideguchi, K. ichiro Iwakiri, T. Kawakatsu, I. Taniguchi, and T. Hase. Comparison of the electrostatic binding sites on the surface of ferredoxin for two ferredoxin-dependent enzymes, Ferredoxin-NADP+ reductase and sulfite reductase. *Journal of Biological Chemistry*, 274(41):29399–29405, Oct. 1999.

A. Aliverti, B. Curti, and M. Vanoni. Identifying and quantitating FAD and FMN in simple and in iron-sulfur-containing flavoproteins. *Methods Mol Biol*, 131:9–23, 1999.

A. Aliverti, R. Faber, C. M. Finnerty, C. Ferioli, V. Pandini, A. Negri, P. A. Karplus, and G. Zanetti. Biochemical and crystallographic characterization of Ferredoxin-NADP+ reductase from non-photosynthetic tissues. *Biochemistry*, 40(48):14501–14508, Dec. 2001.

A. Aliverti, W. R. Hagen, and G. Zanetti. Direct electrochemistry and EPR spectroscopy of spinach ferredoxin mutants with modified electron transfer properties. *FEBS Letters*, 368(2):220–224, July 1995.

A. Aliverti, V. Pandini, and G. Zanetti. Domain exchange between isoforms of ferredoxin-NADP+ reductase produces a functional enzyme. *Biochimica et Biophysica Acta (BBA) - Proteins & Proteomics*, 1696(1):93–101, 2004.

J. F. Allen. Photosynthesis of ATP—Electrons, proton pumps, rotors, and poise. *Cell*, 110(3): 273–276, 2002.

J. F. Allen. Cyclic, pseudocyclic and noncyclic photophosphorylation: new links in the chain. *Trends in Plant Science*, 8(1):15–19, 2003.

M. M. Allen. Simple conditions for growth of unicellular blue-green algae on plates. *Journal of Phycology*, 4(1):1–4, 1968.

A. A. Arteni, G. Ajlani, and E. J. Boekema. Structural organisation of phycobilisomes from synechocystis sp. strain PCC6803 and their interaction with the membrane. *Biochimica et Biophysica Acta (BBA) - Bioenergetics*, 1787(4):272–279, Apr. 2009.

K. Asada. The water-water cycle in chloroplasts: scavenging of active oxygens and dissipation of excess photons. *Annual Review of Plant Physiology and Plant Molecular Biology*, 50(1):601–639, 1999.

M. R. Badger, G. D. Price, B. M. Long, and F. J. Woodger. The environmental plasticity and ecological genomics of the cyanobacterial CO2 concentrating mechanism. *Journal of Experimental Botany*, 57(2):249–265, 2006.

M. R. Badger, S. von Caemmerer, S. Ruuska, and H. Nakano. Electron flow to oxygen in higher plants and algae: rates and control of direct photoreduction (Mehler reaction) and rubisco oxygenase. *Philosophical Transactions of the Royal Society of London. Series B, Biological Sciences*, 355(1402):1433–1446, Oct. 2000.

P. Barth, I. Guillouard, P. Setif, and B. Lagoutte. Essential role of a single arginine of photosystem i in stabilizing the electron transfer complex with ferredoxin. *J. Biol. Chem.*, 275(10):7030–7036, Mar. 2000.

C. J. Batie and H. Kamin. Association of ferredoxin-NADP+ reductase with NADP(H) specificity and oxidation-reduction properties. *The Journal of Biological Chemistry*, 261(24):11214–11223, Aug. 1986.

C. Batie and H. Kamin. Electron transfer by ferredoxin:NADP+ reductase. rapid-reaction evidence for participation of a ternary complex. *J. Biol. Chem.*, 259(19):11976–11985, Oct. 1984a.

C. Batie and H. Kamin. Ferredoxin:NADP+ oxidoreductase. equilibria in binary and ternary complexes with NADP+ and ferredoxin. *J. Biol. Chem.*, 259(14):8832–8839, July 1984b.

N. Battchikova and E. Aro. Cyanobacterial NDH-1 complexes: multiplicity in function and subunit composition. *Physiologia Plantarum*, 131(1):22–32, Sept. 2007.

P. Bennoun. Evidence for a respiratory chain in the chloroplast. *Proceedings of the National Academy of Sciences of the United States of America*, 79(14):4352–4356, July 1982.

A. Ben-Shem, F. Frolow, and N. Nelson. Crystal structure of plant photosystem i. *Nature*, 426 (6967):630–635, Dec. 2003.

R. E. Blankenship. *Molecular mechanisms of photosynthesis*. Wiley-Blackwell, 2002. ISBN 0632043210, 9780632043217.

C. Bordot. Construction et purification d'une forme modifiée de la ferredoxin NADP(H) oxydoréductase chez la cyanobactérie synechocystis sp. PCC6803. 2005.

H. Bottin and B. Lagoutte. Ferredoxin and flavodoxin from the cyanobacterium synechocystis sp PCC 6803. *Biochimica Et Biophysica Acta*, 1101(1):48–56, July 1992.

K. Brettel and W. Leibl. Electron transfer in photosystem i. *Biochimica et Biophysica Acta (BBA) - Bioenergetics*, 1507(1-3):100–114, Oct. 2001.

C. Breyton, B. Nandha, G. N. Johnson, P. Joliot, and G. Finazzi. Redox modulation of cyclic electron flow around photosystem i in c3 plants†. *Biochemistry*, 45(45):13465–13475, Nov. 2006.

V. Capuano, A. S. Braux, N. T. de Marsac, and J. Houmard. The "anchor polypeptide" of cyanobacterial phycobilisomes. molecular characterization of the synechococcus sp. PCC 6301 apce gene. *The Journal of Biological Chemistry*, 266(11):7239–7247, Apr. 1991.

N. Carrillo and E. A. Ceccarelli. Open questions in ferredoxin-NADP+ reductase catalytic mechanism. *European Journal of Biochemistry*, 270(9):1900–1915, May 2003.

N. Cassan, B. Lagoutte, and P. Setif. Ferredoxin-NADP+ reductase: Kinetics of electron transfer, transient intermediates, and catalytic activities studied by flash-absorption spectroscopy with isolated photosystem i and ferredoxin. *J. Biol. Chem.*, 280(28):25960–25972, July 2005.

E. A. Ceccarelli, A. K. Arakaki, N. Cortez, and N. Carrillo. Functional plasticity and catalytic efficiency in plant and bacterial ferredoxin-NADP(H) reductases. *Biochimica et Biophysica Acta (BBA) - Proteins & Proteomics*, 1698(2):155–165, May 2004.

J. W. Cooley, C. A. Howitt, and W. F. Vermaas. Succinate:quinol oxidoreductases in the cyanobacterium synechocystis sp. strain PCC 6803: presence and function in metabolism and electron transport. *Journal of Bacteriology*, 182(3):714–722, Feb. 2000.

J. W. Cooley and W. F. J. Vermaas. Succinate dehydrogenase and other respiratory pathways in thylakoid membranes of synechocystis sp. strain PCC 6803: Capacity comparisons and physiological function. *J. Bacteriol.*, 183(14):4251–4258, July 2001.

M. E. Corrado, A. Aliverti, G. Zanetti, and S. G. Mayhew. Analysis of the oxidation-reduction potentials of recombinant ferredoxin-NADP+ reductase from spinach chloroplasts. *European Journal of Biochemistry / FEBS*, 239(3):662–667, Aug. 1996.

G. DalCorso, P. Pesaresi, S. Masiero, E. Aseeva, D. Schunemann, G. Finazzi, P. Joliot, R. Barbato, and D. Leister. A complex containing PGRL1 and PGR5 is involved in the switch between linear and cyclic electron flow in arabidopsis. *Cell*, 132(2):273–285, 2008.

Y. Deng, J. Ye, and H. Mi. Effects of low CO2 on NAD(P)H dehydrogenase, a mediator of cyclic electron transport around photosystem i in the cyanobacterium synechocystis PCC6803. *Plant & Cell Physiology*, 44(5):534–540, May 2003.

Z. Deng, A. Aliverti, G. Zanetti, A. Arakaki, J. Ottado, E. Orellano, N. Calcaterra, E. Ceccarelli, N. Carrillo, and P. Karplus. A productive NADP+ binding mode of ferredoxin-NADP + reductase revealed by protein engineering and crystallographic studies. *Nat Struct Biol*, 6(9): 847–853, 1999.

J. M. Dubbs and F. R. Tabita. Regulators of nonsulfur purple phototrophic bacteria and the interactive control of CO2 assimilation, nitrogen fixation, hydrogen metabolism and energy generation. *FEMS Microbiology Reviews*, 28(3):353–376, June 2004.

A. Ducret, S. A. Müller, K. N. Goldie, A. Hefti, W. A. Sidler, H. Zuber, and A. Engel. Reconstitution, characterisation and mass analysis of the pentacylindrical allophycocyanin core complex from the cyanobacterium anabaena sp. PCC 7120. *Journal of Molecular Biology*, 278(2):369–388, May 1998.

M. Eisenhut, W. Ruth, M. Haimovich, H. Bauwe, A. Kaplan, and M. Hagemann. The photorespiratory glycolate metabolism is essential for cyanobacteria and might have been conveyed endosymbiontically to plants. *Proceedings of the National Academy of Sciences*, 105(44):17199–17204, 2008.

M. Eisenhut, E. A. von Wobeser, L. Jonas, H. Schubert, B. W. Ibelings, H. Bauwe, H. C. P. Matthijs, and M. Hagemann. Long-term response toward inorganic carbon limitation in wild type and

glycolate turnover mutants of the cyanobacterium synechocystis sp. strain PCC 6803. *Plant Physiology*, 144(4):1946–1959, Aug. 2007.

K. Elmorjani, J. C. Thomas, and P. Sebban. Phycobilisomes of wild type and pigment mutants of the cyanobacterium synechocystis PCC 6803. *Archives of Microbiology*, 146(2):186–191, Nov. 1986.

P. C. Engel and V. Massey. The purification and properties of butyryl-coenzyme a dehydrogenase from peptostreptococcus elsdenii. *The Biochemical Journal*, 125(3):879–887, Dec. 1971.

K. N. Ferreira, T. M. Iverson, K. Maghlaoui, J. Barber, and S. Iwata. Architecture of the photosynthetic Oxygen-Evolving center. *Science*, 303(5665):1831–1838, Mar. 2004.

G. Forti and E. Sturani. On the structure and function of reduced nicotinamide adenine dinucleotide phosphate-cytochrome f reductase of spinach chloroplasts. *Eur.J.Biochem.*, 3(4):461–472, Feb. 1968.

G. Forti. Studies on NADPH-cytochrome f reductase of chloroplasts. *Brookhaven Symposia in Biology*, 19:195–201, 1966.

G. P. Foust, S. G. Mayhew, and V. Massey. Complex formation between ferredoxin triphosphopyridine nucleotide reductase and electron transfer proteins. *The Journal of Biological Chemistry*, 244(3):964–970, Feb. 1969.

E. Gantt and C. A. Lipschultz. Phycobilisomes of porphyridium cruentum. i. isolation. *The Journal of Cell Biology*, 54(2):313–324, Aug. 1972.

C. Gibbons, M. G. Montgomery, A. G. W. Leslie, and J. E. Walker. The structure of the central stalk in bovine F1-ATPase at 2.4 a resolution. *Nat Struct Mol Biol*, 7(11):1055–1061, Nov. 2000.

A. N. Glazer. Light guides. directional energy transfer in a photosynthetic antenna. *The Journal of Biological Chemistry*, 264(1):1–4, 1989.

A. J. Golding, G. Finazzi, and G. N. Johnson. Reduction of the thylakoid electron transport chain by stromal reductants—evidence for activation of cyclic electron transport upon dark adaptation or under drought. *Planta*, 220(2):356–363, Dec. 2004.

C. Gómez-Lojero, B. Pérez-Gómez, G. Shen, W. M. Schluchter, and D. A. Bryant. Interaction of Ferredoxin:NADP+ oxidoreductase with phycobilisomes and phycobilisome substructures of the cyanobacterium synechococcus sp. strain PCC 7002†. *Biochemistry*, 42(47):13800–13811, Dec. 2003.

P. Gou, G. T. Hanke, Y. Kimata-Ariga, D. M. Standley, A. Kubo, I. Taniguchi, H. Nakamura, and T. Hase. Higher order structure contributes to specific differences in redox potential and electron transfer efficiency of root and leaf ferredoxins†. *Biochemistry*, 45(48):14389–14396, Dec. 2006.

L. S. Green, B. C. Yee, B. B. Buchanan, K. Kamide, Y. Sanada, and K. Wada. Ferredoxin and ferredoxin-NADP reductase from photosynthetic and nonphotosynthetic tissues of tomato. *Plant Physiology*, 96:1207–1213, 1991.

G. Guedeney, S. Corneille, S. Cuiné, and G. Peltier. Evidence for an association of ndh b, ndh j gene products and ferredoxin-NADP-reductase as components of a chloroplastic NAD(P)H dehydrogenase complex. *FEBS Letters*, 378(3):277–280, 1996.

J. O. Gummadova, G. J. Fletcher, A. Moolna, G. T. Hanke, T. Hase, and C. G. Bowsher. Expression of multiple forms of ferredoxin NADP+ oxidoreductase in wheat leaves. *J. Exp. Bot.*, 58(14): 3971–3985, Nov. 2007.

C. Hackenberg, A. Engelhardt, H. Matthijs, F. Wittink, H. Bauwe, A. Kaplan, and M. Hagemann. Photorespiratory 2-phosphoglycolate metabolism and photoreduction of o2 cooperate in high-light acclimation of synechocystis sp. strain PCC 6803. *Planta*, 230(4):625–637, 2009.

G. T. Hanke, T. Endo, F. Satoh, and T. Hase. Altered photosynthetic electron channelling into cyclic electron flow and nitrite assimilation in a mutant of ferredoxin:NADP(H) reductase. *Plant, Cell & Environment*, 31(7):1017–1028, July 2008.

G. T. Hanke, Y. Kimata-Ariga, I. Taniguchi, and T. Hase. A post genomic characterization of arabidopsis ferredoxins. *Plant Physiol.*, 134(1):255–264, 2004a.

G. T. Hanke, S. Okutani, Y. Satomi, T. Takao, A. Suzuki, and T. Hase. Multiple iso-proteins of FNR in arabidopsis: evidence for different contributions to chloroplast function and nitrogen assimilation. *Plant, Cell & Environment*, 28(9):1146–1157, 2005.

G. Hanke, G. Kurisu, M. Kusunoki, and T. Hase. Fd : FNR electron transfer complexes: Evolutionary refinement of structural interactions. *Photosynthesis Research*, 81(3):317–327, 2004b.

J. Harbinson and C. H. Foyer. Relationships between the efficiencies of photosystems i and II and stromal redox state in CO(2)-Free air : Evidence for cyclic electron flow in vivo. *Plant Physiology*, 97(1):41–49, Sept. 1991.

S. E. Hart, B. G. Schlarb-Ridley, D. S. Bendall, and C. J. Howe. Terminal oxidases of cyanobacteria. *Biochemical Society Transactions*, 33(Pt 4):832–835, Aug. 2005.

U. Heber and D. Walker. Concerning a dual function of coupled cyclic electron transport in leaves. *Plant Physiology*, 100(4):1621–1626, Dec. 1992.

Y. Helman, D. Tchernov, L. Reinhold, M. Shibata, T. Ogawa, R. Schwarz, I. Ohad, and A. Kaplan. Genes encoding A-Type flavoproteins are essential for photoreduction of o2 in cyanobacteria. *Current Biology*, 13(3):230–235, Feb. 2003.

J. A. Hermoso, T. Mayoral, M. Faro, C. Gomez-Moreno, J. Sanz-Aparicio, and M. Medina. Mechanism of coenzyme recognition and binding revealed by crystal structure analysis of Ferredoxin-NADP+ reductase complexed with NADP+. *Journal of Molecular Biology*, 319(5):1133–1142, June 2002.

J. K. Hurley, R. Morales, M. Martinez-Julvez, T. B. Brodie, M. Medina, C. Gomez-Moreno, and G. Tollin. Structure-function relationships in anabaena ferredoxin/ferredoxin:NADP+ reductase electron transfer: insights from site-directed mutagenesis, transient absorption spectroscopy and x-ray crystallography. *Biochimica et Biophysica Acta (BBA) - Bioenergetics*, 1554 (1-2):5–21, Apr. 2002.

B. Ivanov, K. Asada, and G. Edwards. Analysis of donors of electrons to photosystem i and cyclic electron flow by redox kinetics of p700 in chloroplasts of isolated bundle sheath strands of maize. *Photosynthesis Research*, 92(1):65–74, Apr. 2007.

P. Joliot and A. Joliot. Quantification of cyclic and linear flows in plants. *Proc.Natl.Acad.Sci.U.S.A*, 102(13):4913–4918, Mar. 2005.

P. Jordan, P. Fromme, H. T. Witt, O. Klukas, W. Saenger, and N. Krausz. Three-dimensional structure of cyanobacterial photosystem i at 2.5 a resolution. *Nature*, 411(6840):909–917, June 2001.

T. Kaneko, S. Sato, H. Kotani, A. Tanaka, E. Asamizu, Y. Nakamura, N. Miyajima, M. Hirosawa, M. Sugiura, S. Sasamoto, T. Kimura, T. Hosouchi, A. Matsuno, A. Muraki, N. Nakazaki, K. Naruo, S. Okumura, S. Shimpo, C. Takeuchi, T. Wada, A. Watanabe, M. Yamada, M. Yasuda, and S. Tabata. Sequence analysis of the genome of the unicellular cyanobacterium synechocystis sp. strain PCC6803. II. sequence determination of the entire genome and assignment of potential protein-coding regions (supplement). *DNA Research: An International Journal for Rapid Publication of Reports on Genes and Genomes*, 3(3):185–209, June 1996.

P. Karplus, M. Daniels, and Herriott. Atomic structure of ferredoxin-NADP+ reductase: prototype for a structurally novel flavoenzyme family. *Science*, 251(4989):60–66, 1991.

P. Karplus and H. Faber. Structural aspects of plant ferredoxin : NADP+ oxidoreductases. *Photosynthesis Research*, 81(3):303–315, 2004.

N. Y. Kiang, A. Segura, G. Tinetti, Govindjee, R. E. Blankenship, M. Cohen, J. Siefert, D. Crisp, and V. S. Meadows. Spectral signatures of photosynthesis. II. coevolution with other stars and the atmosphere on extrasolar worlds. *Astrobiology*, 7(1):252–274, Feb. 2007.

C. Klughammer and U. Schreiber. Saturation pulse method for assessment of energy conversion in PS i. *PAM Application Notes (PAN)*, (1):11–14, 2008.

D. B. Knaff. Ferredoxin and Ferredoxin-Dependent enzymes. In *Oxygenic Photosynthesis: The Light Reactions*, volume 4, pages 333–361. Kluwer Academic Publishers, 1996. ISBN 0-7923-3683-6, 0-7923-3684-4.

K. Kondo, X. X. Geng, M. Katayama, and M. Ikeuchi. Distinct roles of CpcG1 and CpcG2 in phycobilisome assembly in the cyanobacterium synechocystis sp. PCC 6803. *Photosynthesis Research*, 84(1):269–273, June 2005.

K. Kondo, C. Mullineaux, and M. Ikeuchi. Distinct roles of CpcG1-phycobilisome and CpcG2-phycobilisome in state transitions in a cyanobacterium synechocystis sp. PCC 6803. *Photosynthesis Research*, 99(3):217–225, Mar. 2009.

K. Kondo, Y. Ochiai, M. Katayama, and M. Ikeuchi. The Membrane-Associated CpcG2-Phycobilisome in synechocystis: A new photosystem i antenna. *Plant Physiol.*, 144(2):1200–1210, June 2007.

A. Korn, G. Ajlani, B. Lagoutte, A. Gall, and P. Sétif. Ferredoxin:NADP+ oxidoreductase association with phycocyanin modulates its properties. *Journal of Biological Chemistry*, 284(46): 31789–31797, Nov. 2009.

G. Kurisu, M. Kusunoki, E. Katoh, T. Yamazaki, K. Teshima, Y. Onda, Y. Kimata-Ariga, and T. Hase. Structure of the electron transfer complex between ferredoxin and ferredoxin-NADP+ reductase. *Nat Struct Mol Biol*, 8(2):117–121, Feb. 2001.

G. Kurisu, H. Zhang, J. L. Smith, and W. A. Cramer. Structure of the cytochrome b6f complex of oxygenic photosynthesis: Tuning the cavity. *Science*, 302(5647):1009–1014, Nov. 2003.

M. Liberton, R. H. Berg, J. Heuser, R. Roth, and H. B. Pakrasi. Ultrastructure of the membrane systems in the unicellular cyanobacterium synechocystis sp. strain PCC 6803. *Protoplasma*, 227 (2):129–138, May 2006.

M. Lintala, Y. Allahverdiyeva, S. Kangasjärvi, N. Lehtimäki, M. Keränen, E. Rintamäki, E. Aro, and P. Mulo. Comparative analysis of leaf-type ferredoxin-NADP+ oxidoreductase isoforms in arabidopsis thaliana. *The Plant Journal*, 57(6):1103–1115, 2009.

M. Lintala, Y. Allahverdiyeva, H. Kidron, M. Piippo, N. Battchikova, M. Suorsa, E. Rintamäki, T. A. Salminen, E. Aro, and P. Mulo. Structural and functional characterization of ferredoxin-NADP⁺-oxidoreductase using knock-out mutants of arabidopsis. *The Plant Journal*, 49(6):1041–1052, 2007.

J. Liu, T. Jiang, J. Zhang, and D. Liang. Crystal structure of allophycocyanin from red AlgaePorphyra yezoensis at 2.2-? resolution. *Journal of Biological Chemistry*, 274(24):16945–16952, June 1999.

R. MacColl. Cyanobacterial phycobilisomes. *Journal of Structural Biology*, 124(2-3):311–334, Dec. 1998.

V. Massey, P. Hemmerich, W. Knappe, H. Duchstein, and H. Fenner. Photoreduction of flavoproteins and other biological compounds catalyzed by deazaflavins. appendix: photochemical formation of deazaflavin dimers. *Biochemistry*, 17(1):9–17, 1978.

M. Matsuo, T. Endo, and K. Asada. Properties of the respiratory NAD(P)H dehydrogenase isolated from the cyanobacterium synechocystis PCC6803. *Plant and Cell Physiology*, 39(3): 263–267, Mar. 1998.

W. Ma and H. Mi. Expression and activity of type 1 NAD(P)H dehydrogenase at different growth phases of the cyanobacterium synechocystis PCC 6803. *Physiologia Plantarum*, 125:135–140, 2005.

M. Medina, M. Martinez-Julvez, J. K. Hurley, G. Tollin, and C. Gomez-Moreno. Involvement of glutamic acid 301 in the catalytic mechanism of Ferredoxin-NADP+ reductase from anabaena PCC 7119†. *Biochemistry*, 37(9):2715–2728, Mar. 1998.

A. H. Mehler. Studies on reactions of illuminated chloroplasts. i. mechanism of the reduction of oxygen and other hill reagents. *Archives of Biochemistry*, 33(1):65–77, Aug. 1951.

J. Messinger, A. Alia, Govindjee, and Govindjee. Special educational issue on 'Basics and application of biophysical techniques in photosynthesis and related processes'—Part b. *Photosynthesis Research*, 102(2):103–106, Dec. 2009.

P. Mitchell. Possible molecular mechanisms of the protonmotive function of cytochrome systems. *Journal of Theoretical Biology*, 62(2):327–367, Oct. 1976.

C. Miyake, M. Miyata, Y. Shinzaki, and K. ichi Tomizawa. CO2 response of cyclic electron flow around PSI (CEF-PSI) in tobacco Leaves–Relative electron fluxes through PSI and PSII determine the magnitude of non-photochemical quenching (NPQ) of chl fluorescence. *Plant Cell Physiol.*, 46(4):629–637, Apr. 2005.

H. Mi, T. Endo, T. Ogawa, and K. Asada. Thylakoid Membrane-Bound, NADPH-Specific pyridine nucleotide dehydrogenase complex mediates cyclic electron transport in the cyanobacterium synechocystis sp. PCC 6803. *Plant Cell Physiol.*, 36(4):661–668, June 1995.

H. Mi, T. Endo, U. Schreiber, and K. Asada. Donation of electrons from cytosolic components to the intersystem chain in the cyanobacterium synechococcus sp. PCC 7002 as determined by the reduction of p700+. *Plant Cell Physiol.*, 33(8):1099–1105, Dec. 1992a.

H. Mi, T. Endo, U. Schreiber, T. Ogawa, and K. Asada. Electron donation from cyclic and respiratory flows to the photosynthetic intersystem chain is mediated by pyridine nucleotide dehydrogenase in the cyanobacterium synechocystis PCC 6803. *Plant Cell Physiol.*, 33(8):1233–1237, Dec. 1992b.

H. Mi, T. Endo, U. Schreiber, T. Ogawa, and K. Asada. NAD(P)H Dehydrogenase-Dependent cyclic electron flow around photosystem i in the cyanobacterium synechocystis PCC 6803: a study of Dark-Starved cells and spheroplasts. *Plant Cell Physiol.*, 35(2):163–173, 1994.

H. Mi, C. Klughammer, and U. Schreiber. Light-Induced dynamic changes of NADPH fluorescence in synechocystis PCC 6803 and its ndhB-Defective mutant m55. *Plant and Cell Physiology*, 41(10):1129–1135, Oct. 2000.

R. Morales, M. Charon, G. Kachalova, L. Serre, M. Medina, C. Gomez-Moreno, and M. Frey. A redox-dependent interaction between two electron-transfer partners involved in photosynthesis. *EMBO Rep.*, 1(3):271–276, 2000.

S. Morigasaki, K. Takata, T. Suzuki, and K. Wada. Purification and characterization of a Ferredoxin-NADP+ Oxidoreductase-Like enzyme from radish root tissues. *Plant Physiol.*, 93 (3):896–901, July 1990.

C. W. Mullineaux. FRAP analysis of photosynthetic membranes. *Journal of Experimental Botany*, 55(400):1207–1211, June 2004.

Y. Munekage, B. Genty, and G. Peltier. Effect of PGR5 impairment on photosynthesis and growth in arabidopsis thaliana. *Plant Cell Physiol*, 2008.

Y. Munekage, M. Hashimoto, C. Miyake, K. ichi Tomizawa, T. Endo, M. Tasaka, and T. Shikanai. Cyclic electron flow around photosystem i is essential for photosynthesis. *Nature*, 429(6991): 579–582, June 2004.

Y. Munekage, M. Hojo, J. Meurer, T. Endo, M. Tasaka, and T. Shikanai. PGR5 is involved in cyclic electron flow around photosystem i and is essential for photoprotection in arabidopsis. *Cell*, 110(3):361–371, Aug. 2002.

M. Nakajima, T. Sakamoto, and K. Wada. The complete purification and characterization of three forms of ferredoxin-NADP(+) oxidoreductase from a thermophilic cyanobacterium synechococcus elongatus. *Plant & Cell Physiology*, 43(5):484–493, May 2002.

N. Nelson and A. Ben-Shem. The complex architecture of oxygenic photosynthesis. *Nat Rev Mol Cell Biol*, 5(12):971–982, Dec. 2004.

J. Nield, P. J. Rizkallah, J. Barber, and N. E. Chayen. The 1.45 ? three-dimensional structure of c-phycocyanin from the thermophilic cyanobacterium synechococcus elongatus. *Journal of Structural Biology*, 141(2):149–155, Feb. 2003.

T. Ogawa. A gene homologous to the subunit-2 gene of NADH dehydrogenase is essential to inorganic carbon transport of synechocystis PCC6803. *Proceedings of the National Academy of Sciences of the United States of America*, 88(10):4275–4279, May 1991.

H. Ohkawa, H. B. Pakrasi, and T. Ogawa. Two types of functionally distinct NAD(P)H dehydrogenases inSynechocystis sp. strain PCC6803. *Journal of Biological Chemistry*, 275(41):31630–31634, Oct. 2000.

H. Ohyanagi, T. Tanaka, H. Sakai, Y. Shigemoto, K. Yamaguchi, T. Habara, Y. Fujii, B. A. Antonio, Y. Nagamura, T. Imanishi, K. Ikeo, T. Itoh, T. Gojobori, and T. Sasaki. The rice annotation project database (RAP-DB): hub for oryza sativa ssp. japonica genome information. *Nucl. Acids Res.*, 34(suppl_1):D741–744, 2006.

S. Okutani, G. T. Hanke, Y. Satomi, T. Takao, G. Kurisu, A. Suzuki, and T. Hase. Three maize leaf Ferredoxin:NADPH oxidoreductases vary in subchloroplast location, expression, and interaction with ferredoxin. *Plant Physiol.*, 139(3):1451–1459, Nov. 2005.

Y. Onda, T. Matsumura, Y. Kimata-Ariga, H. Sakakibara, T. Sugiyama, and T. Hase. Differential interaction of maize root Ferredoxin:NADP+ oxidoreductase with photosynthetic and Non-Photosynthetic ferredoxin isoproteins. *Plant Physiol.*, 123(3):1037–1046, July 2000.

J. F. Palatnik, E. M. Valle, and N. Carrillo. Oxidative stress causes ferredoxin-NADP+ reductase solubilization from the thylakoid membranes in methyl viologen-treated plants. *Plant Physiology*, 115(4):1721–1727, Dec. 1997.

L. Peng, H. Shimizu, and T. Shikanai. The chloroplast NAD(P)H dehydrogenase complex interacts with photosystem i in arabidopsis. *Journal of Biological Chemistry*, 283(50):34873–34879, Dec. 2008.

D. Pils and G. Schmetterer. Characterization of three bioenergetically active respiratory terminal oxidases in the cyanobacterium synechocystis sp. strain PCC 6803. *FEMS Microbiology Letters*, 203(2):217–222, Sept. 2001.

L. Piubelli, A. Aliverti, A. K. Arakaki, N. Carrillo, E. A. Ceccarelli, P. A. Karplus, and G. Zanetti. Competition between c-terminal tyrosine and nicotinamide modulates pyridine nucleotide affinity and specificity in plant ferredoxin-NADP(+) reductase. *The Journal of Biological Chemistry*, 275(14):10472–10476, Apr. 2000.

M. Poncelet, C. Cassier-Chauvat, X. Leschelle, H. Bottin, and F. Chauvat. Targeted deletion and mutational analysis of the essential (2Fe-2S) plant-like ferredoxin in synechocystis PCC6803 by plasmid shuffling. *Molecular Microbiology*, 28(4):813–821, May 1998.

W. Reuter, G. Wiegand, R. Huber, and M. E. Than. Structural analysis at 2.2 a of orthorhombic crystals presents the asymmetry of the allophycocyanin-linker complex, AP.LC7.8, from phycobilisomes of mastigocladus laminosus. *Proceedings of the National Academy of Sciences of the United States of America*, 96(4):1363–1368, Feb. 1999.

M. Rogner, U. Muhlenhoff, E. Boekema, and H. Witt. Monomeric, dimeric and trimeric PSI-reaction center complexes isolated from the thermophilic cyanobacterium synechococcus sp - size, shape and activity. *BIOCHIMICA ET BIOPHYSICA ACTA*, 1015(3):415–424, Feb. 1990.

D. Rumeau, G. Peltier, and L. Cournac. Chlororespiration and cyclic electron flow around PSI during photosynthesis and plant stress response. *Plant, Cell & Environment*, 30(9):1041–1051, 2007.

W. M. Schluchter and D. A. Bryant. Molecular characterization of ferredoxin-NADP+ oxidoreductase in cyanobacteria: cloning and sequence of the petH gene of synechococcus sp. PCC 7002 and studies on the gene product. *Biochemistry*, 31(12):3092–3102, Mar. 1992.

U. Schreiber, C. Klughammer, and C. Neubauer. Measuring p700 absorbance changes around 830 nm with a new type of pulse-modulation system. *Zeitschrift für Naturforschung C-A Journal of Biosciences*, 43(9-10):686–698, Oct. 1988.

U. Schreiber and C. Klughammer. New NADPH/9-AA module for the DUAL-PAM-100: description, operation and examples of application. *PAM Application Notes (PAN)*, (2):1–13, 2009.

U. Schreiber, U. Schliwa, and W. Bilger. Continuous recording of photochemical and non-photochemical chlorophyll fluorescence quenching with a new type of modulation fluorometer. *Photosynthesis Research*, 10(1):51–62, 1986.

U. Schreiber. Detection of rapid induction kinetics with a new type of high-frequency modulated chlorophyll fluorometer. *Photosynthesis Research*, 9(1):261–272, 1986.

H. Seelert, A. Poetsch, N. A. Dencher, A. Engel, H. Stahlberg, and D. J. Muller. Structural biology: Proton-powered turbine of a plant motor. *Nature*, 405(6785):418–419, May 2000.

P. Q. Y. Setif and H. Bottin. Laser flash absorption spectroscopy study of ferredoxin reduction by photosystem i in synechocystis sp. PCC 6803: Evidence for submicrosecond and microsecond kinetics. *Biochemistry*, 33(28):8495–8504, July 1994.

P. Setif, N. Fischer, B. Lagoutte, H. Bottin, and J. Rochaix. The ferredoxin docking site of photosystem i. *Biochimica et Biophysica Acta (BBA) - Bioenergetics*, 1555(1-3):204–209, Sept. 2002.

P. Setif. Ferredoxin and flavodoxin reduction by photosystem i. *Biochimica et Biophysica Acta (BBA) - Bioenergetics*, 1507(1-3):161–179, Oct. 2001.

T. Shikanai, T. Endo, T. Hashimoto, Y. Yamada, K. Asada, and A. Yokota. Directed disruption of the tobacco ndhB gene impairs cyclic electron flow around photosystem i. *Proceedings of the National Academy of Sciences of the United States of America*, 95(16):9705–9709, 1998.

T. Shikanai. Cyclic electron transport around photosystem i: genetic approaches. *Annual Review of Plant Biology*, 58:199–217, 2007.

M. Shin and D. I. Arnon. Enzymatic mechanisms of pyridine nucleotide reduction in chloroplasts. *The Journal of Biological Chemistry*, 240:1405–1411, Mar. 1965.

M. Shin and A. S. Pietro. [40] Ferredoxin-NADP reductase from spinach. In *Photosynthesis and Nitrogen Part A*, volume Volume 23, pages 440–447. Academic Press, 1971. ISBN 0076-6879.

W. Sidler. Phycobilisome and phycobiliprotein structure. In *The Molecular Biology of Cyanobacteria*, pages 139–216. Kluwer Academic Publishers, 1994. ISBN 0-7923-3222-9, 0-7923-3273-3. Chapter 7.

D. Stock, A. G. W. Leslie, and J. E. Walker. Molecular architecture of the rotary motor in ATP synthase. *Science*, 286(5445):1700–1705, Nov. 1999.

D. Stroebel, Y. Choquet, J. Popot, and D. Picot. An atypical haem in the cytochrome b6f complex. *Nature*, 426(6965):413–418, Nov. 2003.

J. Thomas, B. Ughy, B. Lagoutte, and G. Ajlani. A second isoform of the ferredoxin:NADP oxidoreductase generated by an in-frame initiation of translation. *Proceedings of the National Academy of Sciences*, 103(48):18368–18373, Nov. 2006.

B. V. Trubitsin, V. V. Ptushenko, O. A. Koksharova, M. D. Mamedov, L. A. Vitukhnovskaya, I. A. Grigor'ev, A. Y. Semenov, and A. N. Tikhonov. EPR study of electron transport in the cyanobacterium synechocystis sp. PCC 6803: Oxygen-dependent interrelations between photosynthetic and respiratory electron transport chains. *Biochimica et Biophysica Acta (BBA) - Bioenergetics*, 1708(2):238–249, June 2005.

B. L. Trumpower. The protonmotive q cycle. energy transduction by coupling of proton translocation to electron transfer by the cytochrome bc1 complex. *The Journal of Biological Chemistry*, 265(20):11409–11412, July 1990.

P. Turina, D. Samoray, and P. Gräber. H+/ATP ratio of proton transport-coupled ATP synthesis and hydrolysis catalysed by CF0F1-liposomes. *The EMBO Journal*, 22(3):418–426, Feb. 2003.

B. Ughy and G. Ajlani. Phycobilisome rod mutants in synechocystis sp. strain PCC6803. *Microbiology*, 150(12):4147–4156, Dec. 2004.

B. Ughy. *Phycobilisome assembly in Synechocystis sp. strain PCC6803*. PhD thesis, 2005.

G. M. Ullmann, M. Hauswald, A. Jensen, and E. Knapp. Structural alignment of ferredoxin and flavodoxin based on electrostatic potentials: Implications for their interactions with photosystem i and ferredoxin-NADP reductase. *Proteins: Structure, Function, and Genetics*, 38(3):301–309, 2000.

A. van de Meene, M. Hohmann-Marriott, W. Vermaas, and R. Roberson. The three-dimensional structure of the cyanobacterium synechocystis sp. PCC 6803. *Archives of Microbiology*, 184(5): 259–270, 2006.

J. J. van Thor, T. H. Geerlings, H. C. P. Matthijs, and K. J. Hellingwerf. Kinetic evidence for the PsaE-Dependent transient ternary complex photosystem I/Ferredoxin/Ferredoxin:NADP+ reductase in a cyanobacterium†. *Biochemistry*, 38(39):12735–12746, 1999a.

J. J. van Thor, R. Jeanjean, M. Havaux, K. A. Sjollema, F. Joset, K. J. Hellingwerf, and H. C. P. Matthijs. Salt shock-inducible photosystem i cyclic electron transfer in synechocystis PCC6803 relies on binding of ferredoxin:NADP+ reductase to the thylakoid membranes via its CpcD phycobilisome-linker homologous n-terminal domain. *Biochimica et Biophysica Acta (BBA) - Bioenergetics*, 1457(3):129–144, Apr. 2000.

J. van Thor, O. Gruters, H. Matthijs, and K. Hellingwerf. Localization and function of ferredoxin:NADP(+) reductase bound to the phycobilisomes of synechocystis. *EMBO J.*, 18(15): 4128–4136, 1999b.

L. Vara and C. Gómez-Lojero. Participation of plastoquinone, cytochrome c553 and ferrodoxin-NADP+ oxido-reductase in both photosynthesis and respiration in spirulina maxima. *Photosynthesis Research*, 8(1):65–78, 1986.

G. Zanetti, B. Curti, and S. P. Anthony. [22] Ferredoxin-NADP+ oxidoreductase. In *Methods in Enzymology Part C: Photosynthesis and Nitrogen Fixation*, volume Volume 69, pages 250–255. Academic Press, 1980.

H. Zhang, J. P. Whitelegge, and W. A. Cramer. Ferredoxin:NADP+ oxidoreductase is a subunit of the chloroplast cytochrome b6fComplex. *Journal of Biological Chemistry*, 276(41):38159–38165, Oct. 2001.

P. Zhang, Y. Allahverdiyeva, M. Eisenhut, and E. Aro. Flavodiiron proteins in oxygenic photosynthetic organisms: Photoprotection of photosystem II by flv2 and flv4 in synechocystis sp. PCC 6803. *PLoS ONE*, 4(4):e5331, Apr. 2009.

P. Zhang. *Novel insights into cyanobacterial NDH-1 complexes*. PhD thesis, 2006.

THE JOURNAL OF BIOLOGICAL CHEMISTRY VOL. 284, NO. 46, pp. 31789–31797, November 13, 2009

Ferredoxin:NADP$^+$ Oxidoreductase Association with Phycocyanin Modulates Its Properties*[S]

Received for publication, May 23, 2009, and in revised form, September 11, 2009 Published, JBC Papers in Press, September 15, 2009, DOI 10.1074/jbc.M109.024638

Anja Korn, Ghada Ajlani[1], Bernard Lagoutte, Andrew Gall, and Pierre Sétif[2]
From the Institut de Biologie et de Technologie de Saclay, Commissariat à L'Energie Atomique, CNRS, F-91191 Gif sur Yvette, France

In photosynthetic organisms, ferredoxin:NADP$^+$ oxidoreductase (FNR) is known to provide NADPH for CO_2 assimilation, but it also utilizes NADPH to provide reduced ferredoxin. The cyanobacterium *Synechocystis* sp. strain PCC6803 produces two FNR isoforms, a small one (FNR_S) similar to the one found in plant plastids and a large one (FNR_L) that is associated with the phycobilisome, a light-harvesting complex. Here we show that a mutant lacking FNR_L exhibits a higher NADP$^+$/NADPH ratio. We also purified to homogeneity a phycobilisome subcomplex comprising FNR_L, named FNR_L-PC. The enzymatic activities of FNR_L-PC were compared with those of FNR_S. During NADPH oxidation, FNR_L-PC exhibits a 30% decrease in the Michaelis constant $K_{m(\text{NADPH})}$, and a 70% increase in $K_{m(\text{ferredoxin})}$, which is in agreement with its predicted lower activity of ferredoxin reduction. During NADP$^+$ reduction, the FNR_L-PC shows a 29/43% decrease in the rate of single electron transfer from reduced ferredoxin in the presence/absence of NADP$^+$. The increase in $K_{m(\text{ferredoxin})}$ and the rate decrease of single reduction are attributed to steric hindrance by the phycocyanin moiety of FNR_L-PC. Both isoforms are capable of catalyzing the NADP$^+$ reduction under multiple turnover conditions. Furthermore, we obtained evidence that, under high ionic strength conditions, electron transfer from reduced ferredoxin is rate limiting during this process. The differences that we observe might not fully explain the *in vivo* properties of the *Synechocystis* mutants expressing only one of the isoforms. Therefore, we advocate that FNR localization and/or substrates availability are essential *in vivo*.

In cyanobacteria and plastids, ferredoxin:NADP$^+$ oxidoreductase (FNR)[3] catalyzes the exchange of electrons between the one-electron carrier ferredoxin (Fd) and the two-electron carrier NADP$^+$ (1–5): 2 Fd_{red} + NADP$^+$ + H^+ $\leftrightarrows$ 2 Fd_{ox} + NADPH. FNR contains the noncovalently bound FAD cofactor. The NADP$^+$-reductase catalytic cycle involves the reduction of FAD to the neutral semiquinone FADH$^\bullet$ (FNR_{sq}) followed by its further reduction to the fully reduced FADH$^-$ (FNR_{red}), with reduced Fd (Fd_{red}) binding at a single site (4, 6). Hydride transfer from FADH$^-$ to NADP$^+$ completes the catalytic cycle (7) and NADPH is then released. Ternary complexes between the three partners FNR, NADP$^+$ and Fd have been shown to be involved in NADP$^+$-reductase activity (1, 8). This is in line with the fact that fast turnover requires NADP$^+$ binding before Fd_{red} binding, FAD reduction, and Fd_{ox} release (1). Such ternary complexes may not be required during the NADPH-oxidase catalytic cycle (7, 9), although this has yet to be established. In the final step of linear photosynthetic electron flow, FNR is involved in NADPH production, which in turn is used in the Calvin cycle. In plant plastids several FNR isoforms are encoded by different genes (10–12). The expressed enzymes are processed to give molecular masses of ~35 kDa. The different isoforms are differentially expressed in roots and leaves (13). The root enzyme is involved in NADPH consumption, reducing Fd for nitrogen fixation, while the leaf enzyme is involved in NADPH formation (14–17).

The biochemical and structural properties of cyanobacterial and plastid FNR are highly similar except that in most phycobilisome (PBS)-containing cyanobacteria, FNR contains an N-terminal domain whose sequence is similar to PBS-linker polypeptides (18). This extension is responsible for FNR_L attachment to the PBS (18). The conventional PBS is composed of two substructures, the core and the rods. In *Synechocystis* sp. strain PCC6803 (hereafter named *Synechocystis*), the core is composed of allophycocyanin (AP) and each rod contains three phycocyanin (PC) discs. Different linkers are specifically responsible for each level of phycobiliprotein assembly and function to stabilize the PBS and optimize its absorption and energy transfer characteristics (19). FNR_L has been shown to bind to the PBS rods but its precise binding site is still controversial (20–22). Smaller FNR isoforms have been purified from several cyanobacteria and this was attributed to proteolytic degradation of the N-terminal domain (18, 23). However, it has been recently demonstrated that in *Synechocystis* the small isoform (FNR_S, ≈34 kDa) results from an internal translation initiation and not from proteolysis of the large isoform (24). The same authors proposed that FNR_L functions as an NADP$^+$ reductase whereas FNR_S is a better NADPH oxidase. More precisely, FNR_L was shown to support photoautotrophic growth in *Synechocystis* whereas it is the only isoform found in obligate

* This work was supported in part by the Agence Nationale de la Recherche, France (PHYCOSYN, to G. A. and ANR-07-CEXC-009, to A. G.) and the European Commission (EU FP7-ENERGY-2007-1-RTD SOLAR-H2, to P. S.).
[S] The on-line version of this article (available at http://www.jbc.org) contains supplemental Figs. S1 and S2 and Table S1.
[1] To whom correspondence may be addressed: CEA Saclay, iBiTecS, F-91191 Gif sur Yvette, France. Tel.: 33-169086569; Fax: 33-169088717; E-mail: gajlani@cea.fr.
[2] To whom correspondence may be addressed: CEA Saclay, iBiTecS, F-91191 Gif sur Yvette, France. Tel.: 33-169089867; Fax: 33-169088717; E-mail: pierre.setif@cea.fr.
[3] The abbreviations used are: FNR, ferredoxin:NADP$^+$ oxidoreductase; AP, allophycocyanin; α^{PC} and β^{PC}, the two subunits of phycocyanin; cyt *c*, cytochrome *c*; E_m, midpoint redox potential; Fd, ferredoxin; red, reduced; ox, oxidized; FNR_{sq}, singly reduced FNR/semiquinone form; FNR_S, small *Synechocystis* FNR isoform; FNR_L, large *Synechocystis* FNR isoform; PBS, phycobilisome; PC, phycocyanin, an $\alpha\beta$ protomer; PSI, photosystem I; P700, primary electron donor of photosystem I; *Synechocystis*, *Synechocystis* sp. PCC6803; L_{CM}, core-membrane linker; L_{RC}, rod-core linker.

phototrophic cyanobacteria. Conversely, FNR_S accumulates when photosynthesis is slowed down, *i.e.* under heterotrophic or starvation conditions (24). These observations support the idea that the two isoforms differ in their $NADP^+$-reductase/NADPH-oxidase activities. This can be regarded as analogous to the leaf and root isoforms of plants.

Both *Synechocystis* isoforms being encoded by the same gene, they share identical catalytic domains. The N-terminal extension of FNR_L or its association to PBS could somehow modify its catalytic properties. As FNR_L is bound *in vivo* to the core-containing PBS and undergoes proteolysis when not bound to it (25), it is crucial to compare the enzymatic properties of FNR_S to those of PBS-bound FNR_L. However, in practical terms, the large extinction coefficient of the PBS makes such experiments virtually impossible since they are based on absorption measurements. This was circumvented by the purification of a PBS subcomplex, termed FNR_L-PC that contained FNR_L, a PC hexamer and a PBS rod-core linker (L_{RC}). The FNR_L-PC complex possesses a lower extinction coefficient than that of the whole PBS and thus permits absorption measurements to be undertaken.

In this work, we established that the $NADP^+$/NADPH ratio is higher in a mutant containing only FNR_S. An FNR_L-PC complex was purified to homogeneity and shown to be stable for several days in 150 mM phosphate buffer. Finally, the catalytic activities and kinetic constants of the two FNR isoforms are compared with each other and to their plant homologues.

EXPERIMENTAL PROCEDURES

Materials—Synechocystis strains were grown at 34 °C in a CO_2 enriched atmosphere under 60 $\mu E\ m^{-2}\ s^{-1}$ illumination in a modified Allen's medium (26). Photosystem I (PSI) was purified from *Synechocystis* wild type (27), whereas Fd, FNR_S, and FNR_L were overexpressed in *Escherichia coli* and purified as previously described (5, 28). NADPH and horse-heart cytochrome *c* (cyt *c*) were purchased from Sigma-Aldrich. ProBond Ni-resin was obtained from Invitrogen. An antiprotease mixture (Complete, Roche Applied Sciences) was used during the isolation of FNR_L-PC.

$NADP^+$/NADPH Quantification—Absolute and relative amounts of pyridine nucleotides were obtained using an EnzyChrom™ $NADP^+$/NADPH assay kit (Gentaur, France) for the wild type and the two mutants where only one FNR isoform is expressed, *i.e.* FNR_S and FNR_L in the FS1 and MI6 mutants, respectively (24). These measurements were performed with cells in their exponential growth phase under photoautotrophic conditions.

Construction and Purification of His-tagged FNR_L in Synechocystis—Because the N- and C-terminal domains of the enzyme are buried in the PC hexamer and the NADP binding site of the FNR, respectively, a His tag was inserted into the exposed hinge domain preceding the catalytic FNR_S domain (Fig. 1). PCR mutagenesis was performed on the *petH* gene of *Synechocystis* to introduce 6 histidines (between Gly-98 and Ser-99). The mutagenic primers were HIF (5′-CCATCATCACCATCACTCAGGAGCGGTGGC-3′) and HIR (5′-GATGGTGATGATGGTGACCACTTCCCTCGG-3′). The overall method was similar to that used in Ref. 24. The modified gene was introduced in CB, a *Synechocystis* mutant that contains only one PC hexamer per rod instead of three as expressed in the wild type (26). The resulting strain was named CBH.

Phycobilisomes were purified from CBH under conditions that are known (29–31) to preserve PBS-subunit interactions, *i.e.* 0.8 M phosphate (KP: potassium phosphate buffer, pH 8.0). Membranes and chlorophylls were eliminated by Triton X-100 extraction. The PBS complex was then allowed to dissociate overnight at 4 °C by lowering the phosphate concentration to 150 mM KP. The sample was then added to a Ni-resin equilibrated in 250 mM KP and allowed to bind for 1 h. After two washes in the same buffer, the resin was poured into a column. After extensive washing with 150 mM KP, FNR_L was eluted in the presence of 150 mM imidazole. The eluted fractions were concentrated using Vivaspin concentrators (100 kDa cut-off). For each fraction, the PC hexamer concentration was determined by absorption spectroscopy ($\epsilon_{620\ nm} = 2.37\ \mu M^{-1}\ cm^{-1}$, Ref. 32) prior to gel filtration chromatography (250 mM KP, 26/85 Superdex 200, GE Healthcare). Elution profiles were obtained by monitoring the absorbance at 280, 460, and 620 nm, which are indicative of the relative amounts of protein, FAD, and PC, respectively (supplemental Fig. S1). The polypeptide composition of each fraction was analyzed by SDS-PAGE. Polypeptide quantifications were achieved by measuring the Coomassie Blue density of the different bands using an Image scanner II (GE Healthcare). Different amounts of FNR_L-PC were loaded and the staining of the FNR_L polypeptide was compared with known amounts of recombinant FNR_L that were loaded in neighboring lanes.

Measurements of FAD Content in the FNR_L-PC Complex—The polypeptides of FNR_L-PC from three different batches were precipitated by the addition of trichloroacetic acid (5% w/v). Under these conditions, the released FAD cofactor is recovered in the supernatant (33). FAD concentrations were calculated from the absorption maxima at 450 nm ($\epsilon_{450\ nm}$ = 11,300 $M^{-1}\ cm^{-1}$, Ref. 34). This is illustrated in supplemental Fig. S2. In parallel, the pelleted polypeptides were solubilized for SDS-PAGE, and FNR_L quantified after electrophoretic separation. These two approaches allowed us to compare the FNR_L and FAD contents.

Determination of the Absorption Coefficients of FNR_S and FNR_L—As detailed in supplemental data, the FAD cofactor from recombinant FNR_S and FNR_L was released and quantified in the presence of 0.02% SDS (w/v). This allowed us to reevaluate the absorption coefficients of both FNR isoforms. They were determined to be 9,000 $M^{-1}\ cm^{-1}$ at 461 nm instead of 10,800 $M^{-1}\ cm^{-1}$ that was previously reported for plant FNR (35).

Oxidase Activities—Enzymatic reactions were monitored with a Uvikon-XL spectrophotometer. The initial velocities were fitted with Origin 7.5 (OriginLab Corp., Northampton, MA) to obtain Henri-Michaelis-Menten curves. Ferricyanide reductase activity was measured at room temperature in duplicate with NADPH and potassium ferricyanide as the electron donor and acceptor molecules, respectively (36). A series of FNR_S/FNR_L-PC concentrations (0.025–0.1 μM) was mixed with 0.7 mM potassium ferricyanide and 5 mM $MgCl_2$ in 150 mM KP. The reactions were initiated by the addition of a range of

different NADPH concentrations (25–400 μM). The absorption decrease at 420 nm (reduction of ferricyanide) was recorded to determine the steady-state kinetic parameters.

The Fd-mediated cyt *c* reductase activity of FNR_S/FNR_L-PC was measured at 25 °C in triplicate with Fd and cyt *c* acting as intermediate and terminal electron acceptors (35, 36). The reaction was started by the addition of NADPH (400 μM final concentration). Steady-state kinetic parameters for the Fd-dependent cyt *c* reductase activity were determined by varying the concentrations of Fd (2.5–40 μM) in the reaction mixtures and monitoring the resulting absorption increases at 550 nm (reduction of cyt *c*). Fd from *Thermosynechococcus elongatus* was used for these experiments as it was available in large quantities. A few control measurements were performed with *Synechocystis* Fd giving results identical to those obtained with *T. elongatus* Fd.

Flash Absorption Experiments for the Measurements of Reductase Activities—Flash absorption measurements with a time resolution of 10 μs were performed as described previously (5) at 22 °C. Laser excitation (700 nm) was provided by a dye laser (Continuum, Excel Technology, Villebon sur Yvette, France) pumped by a frequency-doubled Nd-Yag laser and was saturating for PSI photochemistry. Conditions were chosen to eliminate any actinic effect of the measuring light.

All spectroscopic measurements were performed under aerobic conditions in 150 mM KP containing 30 mM NaCl and 0.03% (w/v) β-dodecyl maltoside (Biomol, Hamburg, Germany). Sodium ascorbate (2 mM) and 2.6-dichlorophenolindophenol (5–25 μM) were used to reduce the oxidized P700 between two consecutive flashes. The PSI concentration was estimated using the absorption coefficient $\epsilon_{800\ nm} = 7.74\ mM^{-1}\ cm^{-1}$ for $P700^+$ (5). For all flash experiments, the kinetics is shown after subtraction of the $P700^+$ contribution. This was achieved by measuring, in the absence of Fd, the differential absorption coefficients of $P700^+$ at 520/540 nm and at 800 nm, using methyl viologen as an electron acceptor that results in fast reoxidation of the terminal PSI acceptor $(F_A,F_B)^-$. Using this procedure, the differential absorption coefficient of $P700^+$ at 520/540 nm was found to be 50%/34% that of $P700^+$ at 800 nm ($\Delta\epsilon_{520\ nm} = 3.9\ mM^{-1}\ cm^{-1} \approx 7.74\ mM^{-1}\ cm^{-1} \times 0.50$; $\Delta\epsilon_{540\ nm} = 2.6\ mM^{-1}\ cm^{-1} \approx 7.74\ mM^{-1}\ cm^{-1} \times 0.34$). The kinetics probed at 800 nm was subtracted, after multiplication by the normalization factor of 0.50/0.34. In this way, all absorption changes are associated with the reduction of the electron acceptors, *i.e.* those due to (F_A, F_B), Fd, and FNR.

Single reduction of FNR by reduced Fd was triggered by flash excitation of PSI. These experiments were performed in the presence/absence of $NADP^+$ with FNR in excess over PSI. Under this condition, a single reduction event is favored where the neutral protonated semiquinone is produced. These measurements were performed at 520 nm, which corresponds to an absorption minimum of the PSI/FNR_L-PC mixture (Fd absorbance is small compared with those of PSI and PC). Moreover, a large signal is expected at 520 nm for formation of the FNR semireduced form FNR_{sq}.

To promote multiple catalytic turnover, the PSI concentration was >10-fold greater than that of the investigated enzyme (either FNR_S or FNR_L-PC). Under these conditions, FNR receives two electrons from Fd and NADPH is formed via hydride transfer. This multiple turnover reaction was monitored by the reoxidation of Fd_{red} at 540 nm. This wavelength was chosen because of the minimal PSI absorption, which allows actinic effects of the measuring light to be minimized in these measurements made on a long time scale (5).

Fittings and Calculations—The kinetic model used to interpret the single FNR reduction experiments is shown under "Results." It involves two reactions, the first one describes Fd reduction by PSI and the second one corresponds to the redox equilibrium of the first FNR reduction by Fd_{red}. Such a model does not take into account complex formation and dissociation, because of the large ionic strength of the medium, which impedes formation of complexes (2, 37) and hence only considers second-order processes. We assume also that the PSI charge separation leading to the formation of $(F_A, F_B)^-$ is much faster than the subsequent steps since it occurs in the submicrosecond range (38). The kinetic analysis is further simplified as the experiments were performed under conditions where one partner is in large excess over the other one for each of the reactions: $[Fd_{ox}] \gg [PSI_{red}]$, $[FNR_{ox}] \gg [Fd_{red}]$, $[Fd_{ox}] \gg [FNR_{sq}]$. This allows the system of time-differential equations corresponding to the model to be solved analytically, using the three following first-order rate Equations 1–3,

$$k_{rFd} = k_r \times [Fd] \quad \text{(Eq. 1)}$$

with [Fd] as the total Fd concentration ($[Fd_{red}] \ll [Fd_{ox}]$),

$$k_{red} = k_1 \times [FNR] \quad \text{(Eq. 2)}$$

with [FNR] as the total FNR concentration ($[FNR_{sq}] \ll [FNR_{ox}]$).

$$k_{ox} = k_{-1} \times [Fd] \quad \text{(Eq. 3)}$$

The solution is then shown in Equations 4–6,

$$[PSI_{red}](t) = [PSI] \times e^{-k_{rFd}t} \quad \text{(Eq. 4)}$$

$$[Fd_{red}](t) = [PSI] \times \left[\frac{k_{rFd} - k_{ox}}{k_{ox} + k_{red} - k_{rFd}} \times e^{-k_{rFd}t} - \frac{k_{red}k_{rFd}}{(k_{ox} + k_{red} - k_{rFd})(k_{ox} + k_{red})} \times e^{-(k_{ox} + k_{red})t} + \frac{k_{ox}}{k_{ox} + k_{red}}\right] \quad \text{(Eq. 5)}$$

$$[FNR_{sq}](t) = [PSI] \times \left[\frac{-k_{red}}{k_{ox} + k_{red} - k_{rFd}} \times e^{-k_{rFd}t} + \frac{k_{red}k_{rFd}}{(k_{ox} + k_{red} - k_{rFd})(k_{ox} + k_{red})} \times e^{-(k_{ox} + k_{red})t} + \frac{k_{red}}{k_{ox} + k_{red}}\right] \quad \text{(Eq. 6)}$$

with [PSI] as the total PSI concentration. The Excel solver (V. 2003, Microsoft) was used to fit the experimental results with the above equations.

When measuring multiple turnover event from reoxidation of Fd_{red}, the decay kinetics were able to be fitted with a single exponential component (5). The initial decay rate k_{noFNR} in the absence

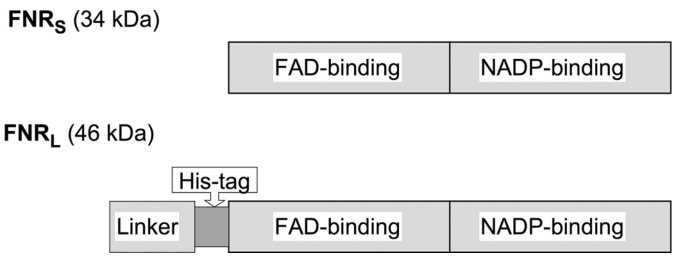

FIGURE 1. **Representation of the FNR primary structures highlighting their functional domains.** FNR_S is restricted to the catalytic part that is divided into the FAD binding domain and the NADP binding domain. FNR_L contains an N-terminal extension that comprises the PBS-linker domain and a hinge domain, whose length and primary sequence are variable depending on the cyanobacterium. Because the N- and C-terminal domains of the enzyme are buried in the PBS and the NADP binding site, respectively, the His tag was inserted into the hinge domain.

of FNR was subtracted from the exponential rate k_{FNR} in its presence. The initial turnover rate was then calculated from Equation 7,

$$-(d[Fd_{red}]/dt)_{t=0}/[FNR] = (k_{FNR} - k_{noFNR}) \times [PSI]/[FNR] \quad \text{(Eq. 7)}$$

as $[PSI] = [Fd_{red}]_{t=0}$.

This rate can also be calculated from rate k_1 of Reaction 2 (see "Results") when this reaction is rate limiting. From Reaction 2, the decay rate of Fd_{red} is shown in Equation 8,

$$d[Fd_{red}]/dt = -k_1[Fd_{red}][FNR_{ox}] + k_{-1}[Fd_{ox}][FNR_{sq}] \quad \text{(Eq. 8)}$$

which gives, for $t = 0$, Equation 9,

$$(d[Fd_{red}]/dt)_{t=0} = -k_1[Fd_{red}]_{t=0}[FNR] \quad \text{(Eq. 9)}$$

with [FNR] as the total concentration of FNR. With $[PSI] = [Fd_{red}]_{t=0}$ one gets Equation 10.

$$-(d[Fd_{red}]/dt)_{t=0}/[FNR] = k_1[PSI] \quad \text{(Eq. 10)}$$

RESULTS

Quantification of $NADP^+$ and NADPH in Cell Extracts—The cellular contents of $NADP^+$ and NADPH were measured in three *Synechocystis* strains grown under photoautotrophic conditions, the wild type and two mutants containing only one of the FNR isoforms, *i.e.* FNR_L and FNR_S in MI6 and FS1, respectively (24). The $NADP^+$/NADPH ratios were 2.6 ± 0.2, 2.0 ± 0.4, and 4.3 ± 0.8 for the wild type, MI6, and FS1 strains, respectively. Whereas the wild type and MI6 strains exhibit similar $NADP^+$/NADPH ratios, FS1 contained a significantly more oxidized NADP pool. As the $NADP^+$/NADPH ratio is expected to depend on the PSI/PSII content, we measured the PSI/PSII ratios in the thylakoids by EPR (39). The ratios were found to be similar in the three strains in the 2.5–2.9 range (data not shown).

Purification of an FNR_L-PC Complex—To study FNR_L under conditions as close as possible to its native conformation, we purified an FNR_L-PBS subcomplex from CBH, a *Synechocystis* mutant that contained a His tag in FNR_L (Fig. 1). The tag had no effect on either the cell growth characteristics or its PBS composition (data not shown).

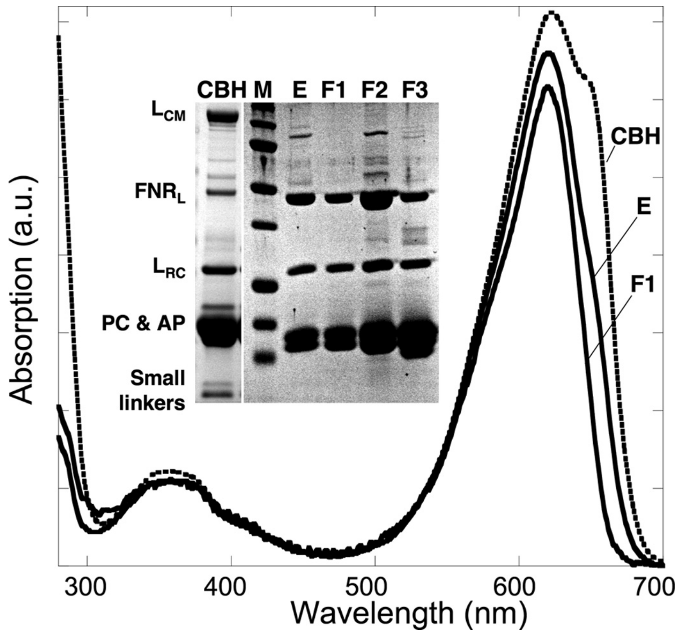

FIGURE 2. **Purification of the FNR_L-PC complex.** Absorption spectra of sample fractions during the purification steps, CBH: PBS preparation (*dotted line*) where AP (λ_{max}, 650 nm) and PC (λ_{max}, 620 nm) peaks are visible, *E*, the sample after Ni-affinity chromatography contains PC and a shoulder at 650 nm due to traces of AP; *F1*, the major fraction from gel filtration chromatography exhibits a PC spectrum with a shoulder at 580 nm indicating the presence of L_{RC}. The polypeptide composition of the samples was analyzed by SDS-PAGE. *Inset*, CBH; *M*, molecular markers, *E1*, after Ni-affinity chromatography; *F1*, first and major fraction; *F2* and *F3*, minor fractions from gel filtration chromatography. The identities of the polypeptides are indicated on the *left*.

Fig. 2 illustrates the purification protocol as followed both by UV/visible absorption spectroscopy and by SDS-PAGE. The specific absorption of the PBS starting material at 650 nm (AP contribution) strongly decreases during the different purification steps (PBS gradient, Ni-affinity chromatography, and gel filtration). Denaturing electrophoresis clearly shows an enrichment of FNR_L after the Ni-column (*lane E*) but the complex contained minor impurities that are ascribed to L_{CM} (the core membrane linker of the phycobilisome) and AP subunits as evidenced by the shoulder at 650 nm in the corresponding spectrum. The impurities were then eliminated from FNR_L-PC by gel filtration. Indeed only Fraction F1 corresponds to pure FNR_L-PC as it contained only FNR_L, α^{PC}, β^{PC}, and L_{RC}, as observed by SDS-PAGE (Fig. 2, *lane F1*). The molecular mass of FNR_L-PC was determined to be 330 kDa. F2 and F3 are minor fractions of lower molecular weight (supplemental Fig. S1).

The polypeptide composition of the purified FNR_L-PC was evaluated by densitometry of the Coomassie Blue-stained SDS-PAGE bands and indicates that the protein partners, FNR_L: L_{RC}: $(\alpha^{PC},\beta^{PC})_6$, are in a 1:1:1 stoichiometry. The estimated mass of the complex (330 kDa) closely matches its theoretical mass (303 kDa), which takes into account one phycocyanin hexamer (229 kDa) binding one FNR_L (46 kDa) and one L_{RC} (28 kDa). A direct measurement of the FAD content at 461 nm was impossible due to the large PC absorption. Therefore, an extraction procedure was applied (see "Experimental Procedures" and supplemental Fig. S2), leading to an occupancy value from 92 to 100% for the FAD cofactor in FNR_L-PC (Table 1).

TABLE 1

Quantification of FNR_L and FAD in FNR_L-PC

Three different FNR_L-PC samples have been trichloroacetic acid precipitated, and analyzed for their FNR_L and FAD contents. For each sample, the result is an average of three measurements. Taking together the results of the three samples, one gets a [FAD]/[FNR_L] ratio of between 0.92 and 1.00.

Sample	FNR_L concentration	FAD concentration	[FAD]/[FNR_L]
	μM	μM	
A	0.43 ± 0.02	0.39 ± 0.02	0.91 ± 0.09
B	0.55 ± 0.04	0.49 ± 0.05	0.89 ± 0.16
C	1.22 ± 0.03	1.19 ± 0.04	0.98 ± 0.06

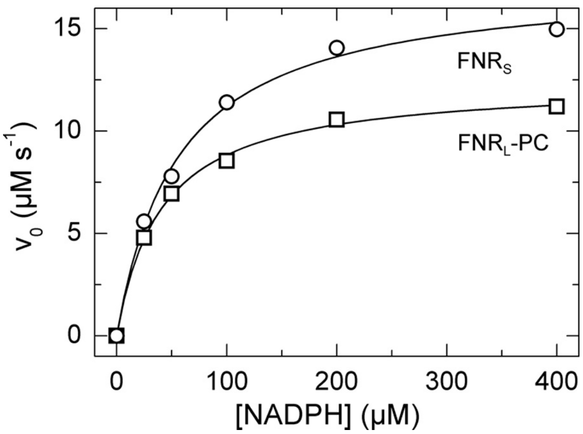

FIGURE 3. **Ferricyanide reductase activities of FNR_S and FNR_L-PC.** $K_3[Fe(CN)_6]$ was premixed with 0.025–0.1 μM $FNR_{S/L}$ in 150 mM KP pH 8 and 5 mM $MgCl_2$ at room temperature. The reaction was started by addition of 25–400 μM NADPH. For the FNR_L-PC preparation, at least two measurements have been carried out at each given point. The data were normalized to an $FNR_{S/L}$ concentration of 0.1 μM and were fitted with the Henri-Michaelis-Menten equation: For FNR_S (*open circles*) and FNR_L-PC (*open squares*), $K_{m(NADPH)}$ values were 55 ± 5 μM and 40 ± 3 μM, respectively. The turnover number k_{cat} for FNR_S and FNR_L-PC were 174 ± 5 s^{-1} and 124 ± 3 s^{-1}, respectively.

It has been recently reported that two types of PBS could be found in *Synechocystis*, the conventional one that contains L_{RC1} encoded by *cpcG1* and another one that lacks the core substructure and contains the *cpcG2* encoded L_{RC2} (40, 41). We analyzed the L_{RC} polypeptide contained in the FNR_L-PC complex by MALDI-TOF mass spectrometry, and this polypeptide was identified as L_{RC1}.

Ferricyanide Reductase Activity—NADPH oxidase activity (also called diaphorase activity) was used to measure the FNR turnover and its affinity for NADPH, in the presence of the artificial electron acceptor potassium ferricyanide. The diaphorase reaction starts with binding of NADPH to FNR, which is followed by the formation of a charge-transfer complex and then hydride transfer from NADPH to FAD (42). Electrons are then transferred to ferricyanide in a non-rate-limiting one-electron reaction. Initial enzyme velocities were plotted as a function of NADPH concentration and fitted according to the Henri-Michaelis-Menten equation (Fig. 3). Both $K_{m(NADPH)}$ and k_{cat} were found to be 30% smaller in FNR_L-PC than in FNR_S, which results in similar catalytic efficiencies (Table 2).

Ferredoxin-mediated Cytochrome c Reductase Activity—This NADPH oxidase activity was used to measure the affinity for Fd and the turnover of FNR in the presence of its natural electron acceptor Fd. After hydride transfer from NADPH to FNR, electrons flow to Fd, which is then reoxidized by cyt *c*. To obtain specific information about the Fd reduction step, the initial

TABLE 2

Catalytic properties of the FNR_L-PC and FNR_S isoforms

FNR catalytic properties (unit)	FNR_L-PC	FNR_S
Ferricyanide reductase activity		
$K_{m(NADPH)}$ (μM)	40 ± 3	55 ± 5
k_{cat} (s^{-1})	124 ± 3	174 ± 5
k_{cat}/K_m ($\mu M^{-1}s^{-1}$)	3.1 ± 0.3	3.2 ± 0.4
Cytochrome c reductase activity		
$K_{m(Fd)}$ (μM)	47 ± 6	28 ± 2
k_{cat} (s^{-1})	144 ± 12	154 ± 6
k_{cat}/K_m ($\mu M^{-1}s^{-1}$)	3.1 ± 0.7	5.5 ± 0.6
Single reduction of FNR by Fd_{red}		
no $NADP^+$		
Second-order forward rate k_1 ($\mu M^{-1}s^{-1}$)	14.1	24.9
Second-order reverse rate k_{-1} ($\mu M^{-1}s^{-1}$)	4.6	10.6
$K_{eq} = k_1/k_{-1}$	3.06	2.35
$E_{m(FNRox/FNRsq)}$[a] (mV)	−384	−390
1 mM $NADP^+$		
Second-order forward rate k_1 ($\mu M^{-1}s^{-1}$)	10.8	15.2
Second-order reverse rate k_{-1} ($\mu M^{-1}s^{-1}$)	4.0	5.4
$K_{eq} = k_1/k_{-1}$	2.73	2.84
$E_{m(FNRox/FNRsq)}$[a] (mV)	−386	−385
Multiple turnover: Initial rate of reoxidation of 3.75 μM Fd_{red} (reoxidized Fd_{red} per second and per FNR)		
Observed rate	50	53/(330)[b]
Calculated rate (with limiting k_1)	40.5	57/(1564)[b]

[a] Vs NHE. Calculated assuming $E_{m(Fdox/Fdred)} = -412$ mV (44).
[b] Numbers in italics were obtained at low ionic strength and recalculated from Ref. 5 by using an absorption coefficient of 9,000 $M^{-1}cm^{-1}$ for FNR_S at 461 nm instead of 10,800 $M^{-1}cm^{-1}$ (giving *e.g.* $k_1 = 417$ $\mu M^{-1}s^{-1}$).

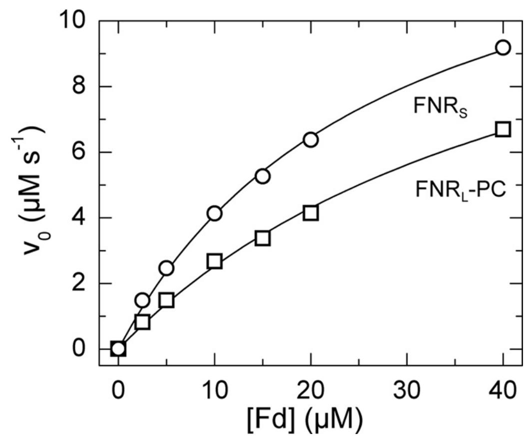

FIGURE 4. **Fd-mediated cyt *c* reductase activities of FNR_S and FNR_L-PC.** $FNR_{L/S}$ was mixed with 2.5–40 μM Fd from *T. elongatus* and 40 μM cyt *c* in 150 mM KP buffer pH 8 at 25 °C. The reaction was started by injection of 400 μM NADPH. The data were normalized to an $FNR_{S/L}$ concentration of 0.1 μM. For FNR_S (*open circles*) and FNR_L-PC (*open squares*), the $K_{m(Fd)}$ values were 28 ± 2 μM and 47 ± 6 μM, respectively. The turnover number k_{cat} for FNR_S and FNR_L-PC were 154 ± 6 s^{-1} and 144 ± 12 s^{-1}, respectively.

enzyme velocities were obtained by varying the amount of Fd under saturating concentrations of NADPH and cyt *c*. The initial rates of cyt *c* reduction were plotted as a function of Fd concentrations (Fig. 4) and fitted after the Henri-Michaelis-Menten equation. Table 2 highlights the similarities and differences between the two FNR isoforms: similar k_{cat} values in both isoforms, $K_{m(Fd)}$ 70% larger and catalytic efficiency 44% smaller in FNR_L-PC than in FNR_S were found.

Single Electron Transfer from Reduced Ferredoxin—The kinetics of FNR reduction in the ternary mixture PSI/Fd/FNR were measured by flash absorption spectroscopy (5). After the actinic flash has triggered a charge separation in PSI, an electron transfer cascade is occurring toward FNR, via Fd. The

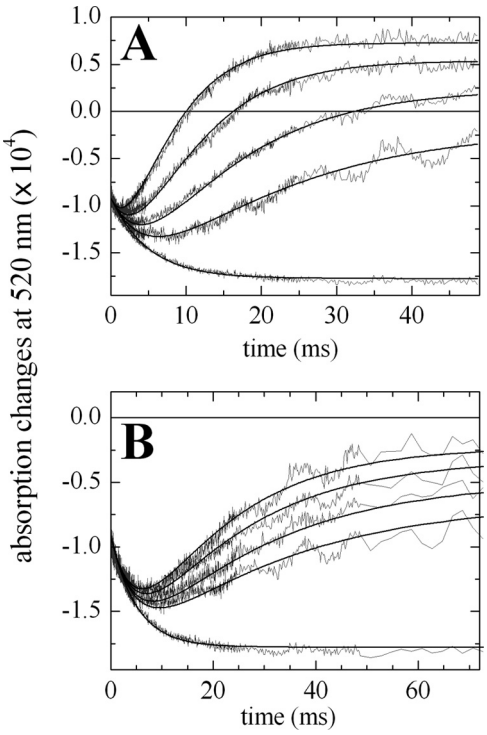

FIGURE 5. **Flash titration of FNR$_S$ and FNR$_L$-PC in the presence of 1 mM NADP$^+$ under single reduction conditions.** The absorption changes at 520 nm are attributed to electron acceptors as the P700$^+$ formation and decay have been subtracted. The *solid line* at zero level corresponds to the baseline before the flash. Concentrations of PSI and Fd were 0.475 μM and 3.96 μM. *A*, concentrations of FNR$_S$ were 0, 2.0, 4.0, 8.0, and 16.0 μM for curves from *bottom to top*. The best fit resulted in k_r = 50 μM^{-1} s^{-1}, k_1 = 15.2 μM^{-1} s^{-1}, and k_{-1} = 5.4 μM^{-1} s^{-1}. *B*, concentrations of FNR$_L$-PC were 0, 1.6, 2.1, 3.0, and 3.7 μM for curves from *bottom to top*. The best fit resulted in k_r = 50 μM^{-1} s^{-1}, k_1 = 10.8 μM^{-1} s^{-1}, and k_{-1} = 4.0 μM^{-1} s^{-1}.

measurements were performed in the absence/presence of NADP$^+$ and, in order to favor single FNR reduction, FNR was in large excess over PSI (and therefore over photoreduced Fd). The kinetics in the presence of 1 mM NADP$^+$ are shown in Fig. 5*A* for different FNR$_S$ concentrations, together with a control experiment without FNR$_S$. The signals are only due to reduction of the PSI electron acceptors, Fd and FNR as the P700$^+$ contribution has been eliminated (see "Experimental Procedures"). In the control experiment (bottom trace), two different kinetic components are present. The fastest component is not time resolved and is attributed to the formation of the reduced PSI terminal acceptor $(F_A, F_B)^-$, as confirmed by a sample without Fd (data not shown). A very small and fast submicrosecond to microsecond signal due to Fd reduction (<10% of the full Fd reduction signal) was observed, corresponding to a small amount of PSI:Fd complex present before flash excitation (data not shown; see also Ref. 43). This is in line with the large dissociation constant K_d that is expected for the PSI:Fd complex under our conditions (150 mM potassium phosphate, pH 8). The slowest millisecond absorption decrease is due to Fd reduction by a second-order diffusion-limited process. In the presence of FNR$_S$, the same initial fast decay is observed but a signal increase, which is ascribed to the reduction of FNR$_S$ by Fd$_{red}$, dominates the subsequent absorption changes. The rates and the final amplitudes of this signal increase when FNR$_S$ concentration increases. The kinetic model we used to simulate the observed kinetics is shown in Reactions 1 and 2.

$$PSI_{red} + Fd_{ox} \xrightarrow{k_r} PSI_{ox} + Fd_{red}$$

REACTION 1

$$Fd_{red} + FNR_{ox} \underset{k_{-1}}{\overset{k_1}{\rightleftharpoons}} Fd_{ox} + FNR_{sq}$$

REACTION 2

In Reaction 1, PSI$_{red}$ stands for PSI with the terminal acceptor (F_A, F_B) reduced. Reduction of (F_A, F_B) occurs in the submicrosecond time range and thus does not need to be considered. This kinetic model can be analytically solved in a simplified version when all reactions are considered as pseudo first-order (see "Experimental Procedures" for the solution equations). This allowed us to perform a global fit analysis resulting in the following values: k_r = 50.0 μM^{-1} s^{-1}, k_1 = 15.2 μM^{-1} s^{-1}, k_{-1} = 5.4 μM^{-1} s^{-1}. The redox equilibrium constant K_{eq} = 2.84 can be calculated for Reaction 2 (k_1/k_{-1}). This constant is related to the difference in midpoint redox potentials (E_m) of the reaction partners in Equation 11.

$$\Delta E_m = E_{m(FNR_{ox}/FNR_{sq})} - E_{m(Fd_{ox}/Fd_{red})} = (RT/F)\ln(K_{eq}) \quad \text{(Eq. 11)}$$

Assuming E_m = −412 mV for *Synechocystis* Fd (44), one gets −385 mV for $E_{m(FNRox/FNRsq)}$, which is very close to the value of −382 mV previously determined under conditions of moderate ionic strength (30 mM NaCl, 5 mM $MgCl_2$; the value of −378 mV in Ref. 5 has been recalculated using $\epsilon_{461\ nm}$ = 9,000 M^{-1} cm^{-1} for FNR). It should be noted that measuring $E_{m(FNRox/FNRsq)}$ by standard methods is fairly difficult because the thermodynamically unstable semiquinone (45) is only marginally observed during a redox titration.

The same experiment was performed with FNR$_L$-PC and the corresponding kinetics are shown in Fig. 5*B*. Fitting these data gave similar values of K_{eq} and hence of $E_{m(FNRox/FNRsq)}$, whereas the second-order rate constants were 25–30% smaller than with FNR$_S$ (Table 2). The smaller rate constants measured with FNR$_L$-PC are in accordance with its larger $K_{m(Fd)}$ observed in the ferredoxin-mediated cyt *c* reduction assay. The above experiments were repeated in the absence of NADP$^+$, to compare the kinetics in the presence or absence of a ternary complex Fd/FNR/NADP$^+$. These results are summarized in Table 2: For both isoforms the E_m is very similar to those measured in the presence of NADP$^+$. This indicates that the electrostatic environment of FAD is not modified by NADP$^+$. In contrast, the k_1 and k_{-1} rates are larger in the absence of NADP$^+$, in agreement with a previous study, where this effect was attributed to a repulsive electrostatic effect between the phosphate moiety of NADP$^+$ and the negatively charged Fd (5).

Catalytic Turnover of the Two FNR Isoforms during NADP$^+$ Reduction—We also measured FNR-reduction kinetics obtained for a ternary mixture PSI/Fd/FNR in the presence of

$NADP^+$ under multiple catalytic turnover conditions (5). These conditions were met by using PSI in large excess over FNR (3.75 μM *versus* 0.15/0.3 μM). Fd (8 μM) is also added in excess over PSI so that Fd_{red}, at a PSI equivalent concentration, is rapidly formed after PSI photoexcitation. Fd_{red} is then slowly monoexponentially reoxidized by FNR (rate k_{FNR}). Taking into account the decay without FNR (rate $k_{no\ FNR}$), we obtained values of 2.2 and 4.1 s^{-1} for ($k_{FNR} - k_{no\ FNR}$) with 0.15 and 0.30 μM FNR_S, respectively. This corresponds to 55 and 51 reoxidized Fd_{red} per second and per FNR_S, respectively and the average value of 53 is indicated in Table 2. Using the same enzyme concentrations, the ($k_{FNR} - k_{no\ FNR}$) rates are quite similar to those of FNR_L-PC (2.14 and 3.69 s^{-1}). This corresponds to an averaged value of 50 reoxidized Fd_{red} per second and per FNR_L-PC (Table 2). Overall, the multiple turnover rates are similar for the two isoforms.

As the second-order rate constants k_1 measured for the first FNR reduction are rather small under our conditions (see "Discussion"), it is worth checking if this process could be rate limiting during the catalysis (see Equation 10 under "Experimental Procedures"). The similarity between the calculated and measured turnover rates (Table 2) indicates that this is indeed the case. Thus we have identified under our conditions a limiting step which has not been identified previously. As a control, we also considered FNR_S under low ionic strength conditions (5) in order to compare the measured and calculated turnovers (bracketed values in Table 2). The 5-fold excess in calculated *versus* measured turnover shows that in this case of faster turnover, FNR_S reduction by Fd_{red} is not rate limiting.

DISCUSSION

Based on the observation that in *Synechocystis* FNR_S accumulates only under heterotrophic or starvation conditions whereas FNR_L is the major isoform detected under photoautotrophic conditions (24), it was proposed that each isoform plays a specific role. In this work, we have shown that under photoautotrophic conditions the $NADP^+$/NADPH ratio is higher in a mutant containing only FNR_S. Furthermore this observation cannot be attributed to a different PSI/PSII ratio as the ratio was shown to be unchanged in FS1 compared with that of the wild type. This reinforces the hypothesis that the FNR isoforms have different roles. FS1 seems unable to accumulate the NADPH amounts produced in the strains (wild type and MI6) where FNR_L is the main isoform. This also explains the fact that photoautotrophic growth is impaired in FS1, while MI6 growth is similar to that of the wild type (24). We decided to check whether the *in vivo* differences could be explained by the *in vitro* properties of the two FNR isoforms. In other words, is there any selectivity of the two isolated FNR isoforms for $NADP^+$ reductase *versus* NADPH oxidase activities? Such a selectivity has been observed in the case of root and leaf FNR isoforms in plants (3, 12, 14–17, 46).

Purification of an L_{RC}-containing FNR_L:PC Complex—The best compromise between approaching the *in vivo* situation and feasibility (stability, compatibility with absorption-spectroscopy studies) was to obtain a PBS subcomplex containing FNR_L and a PC hexamer $(\alpha^{PC}, \beta^{PC})_6$. The purification was facilitated by a His tag in the hinge domain of FNR_L. We obtained a pure and homogeneous complex, as judged by gel filtration, SDS-PAGE analysis, and FAD content. The stoichiometry of FNR_L:L_{RC}:$(\alpha^{PC}, \beta^{PC})_6$ in the 300-kDa complex was found to be 1:1:1. Furthermore it was verified that the L_{RC} polypeptide present in FNR_L-PC was encoded by *cpcG1*, which was expected since conventional PBS were used for its purification. It was recently proposed, using single particle analysis of CBH PBS, that FNR_L is located at the interface between the rod and the core (22). From our purification data, it can be further concluded that FNR_L is bound at only one of the PC hexamers, with no major involvement of the other hexamers. The complex was stable, for at least 2 weeks at 4 °C, with no proteolysis of FNR_L. This is probably due to protection of the FNR_L linker-domain by the PC hexamer.

Effect of High Ionic Strength on the Catalytic Properties of FNR_S—With the aim of comparing FNR_S and FNR_L-PC, we performed a broad set of measurements on NADPH-oxidase and $NADP^+$-reductase activities of the two isoforms as summarized in Table 2. These measurements were performed under high ionic strength conditions (150 mM potassium phosphate) because such conditions are necessary to stabilize the FNR_L-PC complex. We compared our data to those previously obtained for cyanobacterial FNR_S at lower ionic strength. The NADPH-oxidase catalytic parameters (measured via ferricyanide reduction) are quite similar to those previously reported for FNR_S from *Anabaena* sp. (k_{cat} 20% smaller, $K_{m(NADPH)}$ about 2-fold greater in our case; Ref. 47). This implies that this ionic strength is not detrimental for diaphorase activity. Regarding the ferredoxin-mediated NADPH-oxidase activity, we found a 3-fold increase in $K_{m(Fd)}$ and only a 25% decrease in k_{cat}, between our measurements and those previously measured in the same report with *Anabaena* FNR_S (47). The $K_{m(Fd)}$ increase can be attributed to the screening of electrostatic interactions occurring at high ionic strength between FNR and Fd (2). A similar screening effect explains our data concerning FNR_S reduction by Fd_{red} when compared with a previous study, conducted under lower ionic strength (5): the second-order rate constant k_1 of single FNR_S reduction by Fd_{red} is 28-fold smaller and during multiple turnover, the rate of Fd_{red} reoxidation is 6 times smaller in the present study. We also obtained evidence that at high ionic strength, k_1 is rate limiting during multiple turnover, which is not the case at lower ionic strength. Under these last conditions, the enzyme turnover is much faster and is limited by one of the first-order processes (Fd_{ox} dissociation, hydride transfer, or NADPH release).

Comparison of the Catalytic Properties of FNR_S and FNR_L-PC: an Analogous System to Leaf and Root FNR Isoforms?—The following catalytic parameters are quite similar for the two *Synechocystis* isoforms: the catalytic efficiency (k_{cat}/K_m) of NADPH/ferricyanide oxidoreduction, the k_{cat} of the Fd-mediated cyt *c* reduction, the E_m (FNR_{ox}/FNR_{sq}) in the presence/absence of $NADP^+$ and the initial reoxidation rate of Fd_{red} by FNR during multiple catalytic turnover. Differences between the two isoforms were observed: 30% smaller K_m(NADPH) and k_{cat} of FNR_L-PC *versus* FNR_S during NADPH/ferricyanide oxidoreduction, a 70% larger $K_{m(Fd)}$ and a 44% smaller catalytic efficiency of FNR_L-PC for the Fd-mediated cyt *c* reductase activity, and a 29/43% ($NADP^+$ present/absent) decrease in k_1,

the rate of single FNR reduction by Fd_{red}, for FNR_L-PC (Table 2). The slight decrease in $K_{m(NADPH)}$ and k_{cat} during ferricyanide reduction indicates that the presence of the PC hexamer slightly modifies the association of NADPH to FNR and/or the following steps leading to FAD reduction. The increase in $K_{m(Fd)}$ and the decrease in k_1 are likely due to a steric hindrance by, or a conformational effect due to, the PC hexamer moiety of FNR_L-PC. We favor these explanations over electrostatic repulsion brought by PC, because electrostatic interactions are expected to be of limited importance at high ionic strength. Moreover, the electrostatic environment of FAD appears to be unmodified in FNR_L-PC as judged by the similar $E_{m(FNRox/FNRsq)}$ measured for the two isoforms. Overall, the results obtained for the Fd-mediated cyt *c* reductase activity are in agreement with the different predicted roles for the FNR isoforms. Both isoforms are capable of catalyzing $NADP^+$ reduction under multiple turnover conditions. Furthermore, we obtained indications that in our conditions electron transfer from Fd_{red} is rate limiting.

The leaf and root FNR isoforms from plants differ mainly in four catalytic or thermodynamic parameters (supplemental Table S1): 1) $K_{m(NADPH)}$, measured via ferricyanide reduction, is 3–10-fold higher, depending on the authors, for leaf FNR compared with root FNR (14, 16). We observed a 30% decrease in FNR_L-PC *versus* FNR_S. If we tentatively make the parallel between FNR_L-PC and leaf FNR on the one hand, and between FNR_S and root FNR on the other hand, the situation seems reversed; 2) $K_{m(leaf\ Fd)}$, measured by Fd-mediated cyt *c* reduction, is 5–10-fold smaller for leaf FNR than for to root FNR (3, 14, 17, 46). The 70% difference that we observe is also in the unexpected direction; 3) k_{cat} of the Fd-mediated cyt *c* reduction is 3–4-fold smaller for leaf FNR than for root FNR (3, 14, 17, 46). We observed no significant difference in this parameter; 4) The $E_{m(FNRox/FNRred}$ couple, 2-electron reduction) of corn root FNR is 20 mV higher than the midpoint potential of spinach leaf FNR (15). Unfortunately, no comparison is available for two FNR isoforms from the same plant, to our knowledge. We observed no significant difference for $E_{m(FNRox/FNRsq)}$ between the two *Synechocystis* isoforms.

Contrary to the case of *Synechocystis*, there are some differences in the catalytic domains of the plant FNR isoforms. Moreover, the existence of Fd isoforms is essential when comparing the processes of $NADP^+$ reduction and NADPH oxidation in leaves and roots. The E_m of root Fd was found to be much higher than that of leaf Fd (50–100 mV difference; Refs 17, 46, 48, 49). This probably favors NADPH oxidation in roots *versus* $NADP^+$ reduction in leaves. Many different Fd encoding genes have been identified in *Synechocystis* (50). In the present work we studied the major Fd encoded by *fed1*. This Fd shares with the leaf Fd a similar redox potential but both root and leaf Fds appear to be phylogenetically equally distant to the *Synechocystis* Fd (17). At our present state of knowledge, there is no equivalent of the root Fd in cyanobacteria, in terms of redox potential, and the major photosynthetic Fd is generally thought to be involved in all bioenergetically significant electron flows. This was also a basic assumption in our approach. However, the involvement of other Fd isoforms under heterotrophic conditions cannot be excluded.

CONCLUSION

From recent data (24), specific roles were proposed for the two *Synechocystis* FNR isoforms, which seem to parallel the enzymatic selectivity of plant FNR root and leaf isoforms. Such specificity is also supported by the change in the $NADP^+$/NADPH ratios that we measured in *Synechocystis* cells containing only one of the isoforms. However, from a detailed functional characterization, we observed small differences in the $NADP^+$ reductase and NADPH oxidase activities of FNR_S and FNR_L-PC complex. This contrasts with the much larger *in vitro* differences observed between leaf and root FNR isoforms from plants.

If the main photosynthetic Fd (50) is involved *in vivo* in electron transfer with both isoforms (see above), the differences that we observe might not fully explain the *in vivo* properties of the *Synechocystis* mutants expressing only one of the isoforms. Besides the intrinsic catalytic properties of those isoforms, it would be necessary to invoke their localization or association to other complexes. For example, it can be speculated that FNR_S is involved in cyclic/respiratory electron flow because it is free to bind to other membrane complexes such as NADPH dehydrogenase or cytochrome b_6f. Conversely, PBS-bound FNR_L cannot play such a role and is therefore dedicated to $NADP^+$ photoreduction. For both types of activities, substrates availability (Fd_{red}/Fd_{ox} and $NADP^+$/NADPH) might also be key *in vivo* characteristics for the activity of the two isoforms. This situation would be reminiscent of what has been described recently for the different leaf isoforms, where catalytic activities appear to depend upon their variable attachment to the thylakoid membrane (51, 52).

In this context, it would be worth studying the involvement of CpcG2-PBS, which lacks the PBS core, in binding FNR_L, as it has been hypothesized to be directly bound to PSI (53). However the small amount of CpcG2-PBS *versus* CpcG1-PBS in the wild type (40) and the effect of cpcG2 disruption on the PSI/PSII ratio (41) are obstacles, which have to be surmounted for such studies. Further *in vivo* measurements are needed to better understand the reason for which FNR binds the PBS in the majority of PBS-containing cyanobacteria.

Acknowledgments—We thank V. Mary for skillful technical assistance and Dr. F. Haraux for discussions. C. Bordot is acknowledged for initial work on the His-tagged complex and Dr. A. Boussac for the gift of T. elongatus soluble extracts. We thank C. Deladriere and A. Guillot (PAPPSO, Jouy-en-Josas) for mass spectroscopy analysis.

REFERENCES

1. Batie, C. J., and Kamin, H. (1984) *J. Biol. Chem.* **259,** 11976–11985
2. Hurley, J. K., Morales, R., Martínez-Júlvez, M., Brodie, T. B., Medina, M., Gómez-Moreno, C., and Tollin, G. (2002) *Biochim. Biophys. Acta* **1554,** 5–21
3. Hanke, G. T., Kurisu, G., Kusunoki, M., and Hase, T. (2004) *Photosynth. Res.* **81,** 317–327
4. Karplus, P. A., and Faber, H. R. (2004) *Photosynth. Res.* **81,** 303–315
5. Cassan, N., Lagoutte, B., and Sétif, P. (2005) *J. Biol. Chem.* **280,** 25960–25972
6. Bruns, C. M., and Karplus, P. A. (1995) *J. Mol. Biol.* **247,** 125–145
7. Carrillo, N., and Ceccarelli, E. A. (2003) *Eur. J. Biochem.* **270,** 1900–1915
8. Batie, C. J., and Kamin, H. (1984) *J. Biol. Chem.* **259,** 8832–8839

9. Forti, G., and Sturani, E. (1968) *Eur. J. Biochem.* **3,** 461–472
10. Morigasaki, S., Takata, K., Suzuki, T., and Wada, K. (1990) *Plant Physiol.* **93,** 896–901
11. Okutani, S., Hanke, G. T., Satomi, Y., Takao, T., Kurisu, G., Suzuki, A., and Hase, T. (2005) *Plant Physiol.* **139,** 1451–1459
12. Gummadova, J. O., Fletcher, G. J., Moolna, A., Hanke, G. T., Hase, T., and Bowsher, C. G. (2007) *J. Exp. Bot.* **58,** 3971–3985
13. Green, L. S., Yee, B. C., Buchanan, B. B., Kamide, K., Sanada, Y., and Wada, K. (1991) *Plant Physiol.* **96,** 1207–1213
14. Onda, Y., Matsumura, T., Kimata-Ariga, Y., Sakakibara, H., Sugiyama, T., and Hase, T. (2000) *Plant Physiol.* **123,** 1037–1045
15. Aliverti, A., Faber, R., Finnerty, C. M., Ferioli, C., Pandini, V., Negri, A., Karplus, P. A., and Zanetti, G. (2001) *Biochemistry* **40,** 14501–14508
16. Aliverti, A., Pandini, V., and Zanetti, G. (2004) *Biochim. Biophys. Acta* **1696,** 93–101
17. Hanke, G. T., Kimata-Ariga, Y., Taniguchi, I., and Hase, T. (2004) *Plant Physiol.* **134,** 255–264
18. Schluchter, W. M., and Bryant, D. A. (1992) *Biochemistry* **31,** 3092–3102
19. Glazer, A. N. (1989) *J. Biol. Chem.* **264,** 1–4
20. van Thor, J. J., Gruters, O. W., Matthijs, H. C., and Hellingwerf, K. J. (1999) *EMBO J.* **18,** 4128–4136
21. Gómez-Lojero, C., Pérez-Gómez, B., Shen, G. Z., Schluchter, W. M., and Bryant, D. A. (2003) *Biochemistry* **42,** 13800–13811
22. Arteni, A. A., Ajlani, G., and Boekema, E. J. (2009) *Biochim. Biophys. Acta* **1787,** 272–279
23. van Thor, J. J., Jeanjean, R., Havaux, M., Sjollema, K. A., Joset, F., Hellingwerf, K. J., and Matthijs, H. C. P. (2000) *Biochim. Biophys. Acta* **1457,** 129–144
24. Thomas, J. C., Ughy, B., Lagoutte, B., and Ajlani, G. (2006) *Proc. Natl. Acad. Sci. U.S.A.* **103,** 18368–18373
25. Nakajima, M., Sakamoto, T., and Wada, K. (2002) *Plant Cell Physiol.* **43,** 484–493
26. Ughy, B., and Ajlani, G. (2004) *Microbiology* **150,** 4147–4156
27. Rögner, M., Nixon, P. J., and Diner, B. A. (1990) *J. Biol. Chem.* **265,** 6189–6196
28. Barth, P., Guillouard, I., Sétif, P., and Lagoutte, B. (2000) *J. Biol. Chem.* **275,** 7030–7036
29. Gantt, E., and Lipschultz, C. A. (1972) *J. Cell Biol.* **54,** 313–324
30. Elmorjani, K., Thomas, J. C., and Sebban, P. (1986) *Arch. Microbiol.* **146,** 186–191
31. Ajlani, G., Vernotte, C., DiMagno, L., and Haselkorn, R. (1995) *Biochim. Biophys. Acta* **1231,** 189–196
32. Glazer, A. N. (1985) *Annu. Rev. Biophys. Chem.* **14,** 47–77
33. Engel, P. C., and Massey, V. (1971) *Biochem. J.* **125,** 879–887
34. Whitby, L. G. (1953) *Biochem. J.* **54,** 437–442
35. Shin, M. (1971) *Methods Enzymol.* **23,** 440–447
36. Zanetti, G., and Arosio, P. (1980) *FEBS Lett.* **111,** 373–376
37. Sétif, P., Fischer, N., Lagoutte, B., Bottin, H., and Rochaix, J. D. (2002) *Biochim. Biophys. Acta* **1555,** 204–209
38. Brettel, K., and Leibl, W. (2001) *Biochim. Biophys. Acta* **1507,** 100–114
39. Danielsson, R., Albertsson, P. A., Mamedov, F., and Styring, S. (2004) *Biochim. Biophys. Acta* **1608,** 53–61
40. Kondo, K., Geng, X. X., Katayama, M., and Ikeuchi, M. (2005) *Photosynth. Res.* **84,** 269–273
41. Kondo, K., Ochiai, Y., Katayama, M., and Ikeuchi, M. (2007) *Plant Physiol.* **144,** 1200–1210
42. Tejero, J., Peregrina, J. R., Martínez-Júlvez, M., Gutiérrez, A., Gómez-Moreno, C., Scrutton, N. S., and Medina, M. (2007) *Arch. Biochem. Biophys.* **459,** 79–90
43. Sétif, P. Q., and Bottin, H. (1994) *Biochemistry* **33,** 8495–8504
44. Bottin, H., and Lagoutte, B. (1992) *Biochim. Biophys. Acta* **1101,** 48–56
45. Corrado, M. E., Aliverti, A., Zanetti, G., and Mayhew, S. G. (1996) *Eur. J. Biochem.* **239,** 662–667
46. Gou, P., Hanke, G. T., Kimata-Ariga, Y., Standley, D. M., Kubo, A., Taniguchi, I., Nakamura, H., and Hase, T. (2006) *Biochemistry* **45,** 14389–14396
47. Medina, M., Martinez-Júlvez, M., Hurley, J. K., Tollin, G., and Gómez-Moreno, C. (1998) *Biochemistry* **37,** 2715–2728
48. Aliverti, A., Hagen, W. R., and Zanetti, G. (1995) *FEBS Lett.* **368,** 220–224
49. Akashi, T., Matsumura, T., Ideguchi, T., Iwakiri, K., Kawakatsu, T., Taniguchi, I., and Hase, T. (1999) *J. Biol. Chem.* **274,** 29399–29405
50. Poncelet, M., Cassier-Chauvat, C., Leschelle, X., Bottin, H., and Chauvat, F. (1998) *Mol. Microbiol.* **28,** 813–821
51. Palatnik, J. F., Valle, E. M., and Carrillo, N. (1997) *Plant Physiol.* **115,** 1721–1727
52. Hanke, G. T., Endo, T., Satoh, F., and Hase, T. (2008) *Plant Cell Environ.* **31,** 1017–1028
53. Kondo, K., Mullineaux, C. W., and Ikeuchi, M. (2009) *Photosynth. Res.* **99,** 217–225

Abstract

In photosynthetic organisms, ferredoxin:NADP oxidoreductase (FNR) provides NADPH for CO_2 assimilation, but it also utilizes NADPH to provide reduced ferredoxin (Fd). The cyanobacterium *Synechocystis* sp. strain PCC6803 contains two FNR isoforms, a small (FNR_S, 34 kDa) and a large one (FNR_L, 46 kDa) that is associated with the phycobilisome (PBS), a light-harvesting complex. We purified a PBS subcomplex comprising FNR_L (FNR_L-PC) and compared the enzymatic properties of FNR_L-PC to FNR_S. FNR_L-PC exhibits an increased NADPH affinity, and a decreased Fd affinity in agreement with its predicted lower activity of Fd reduction. FNR_L-PC shows also a decrease in the rate of single electron transfer (ET) from Fd_{red}. Most of the obtained differences are attributed to steric hindrance by the phycocyanin moiety of FNR_L-PC. Both isoforms seem to catalyze the $NADP^+$ reduction under multiple turnover conditions to the same extent and we obtained evidence that, under our high ionic strength conditions, ET from Fd_{red} is rate limiting. During *in vivo* studies, we presented evidence supporting an increase of NADPH oxidation by respiratory or cyclic ET in a mutant lacking FNR_L and a similar behavior was observed for the wild type under low CO_2. The measurements clearly showed that FNR_S is implicated in this alternative ET and we propose that FNR_S attaches to NDH-1 acting as the dehydrogenase module. FNR localization and/or substrate availability seem to be essential so that FNR isoforms perform their respective roles *in vivo*. Future studies should result in a more complete *in vivo* view and clarify the important issue of the NADPH-dependent ET into the PQ pool that seems to be enhanced by FNR_S.

Résumé

Dans les organismes photosynthétiques, la ferrédoxine:NADP oxydoréductase (FNR) fournit le NADPH nécessaire à l'assimilation du CO_2, mais elle réduit aussi la ferrédoxine (Fd) à partir du NADPH. La cyanobactérie *Synechocystis* sp. PCC6803 contient deux isoformes de FNR: une forme courte (FNR_S, 34 kDa) et une forme longue (FNR_L, 46 kDa) qui est liée au phycobilisome (PBS), un complexe collecteur de lumière. Nous avons purifié un sous-complexe du PBS qui contient la FNR_L (FNR_L-PC) et comparé les propriétés enzymatiques de FNR_L-PC à FNR_S. Par rapport à FNR_S, FNR_L-PC présente des affinités plus faible/forte pour le NADPH/la Fd, conformément aux prédictions des activités relatives des deux isoformes. La plupart des différences observées sont attribuées à l'encombrement stérique amené par la phycocyanine dans FNR_L-PC. En conditions de turnover multiple, les deux isoformes catalysent de la même manière la réduction de $NADP^+$ et de plus le transfert d'électrons (TE) depuis Fd_{red} est limitant à force ionique élevée. Lors d'études *in vivo*, nous avons observé une augmentation de l'oxydation du NADPH par TE respiratoire ou cyclique chez un mutant ne contenant que la FNR_S et chez le type sauvage à faible CO_2. Les mesures ont montré clairement que FNR_S est impliqué dans ce TE alternative et nous proposons que FNR_S constitue le module déshydrogénase de NDH-1. La localisation de la FNR et/ou la présence de substrats semblent être essentiels dans les rôles respectifs des isoformes de FNR *in vivo*. Des études futures devraient nous donner une vue plus complète des processus de TE *in vivo* et clarifier le rôle du TE dépendant du NADPH et favorisé par FNR_S dans la réduction du pool de PQ.